Floquet Engineering in an Atom-Optics Kicked Rotor

विद्या वाचस्पति की
उपाधि की अपेक्षाओं की आंशिक पूर्ति में प्रस्तुत शोध प्रबंध

A thesis submitted in partial fulfillment of the requirements of the degree of Doctor of Philosophy

द्वारा / By

शिव सागर मौर्या / Shiv Sagar Maurya

पंजीकरण सं. / Registration No.:

20172029

शोध प्रबंध पर्यवेक्षक / Thesis Supervisor:

प्रो. उमाकांत डी. रापोल / Prof. Umakant D. Rapol

भारतीय विज्ञान शिक्षा एवं अनुसंधान संस्थान पुणे
INDIAN INSTITUTE OF SCIENCE EDUCATION AND RESEARCH PUNE

2024

Certificate

Certified that the work incorporated in the thesis entitled **"Floquet Engineering in an Atom-Optics Kicked Rotor"** submitted by **Shiv Sagar Maurya** was carried out by the candidate, under my supervision. The work presented here or any part of it has not been included in any other thesis submitted previously for the award of any degree or diploma from any other university or institution.

Date: 18/11/2024

Prof. Umakant D. Rapol (Supervisor)

Declaration by student

Name of Student : Shiv Sagar Maurya
Reg. No.: 20172029
Thesis Supervisor : Prof. Umakant D. Rapol
Department : Physics
Date of Joining Program : 01/08/2017
Date of Pre-Synopsis Seminar : 12/02/2024

Title of Thesis: Floquet Engineering in an Atom-Optics Kicked Rotor

I declare that this written submission represents my idea in my own words and where others ideas have been included; I have adequately cited and referenced the original sources. I declare that I have acknowledged collaborative work and discussions wherever such work has been included. I also declare that I have adhered to all principles of academic honesty and integrity and have not misrepresented or fabricated or falsified any idea/data/fact/source in my submission. I understand that violation of the above will be cause for disciplinary action by the Institute and can also evoke penal action from the sources which have thus not been properly cited or from whom proper permission has not been taken when needed.

The work reported in this thesis is the original work done by me under the guidance of Prof. Umakant D. Rapol .
Date: 18/11/2024
Signature of the Student: Shiv Sagar Maurya

Abstract

Implementing the Floquet operator in a cold atoms system is a fascinating field of research. This implication opens the path for the study of dynamical localization in the quantum kicked rotor system. The quantum kicked rotor system provides a platform to simulate analogue Anderson localization in both lower and higher dimensions, including the observation of the Anderson insulator-metal transition in three dimensions. It is also a unique tool to study quantum chaos. Since dynamical localization phenomena are based on the destructive quantum interference of the atomic wave-function, this system provides a platform for studying the exponential and non-exponential loss of coherence by coupling the quantum system with an external bath in an arbitrary way.

The present aim of this thesis is to coherently control quantum interference by engineering different dynamical phase evolution without introducing decoherence into the system. As we know, the classical counterpart of the system is fully chaotic in nature. Therefore, coherent control must be systematically engineered; otherwise, quantum interference may be disrupted in the system, causing it to behave classically. This thesis focuses on controlling dynamical localization in periodically kicked ultra-cold atoms with a 1D optical lattice. Two methods are explored: periodic modulation of a control parameter to induce competition between quantum diffusion and localization, leading to enhanced in localization length of localized system. In second method, we demonstrate a simple and intuitive method for controlling dynamical localization using a single parameter with Bose-Einstein condensate. This coherent control approach, operates through a single knob, enables systematic control over dynamical localization across a wide range without introducing any decoherence into the system.

Further in this thesis, our study also investigates the asymmetric dynamical localization and it's stability, by launching the initial wave-function with varying recoil velocities within periodically kicked optical lattices. Noteworthy velocity-dependent features are observed in different time-evolution. Utilizing the velocity dependent feature in early time dynamics, we created a method for direct measurement of micromotion (100's μm/s) of the Bose-Einstein condensate (BEC). This micromotion velocity is order of magnitude less than the one recoil photon momentum, as well as mean velocity associated with BEC temperature. By utilizing a feature coming from broken parity

symmetry due to the micromotion, measurement of such a small velocity is possible, which is not significantly affected by velocity distribution of the BEC, that is a common challenge in spectroscopy techniques. This approach offers a precise measurement of micromotion without relying heavily on the time-of-flight method, which often requires a substantial time for measurable movement, making it unfeasible in many systems. The precise measurement of such low velocities of the BEC contributes significantly to precision measurements, such as in atom interferometers for measuring rotation and acceleration, helping nullify unknown shifts in measurements comes from the micromotion.

Dedicated to my **Family**

Publications from the thesis work

- Interplay between quantum diffusion and localization in the atom-optics kicked rotor; **S. Sagar Maurya**, J. Bharathi Kannan, Kushal Patel, Pranab Dutta, Korak Biswas, Jay Mangaonkar, M. S. Santhanam, and Umakant D. Rapol, ***Phys. Rev. E, 106, 034207 (2022).***

- Asymmetric dynamical localization and precision measurement of the micromotion of a Bose-Einstein condensate; **S. Sagar Maurya**, J. Bharathi Kannan, Kushal Patel, Pranab Dutta, Korak Biswas, M. S. Santhanam, and Umakant D. Rapol, ***Phys. Rev. A, 110, 053307 (2024).***

Publications from other contributions

- Effects of finite momentum width on the reversal dynamics in a BEC based atom optics δ-kicked rotor; Jay Mangaonkar, Chetan Vishwakarma, **S. Sagar Maurya**, Sumit Sarkar, Jamie L. MacLennan, Pranab Dutta and Umakant D. Rapol, ***Journal of Physics B: Atomic, Molecular and Optical Physics, 53, 235502 (2020).***

- A decade of advancement of quantum sensing and metrology in India using cold atoms and ions; Pranab Dutta, **S. Sagar Maurya**, Kushal Patel, Korak Biswas, Jay Mangaonkar, Sumit Sarkar, Umakant D. Rapol, ***Journal of the Indian Institute of Science, 103 (2), 609-632 (2023).***

- Machine-learning-based automated loading of strontium isotopes into magneto-optical trap; Korak Biswas, Kushal Patel, **S. Sagar Maurya**, Pranab Dutta, Umakant D. Rapol, ***AIP Advances, 13 (7), (2023).***

- Comparative analysis of phase noise for different configurations of Bragg lattice for an atomic gravimeter with Bose-Einstein condensate; Pranab Dutta, **S. Sagar Maurya**, Korak Biswas, Kushal Patel, Umakant D. Rapol, ***AIP Advances, 14 (1), (2024).***

- Spectroscopy of the $5s5p\ ^3P_0 \rightarrow 5s5d\ ^3D_1$ transition of strontium using laser-cooled atoms; Kushal Patel, Palki Gakkhar, Korak Biswas, **S. Sagar Maurya**, Pranab Dutta, Vishal Lal, B.K. Mani and Umakant D. Rapol, ***Journal of Physics B: Atomic, Molecular and Optical Physics, 57, 105501 (2024).***

Manuscripts under review

- Evaporative Cooling by pulse-width modulation (PWM) of optical dipole trap; **S. Sagar Maurya**, Joel M. Sunil, Jay Mangaonkar, Monu Bhartiya, Rahul Sawant, Umakant D. Rapol, *In preparation.*
- A three-level cooling technique for enhancing the inter-stage transfer efficiency of strontium atoms; Korak Biswas, Kushal Patel, **S. Sagar Maurya**, Pranab Dutta, Umakant D. Rapol and Yeshpal Singh, *In review.*

Patents

- OVEN FOR GENERATION AND COLLIMATION OF AN ATOMIC BEAM; Umakant D Rapol, Kushal Patel, Korak Biswas, **S. Sagar Maurya**, Pranab Dutta, ***Indian Patent, Application Number-202421000590, filed on January 03, 2024.***

Acknowledgments

I remember each moment at IISER Pune very vividly, I started my M.S. and Ph.D. journey in the Atomic Physics and Quantum Optics (APQO) lab, where I gained a profound understanding of experimental skills and a scientific approach for solving the problems. I would like to acknowledge all those people who were with me during this journey.

Firstly, I would like to express my gratitude to my adviser, Dr. Umakant D. Rapol. I am thankful for the opportunities he has provided me in his super-cool lab. His advice, knowledge, and support have been invaluable during the last six years, and I am deeply appreciative of it. He gave me the freedom to conduct my own experiments and explore setups, which greatly contributed to my knowledge and experience.

I would also like to extend my gratitude to the members of my Research Advisory Committee (RAC), Dr. Subhadeep De, and Dr. M.S. Santhanam. Discussions with Dr. Santhanam on the quantum kicked rotor experiment were always fruitful, and I appreciate his knowledge and patience. Giving me enough time and always being punctual for discussions of experimental results was very helpful. Dr. Subhadeep De motivated me a lot during this journey and helped me think like an experimentalist. I am thankful for all his comments and guidance for the experiment.

I am also thankful to J. Bharathi Kannan, one of Dr. Santhanam's Ph.D. student, for his contributions to the numerical simulation of the quantum kicked rotor experiment and for all our discussions. I would also like to thank Dr. Sreejith G. J. and Dr. Rejish Nath for all the theoretical discussions regarding possible experiments with optical lattices and Bose-Einstein condensates. I would also like to thank Dr. Surjeet Singh for giving me a six-month project in his lab, where I learned many experimental techniques of condensed matter physics.

Now, I would like to express my gratitude to my lab mates past and present. I am thankful for the valuable learning experiences, I gained from my seniors, Sumit and Gunjan. I extend my appreciation to Jay for his guidance in teaching me about the Bose-Einstein condensate setup. I was actively involved in learning the experiments with him, and I am grateful to Jay for having confidence in me to run the Rb setup independently at the beginning of my journey. I also want to thank Chetan for his role in enhancing my experimental skills. Additionally, I am grateful to Jithin for his

guidance. Also a big thanks to visitors Jammie and Harinee for sharing their ideas for experiment and positive energy with us during their time in the lab. After Jay and Chetan completed their Ph.D., the lab underwent significant changes with the rebuilding of the Rubidium setup and new construction of Strontium setup. I and Pranab took over the operation of the Rubidium setup, while Kushal and Korak managed the Strontium setup commands. This marked the beginning of our collaboration, during which we worked together to advance the capabilities of the lab. We rebuilt the Rubidium setup, which had stopped working due to aging, and simultaneously planned the construction of a new Strontium setup. This period, marked by the tireless efforts of our fantastic four, it was a golden time of my Ph.D. journey as we worked relentlessly to achieve the Bose-Einstein condensate setup and get a Red MOT for Strontium setup. Furthermore, I would like to express my gratitude to Korak for his in-depth explanations connecting theory and experiment. I extend my thank to Pranab for his assistance with the BEC setup, and I am grateful to Kushal for his help with the vacuum setup and control system. I also thank mechanical engineer Aditya for all the SolidWorks design and electronic engineer Darshit. I enjoyed working with BS-MS students Anurag, Vishal, and Ruthwik, all of whom are enthusiastic about experiments. Lastly, I express my appreciation to my juniors, Rayees, Joel, Shuvarati, and Monu, who have the great opportunity to take the lab to the next level.

I would also like to thank my integrated Ph.D. 2017 batchmates for the wonderful memories. Additionally, I extend my gratitude to my friends Aakash, Mayank, Shaunak, Pranjal, Taniya, Chetana, Kushal, Sneha, Umashankar, Anupam, Sarvottam, Ratimansee, and Pragya. Special thanks to Aakash and Sarvottam for their help during coursework. I am thankful to Taniya for good discussions about science and culture over tea. I am also thankful to Chetana, can't forget the Rajgad trek. Thanks to Pragya and Ratimansee for discussion about their experiments related to optical tweezers, sharing sweets on festivals and inviting me for dinner on occasions. Thanks to Umashankar and Pranjal for organizing many treks during the monsoon season. I would also like to thank IISER badminton group for fantastic badminton matches.

I would also like to thank the H-Cross support staff: Nilesh Dumbre, Karthikey, Sudhir Lone, Prashant Kale, Daji, and Berman. Furthermore, I extend my gratitude

to the people from the administrative department: Prabhakar, Dhanashree, Sayalee, and Tushar. I specially thank Sayalee ma'am for her assistance in submitting the RAC report to the CSIR portal.

I acknowledge IISER Pune for providing a good environment for research and funding my fellowship during MS. I also acknowledge the CSIR for providing me the fellowship during my Ph.D. as JRF and SRF. I am also thankful for the Infosys Foundation Fellowship.

Finally, I express my sincere gratitude to my joint family for their unwavering love, support, and encouragement, without them, none of this would have been possible. Their immense support and affection have been indispensable in my journey. No words can truly capture the depth of their support, love, and encouragement. Thanks for always being there for me as my strongest supporters.

Date: June 13, 2024 (Shiv Sagar Maurya)

Contents

Declaration **v**

Abstract **vii**

Publications **xi**

Acknowledgments **xiii**

List of figures **xxi**

1 Introduction **1**

1.1 Quantum Interference 1

1.2 Coherent Control of Quantum Interference 2

1.3 Floquet Engineering for Coherent Control 3

1.4 Atom-Optics System for Kicked Rotor and Quantum Engineering . . . 4

1.4.1 Bose-Einstein Condensate 5

1.4.2 Anderson Localization in BEC System: Destructive Quantum Interference 6

1.4.3 Dynamical Localization in Quantum Kicked Rotor 7

1.4.4 Ultra-cold Atoms in Optical Lattices:Quantum Simulator 10

1.4.5 Precision Measurement: Atom Interferometer as Quantum Sensor 12

1.4.6 Quantum Computation in Atom-optics System 13

1.5 Motivation and Objective of the Thesis 14

1.5.1 Motivation 14
1.5.2 Objective 15
1.6 Organization of the Thesis 17

2 The Classical and Quantum Kicked Rotor **19**
2.1 Hamiltonian for the Kicked Rotor 19
2.2 The Classical Kicked Rotor and Phase Space 20
2.2.1 The Classical Diffusion and It's Manipulation in Phase-Space . 21
2.3 Quantum Kicked Rotor 22
2.3.1 Floquet Analysis and Floquet Engineering 23
2.3.2 Quantum Resonance and Quantum Anti-resonance 26
2.3.3 Dynamical Localization in Quantum Kicked Rotor System . . . 30
2.3.4 Coherent Control of Quantum Chaos 32
2.3.5 Anderson Localization vs Dynamical Localization 33
2.4 Quantum Kicked Rotor in Moving Frame of Reference 35
2.4.1 Micromotion in Bose-Einstein Condensates 36
2.4.2 Asymmetric Dynamical Localization 37
2.4.3 Numerical Simulations 38
2.5 Conclusions 38

3 Experimental Setup **41**
3.1 Laser Cooling and Trapping 41
3.2 Scattering Force 42
3.2.1 Zeeman Slower 43
3.3 Magneto-Optical Trap 44
3.4 Dipole Trap and It's Evaporation 46
3.4.1 Machine Learning for Production of BEC and Pulse-Width Modulation for Evaporative Cooling 49
3.5 BEC Machine 50
3.5.1 Experiments with BEC Machine in Our Lab 50
3.6 Optical Lattice and It's Interaction with Cold Atoms 52
3.6.1 The Raman-Nath Regime 53

3.6.2 The Bragg Regime 54
3.7 Conclusions 56

4 Demonstration of Coherent Control of Dynamical Localization in Quantum Chaotic System 57
4.1 Background and Definition of the Problem 58
4.2 Modified Atom-Optics Kicked Rotor 59
4.3 Atom-Optics Experimental Setup 66
4.4 Evolution of Mean Energy 67
4.4.1 $M = 2$ case 69
4.4.2 case of $M > 2$ 72
4.5 Conclusions 74

5 A single Knob Coherent Control of Dynamical Localization 77
5.1 Theory and Scheme for Single Knob Coherent Control 77
5.2 Demonstration of Single Knob Coherent Control of Dynamical Localization 79
5.2.1 Coherent Control by Preparing Different Initial State 80
5.2.2 Coherent Control of Dynamically Localized State 82
5.3 Conclusions 84

6 Asymmetric Dynamical Localization and Precision Measurement of the Micromotion of a Bose-Einstein Condensate 85
6.1 Background and Definition of the Problem 86
6.2 QKR in Moving Frame of Reference 87
6.3 Experimental Setup for QKR 91
6.4 Asymmetric Dynamical Localization in Moving Frame of Reference . . 92
6.5 Measurement of Early Time Dynamics 96
6.6 Measurement of Micromotion of BEC 97
6.7 Conclusion 99

7 Conclusion and Future Outlook 101
7.1 Summary 101

7.2 Future Outlook: 103

List of Figures

1.1 **Coherent control**. A simple illustration of coherent control. Similar to the use of a musical instrument for producing a desired music. 2

1.2 **Floquet engineering**. The concept of Floquet engineering: random delta perturbations sandwiching free evolution, that is used as a control parameter with the corresponding Floquet operator. 4

1.3 **BEC in our lab**: Images show the transition from a thermal state to a Bose-Einstein Condensate (BEC). Colormap is the optical density (OD) of the atomic cloud. 5

1.4 **Anderson localization**. Direct observation of 1D and 2D Anderson localization using BEC. A random disorder can be seen as blue color in 1D and as spikes in 2D. 7

1.5 **Dynamical localization**. The left image shows the dynamical localization with periodic kicks and the right image shows the diffusive nature with random kicks. 9

2.1 **Phase space**. Classical Phase space for stochastic parameters $K = 0.97$ and $K = 5$ 20

2.2 **Modified phase space**. A moving island is generated by an appropriate phase modulation for $K \approx 3$. 21

2.3 **Modified phase space**. (a) Standard phase space (b) Transporting island by change of sign of parameter K to -K after every 2 kick (c) Very small transporting island (not visible) in case of a modulation after every 3 kick, in all cases, $K = 5$. 22
2.4 **Experimental schematic for QKR**. A periodically kicked cloud of cold atoms with standing wave for experimental realization of quantum kicked rotor. The periodic turning on and turning off of the optical lattice acts like strong periodic perturbations-leading to application of kicks 24
2.5 **Resonance in QKR**. Quadratic energy growth at resonance and the momentum distribution after 40 kicks 28
2.6 **Anti-resonance in QKR**. A energy growth showing the revival after even number of kicks and the distribution after 40 kicks. 29
2.7 **Dynamical localization in QKR**: Energy growth for K = 5.5 exhibiting the characteristics of dynamical localization, with an inset showing an exponentially localized momentum distribution after 1000 kicks. 31
2.8 **Coherent control of DL**. A simple illustration demonstrating the concept of coherent control of quantum chaos. 32
2.9 **Anderson vs dynamical localization** . A graphical representation of Anderson and dynamical localization 34

3.1 **Energy level diagram**. A schematic representation of the energy level diagram for the D2 line of ^{87}Rb, featuring cooling and repumping lasers alongside the Zeeman slower (ZS). The spectroscopy signal from saturation absorption spectroscopy is also shown, illustrating its role in stabilizing the laser. 44
3.2 **MOT**. **(Left)** Working principle of MOT. **(Right)** Schematic for confining atoms using six laser beams. The blue square in the middle of the laser beams is the glass cell maintaining UHV. 45
3.3 **Schematic of the dipole trap**. **(Left)** Tightly focussed crossed dipole trap in glass cell. **(Right)** An absorption image of atoms captured in this trap 47

3.4 **Evaporative cooling**. **(Left)** Lowering potential adiabatically for evaporation. **(Right)** A transition to BEC 48

3.5 **Experimental sequence**. A general overview of the steps involve in production of BEC 51

3.6 **Experimental setup**. BEC machine and a bright ^{87}Rb MOT 52

3.7 **Diffraction of a BEC in different momentum states**. Diffraction of BEC with a pulsed optical lattice ^{87}Rb MOT 54

3.8 **Bragg Diffraction**. Bragg Diffraction of ^{87}Rb BEC between $0\hbar k$ and $2\hbar k$ with pulsed optical lattice 55

4.1 **Phase portraits and classical energy growth**. Phase portrait's of the standard ($M = 0$) and modified kicked rotor ($M > 0$). The parameters are kick strength $K = 5$ and (a) $M = 0$, (b) $M = 2$ and (c) $M = 3$. The regular islands in the chaotic sea in (a) are non-transporting whereas those in (b) are transporting in nature, albeit much smaller in size. The inset in (b) shows an enlarged view of one of these islands. No regular structures are visible in (c). The classical energy $\langle E \rangle_c$ growth for various vales of M at $K = 5$ is shown in (d). 62

4.2 **Kicking scheme and quantum energy growth**. (a) Pulse scheme for the regular and modified kicked rotor at $k = 5$ and $\hbar_{eff} = 1$ ($K = 5$). For $M = 2$, the sign of K is flipped alternatively. (b) Simulated energy evolution of KR (dashed line) and MKR with $M = 2$ (solid line). The quantum energy $\langle E \rangle_q$ for $M = 2$ localizes at a higher energy. Inset plots (in a semi-log scale) the momentum distribution of for the same at $t = 1000$. 64

4.3 **Standing wave and lattice laser**. The left image is showing the optical lattice formed by two counter propagating laser beam and diffraction of the atoms. The right image is showing the lattice laser frequency and it's detuning from atoms energy level 67

4.4 **Kicking scheme of MKR and mean energy growth**. (a) Kicking scheme for MAKR with $M = 2, 3, 4$. This scheme also shows the delay time T_d. (b) Mean quantum energy $\langle E \rangle_q$ evolution for different values of M at $K = 5$ and $\hbar_{\text{eff}} = 1$. The solid lines and markers indicate the numerical simulation and the experimental data respectively. 68

4.5 **Momentum distribution and absorption image**. (a) Momentum distribution profiles for $M = 0, 2, 3$ and 4 at the parameters $K = 5$ and $\hbar_{\text{eff}} = 1$. The markers and solid lines denote experimental and simulated momentum profiles respectively. $M = 2$ clearly shows enhanced localization length. (b) Absorption images for different values of M with $\hbar_{\text{eff}} = 1$ and $K = 5$. 70

4.6 **Calculation of IPR**. IPR for experimental data as a function of M for different values of $\hbar_{\text{eff}}$ while maintaining the kick strength constant at $K = 5$. Errors bars for experimental data lie within the marker, hence, they are not shown here. 73

5.1 **Pulse scheme**. Kick sequence for single knob coherent control 78

5.2 **Simulation result**. (a) The normalized population of the zeroth momentum state $f(0)$ is shown as a function of T' over an extended range (0-4π) after 60 kicks (b) Shows the actual control regime which lies in the π to 2π region or 0 to π region. Maximum population is when this time gap matches with periodic kick. 80

5.3 **Experimental results**. (a) The normalized population of the zeroth momentum state $f(0)$ is shown as s function of applied kicks, showing the feature of dynamical localization. (b) Demonstration of coherent control by varying single knob T' 81

5.4 **Localized distribution**. Momentum distribution profile after 60 kick by varying the control knob from π to 2π. It clearly shows the control enhancement of localization length. 81

5.5 **Kicking sequence**. A pulse scheme for control over localized wavefunction 82

5.6 **Simulation result**. (a) The normalized population of the zeroth momentum state $f(0)$ is shown as a function of T' (b) Actual control regime which lies in the π to 2π region. Maximum population is when this time gap matches with periodic kick. 83

5.7 **Experiment result**. (a) The normalized population of the zeroth momentum state $f(0)$ is shown as a function of T' over an extended range (0-4π) after 60 kick, (b) It is showing the actual control regime which lie in π to 2π region or 0 to π region. Maximum population is when this time gap matches with periodic kick 83

6.1 This experimental schematic shows the moving BEC (left side) with velocity v and periodically kicked 1D optical lattice. This relative motion between BEC and lattice provides asymmetry in momentum distribution which we quantify by measuring $\langle p \rangle$. Same asymmetry with opposite nature arises when lattice is in motion, shown in right side. Micromotion is measured by scanning lattice velocity (see Fig. 6.5 for details). Further, dynamical localization sets in for larger number of kicks. . . . 89

6.2 Wavefunction profile for different launch velocity shown at 30, 40 and 50 kicks. In all the cases, dynamical localization has set in for initial velocity corresponds to momenta (a) $0\hbar k/M_{Rb}$, (b) $2\hbar k/M_{Rb}$, and (c) $4\hbar k/M_{Rb}$. In all cases, in left side, symbols are obtained experimental data. In right side, symbols are obtained from kicked rotor simulations with 50 kicks. 93

6.3 Dynamically localization for three different lattice velocity: (a) $\hbar k/M_{Rb}$, (b) $2\hbar k/M_{Rb}$ and (c) $4\hbar k/M_{Rb}$. (left side) experimental data shown as symbols for three different kick numbers, (right side) simulation results shown as symbols at 70th kick. 95

6.4 Oscillatory behavior of $\langle p \rangle$ as a function of lattice velocity. In this experiment, $\langle p \rangle$ is measured after two kicks 97

6.5 Measured $\langle p \rangle$ as a function of lattice velocity by changing the frequency difference α for two different time delays. Micromotion of BEC is measured by scanning over a range of lattice velocity. See text for details. . 98

Chapter 1

Introduction

This chapter begins by explaining the importance of studying quantum systems in atom-optics, starting with a definition of quantum interference. It then reviews existing literature in this area. Following this background, the chapter outlines goals and plans in thesis. The chapter closes with a summary, giving an overview of what follows in the later chapters.

1.1 Quantum Interference

Quantum interference is a phenomenon when wave-functions associated with different quantum states or paths interfere with each other. This interference of wave-functions can be constructive or destructive, leading to an increased probability of a particular outcome, or a decreased probability of an outcome respectively. Quantum interference occurs when quantum particles, such as photons, electrons, atoms, and even molecules that exhibit wave-like behavior and interfere with each other, leading to either constructive or destructive interference patterns. Quantum interference is different from classical interference mainly due to properties in higher-order correlation functions, especially the second-order correlation function [1]. This function, either in spatial or temporal aspects, reveals distinctions between quantum (non-classical) and classical interference.

1.2 Coherent Control of Quantum Interference

Coherent control over quantum interference is a very fascinating and active experimental and theoretical research [2]. Control over quantum interference is one of the pivots of quantum technology, enabling the manipulation and utilization of quantum phenomena for practical applications [3, 4]. Achieving control over this interference is essential for quantum information processing, quantum communication, quantum sensing and for studying fundamental physics. Researchers are developing innovative techniques and pulse schemes to precisely manipulate the quantum states of particles, allowing for desired outcomes. This control is crucial for the implementation of quantum algorithms, quantum communication protocols like quantum key distribution, and the development of ultra-sensitive quantum sensors. As advancements in quantum technology continue, mastering control over quantum interference promises to unlock unprecedented capabilities having far-reaching implications in fields ranging from computing to secure communication and sensing. The different quantum evolution pathways can lead a quantum system from the same initial to different desired final states [5], this quantum interference between the routes leads to enhancement or suppression of the transition. Consider

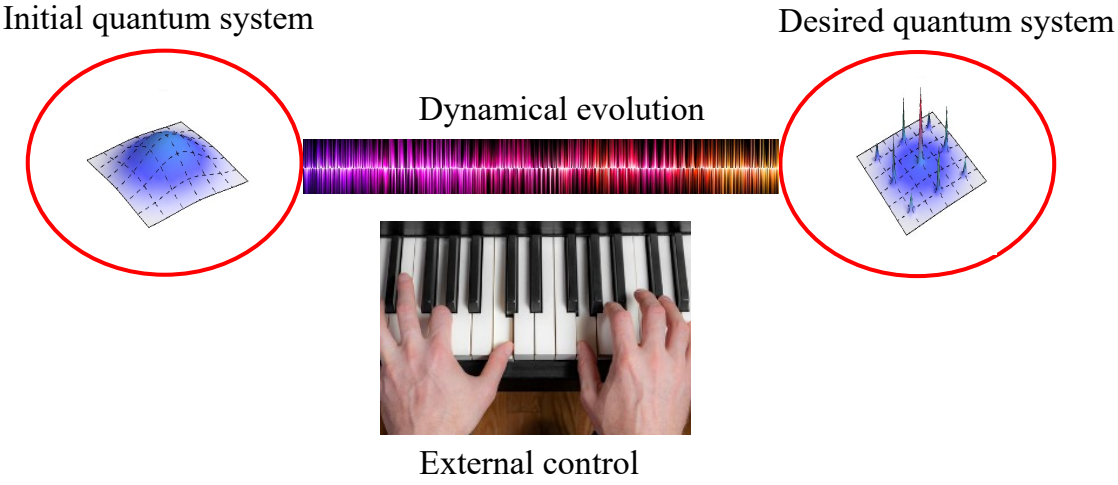

Figure 1.1: Coherent control. A simple illustration of coherent control. Similar to the use of a musical instrument for producing a desired music.

a quantum system with multiple pathways to reach different states. Coherent control involves skillfully manipulating the phases and amplitudes of these pathways (a simple

illustration in the Fig. 1.1), much like adjusting the settings on a musical instrument to produce a desired sound wave. By precisely tuning the phases of quantum interference pathways, one can control the system to end up in a particular state, essentially forcing the quantum dynamics to favor a predefined target state. This complex manipulation of interference forms the core of coherent control, offering a powerful means to guide and shape quantum outcomes.

1.3 Floquet Engineering for Coherent Control

Floquet engineering in the context of quantum systems refers to the deliberate manipulation of periodic time-dependent Hamiltonian to achieve specific target objectives. Coherent control using Floquet engineering involves tailoring the properties of a quantum system during the evolution by playing with the dynamical phase evolution. Identifying the optimal form of an external control to effectively alter a system's properties for a preferential target behavior can also be expressed as an optimal control problem [6]. The basic idea for Floquet engineering comes from Floquet theory. As we know Floquet theory provides the solutions for time-dependent Schrodinger equation for a time-periodic Hamiltonian [7]. For a time-periodic Hamiltonian, a single driving frequency provides a straightforward solution and it's numerically easier.

But, if a system is driven by multiple frequencies, along with other parameters being variable, the number of possibilities of outcomes explodes and the probability of different outcomes increases. Solving such a system analytically and numerically is challenging, as huge parameter space is required to consider variables and frequencies. However, this difficulty can be overcome if we use some controllable quantum system by exactly spanning the parameter space. The external control over parameters and direct measurement with different evolution makes it faster and robust. This concept is known as a quantum simulator [8]. Various quantum systems, including neutral atoms, ions, molecules, electrons in semiconductors, superconducting circuits, NMR, and photons, have been suggested as candidates for quantum simulators.

Let's consider a straightforward example known as a periodically kicked quantum system. In the case of periodic kicks, the dynamics of the system can be precisely understood and mostly solved using Floquet theory, resulting in a predictable outcome.

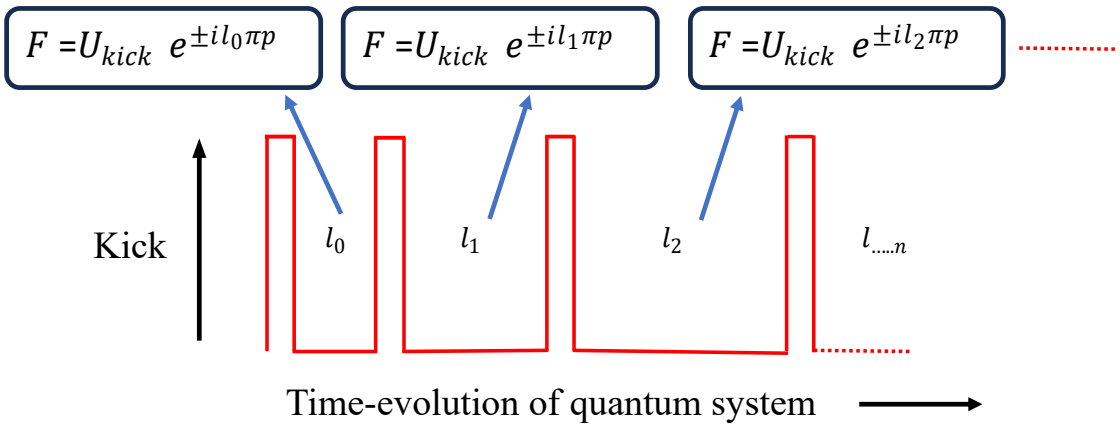

Figure 1.2: Floquet engineering. The concept of Floquet engineering: random delta perturbations sandwiching free evolution, that is used as a control parameter with the corresponding Floquet operator.

Now, let's extend this concept to a system that allows for variable control over the time gap between kicks as shown in Fig. 1.2. Here $l_0, l_1, ...l_n$ are free parameters. The time gap serves as a control parameter for dynamical phases, introducing more flexibility in manipulating the quantum system to get desired output. The dynamics of the system is essentially governed by the one step Floquet operator which is an ordered product of the free evolution operator and the kick operator. The system complexity will grow if we consider the strength of the kicks as a variable and extending system from 1-dimension to higher dimensions.

In summary, Floquet engineering for coherent control entails purposefully manipulating quantum systems through external control. The key condition for coherent manipulation is to attain the desired target state without introducing decoherence into the system [9]. Such approach allows researchers to harness the principles of quantum mechanics for specific applications, making it a valuable tool in the field of quantum science and technology.

1.4 Atom-Optics System for Kicked Rotor and Quantum Engineering

An atom-optics system refers to the experimental and theoretical exploration of the interaction between matter waves and photons, typically in the form of laser-cooled

atoms [10] and optical elements such as laser beams. This active field lies at the intersection of atomic physics and optics, and it has led to a variety of exciting developments in both fundamental physics and practical applications. Particularly this field explores the wave-like properties of matter, specifically focusing on the manipulation and control of atomic matter waves [11–13]. Drawing inspiration from traditional optics that deals with light waves, atom optics extends these principles to matter waves, treating atoms as quantum particles with both particle and wave characteristics.

1.4.1 Bose-Einstein Condensate

The journey into the ultra-cold regime begins with the formation of a Bose-Einstein Condensate (BEC), a remarkable state of matter predicted by Satyendra Nath Bose [14] and Albert Einstein [15] in the early 20th century. In 1995, through advanced cooling techniques such as laser cooling and evaporative cooling, a BEC was created by Eric Cornell and Carl Wieman of the University of Colorado, Boulder using rubidium atoms [16]; later that year, Wolfgang Ketterle of MIT produced a BEC using sodium atoms [17]. In 2001 Cornell, Wieman, and Ketterle shared the Nobel Prize in Physics “for the

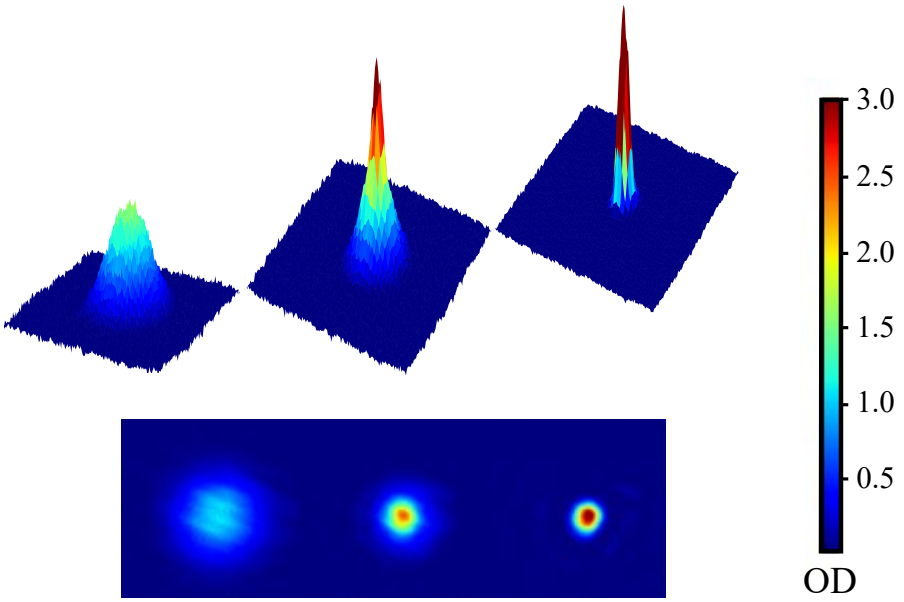

Figure 1.3: BEC in our lab: Images show the transition from a thermal state to a Bose-Einstein Condensate (BEC). Colormap is the optical density (OD) of the atomic cloud.

achievement of Bose-Einstein condensation in dilute gases of alkali atoms, and for early

fundamental studies of the properties of the condensates". A transition to BEC is shown in Fig. 1.3. This macroscopic coherence endows BEC with remarkable properties, including long-range phase coherence, wave-like behavior, and sensitivity to external fields at the quantum scale [18]. The lowest temperature achieved for a BEC is just 38 pico kelvins (pK) away from absolute zero [19].

The study of ultra-cold atoms provides a unique playground for investigating quantum phenomena that were once confined to theoretical realms. This includes the observation of super-fluidity [20], critical quantum interference [21], and the exploration of exotic quantum states such as, spinor BEC [22, 23], Vortices [24, 25], solitons, interactive BEC etc. In atom-optics systems, a Bose-Einstein Condensate (BEC) plays a major role due to its various applications. BEC is used for precision measurements, quantum simulations of complex condensed matter systems, Anderson localization, and dynamical localization. Additionally, it contributes to the exploration of fundamental physics, such as black holes and dark matter [26]. I will go into the observation of Anderson localization with BEC and its analogs, particularly emphasizing dynamical localization in quantum kicked rotor, which is relevant to this thesis.

1.4.2 Anderson Localization in BEC System: Destructive Quantum Interference

Localization of electronic wave-function in disordered crystals was first proposed by Anderson in 1958 [27]. According to Anderson's theory of Localization, electron wave-function in a disorder go through quantum reflections and the interference of all these reflections causes the localization of wave-function. In Anderson's influential paper, he showed that under sufficiently strong disorder, the localization of states would occur irrespective of the dimensionality of the system (denoted by 'D'). Notably, the article primarily focused on the phenomenon of localization, while aspects related to delocalization and critical behavior were not extensively explored or analyzed. For the dimension D=1 and D=2, localization will always happen no matter how small the disorder is, it just needs to be finite [28–30]. The first direct observation of Anderson localization in 1D system was demonstrated in an Atom-optics system using BEC and random disorder made by a laser [31] shown in Fig. 1.4. A very recent observation of

2D-Anderson localization has been demonstrated with BEC using complex optics for making 2D random potential [32], also shown in Fig. 1.4. 3D-Anderson localization shows a transition from localized state to a diffusive state with increasing strength of the disorder. It shows a phase transition from insulator (localized state) to metal (diffusive state) and it's called Anderson insulator-metal transition. Direct observation of Anderson insulator-metal transition is experimentally challenging and has not yet been observed in such a system [33, 34].

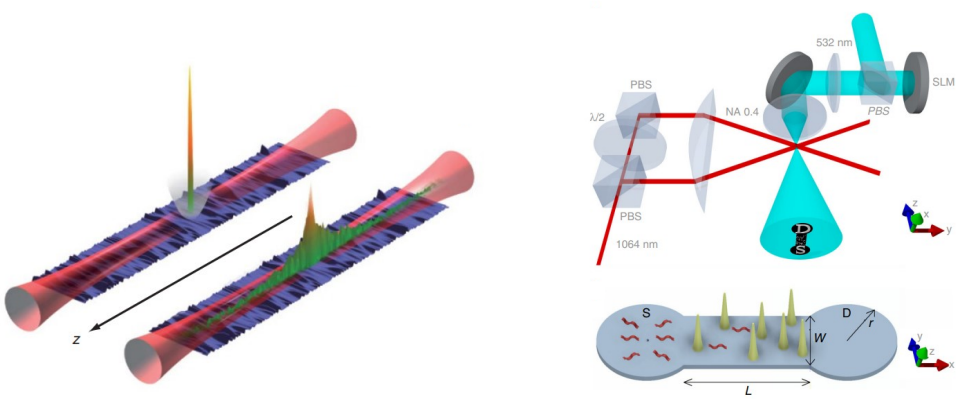

1D 2D

Figure 1.4: Anderson localization. Direct observation of 1D and 2D Anderson localization using BEC. A random disorder can be seen as blue color in 1D and as spikes in 2D.

1.4.3 Dynamical Localization in Quantum Kicked Rotor

The majority of phenomena explained by quantum mechanics are connected to either interference or the closely associated concept of coherence [1, 35, 36]. This is particularly evident in the realm of quantum optics, which investigates and applies the interactions between light and matter at the quantum level. Here, in an atom-optics based kicked rotor, basically in laser cooled atoms, a coherent cloud of atoms is manipulated through laser light to study the interference of matter waves and their dynamics [9, 37, 38]. The quantum kicked rotor system is a great tool to study dynamical localization [39–41], control over quantum system [5, 42–44] and quantum chaos [45–47].

Hamiltonian for this simple system is:

$$\hat{H} = \frac{\hat{p}^2}{2} + K\cos(\hat{x})\sum_{n=1}^{N}\delta(t-n)\ , \tag{1.1}$$

K is related with the strength of the kick and $t \to t/T$ is scaled, where T is the period (more details in next chapter). Now the coordinate to describe dynamics, like position can be described by the angle x (defined by modulo 2π) and the associated momentum p. Although, it is a strictly deterministic Hamiltonian system, it shows chaotic motion beyond certain range of parameters. Controlling the chaos with modulation of an external parameter, makes this Hamiltonian system a popular system for studying chaos in classical and quantum regime. When we apply a periodic kick to an initial wave-function of atoms, after a certain number of kicks, the energy growth of the system freezes and the system becomes dynamically localized in momentum space. It is analogues to Anderson localization in position space [48]. Observation of dynamical localization [49–52] analogue to Anderson localization and Anderson metal-insulator transition in 3D [53–55] has drawn much attention to study the localization in this system. Quantum kicked rotor (QKR) system can be realized with cloud of laser cooled atoms or a BEC subjected to periodic pulsing of an optical lattice [56]. Further investigations in this field are the study from a state of dynamical localization (where energy becomes frozen) to a delocalized state characterized by diffusive energy growth.This transition has been observed through the introduction of various forms of noise, such as variations of kick strength [57], phase noise [58], or introducing spontaneous emission in the system [59]. All such systems shows an exponential loss of coherence in quantum system, also a non-exponential loss of coherence has been studied theoretically [60] and observed experimentally [56] by selected time sequence that follows a levy distribution. Most of the above mentioned experiments are done with the cloud of cold atoms.

In recent years, there has been much interest in studying a QKR with Bose-Einstein condensate [61, 62]. Very narrow initial momentum distribution of BEC is helpful in resolving different momentum eigen states. Accurate phase imprint of lattice on BEC for phase sensitive Hamiltonian, a tunable interaction for interacting quantum kicked rotor and early observations of quantum correlations in dynamics make a BEC system

great to study the localization phenomena.

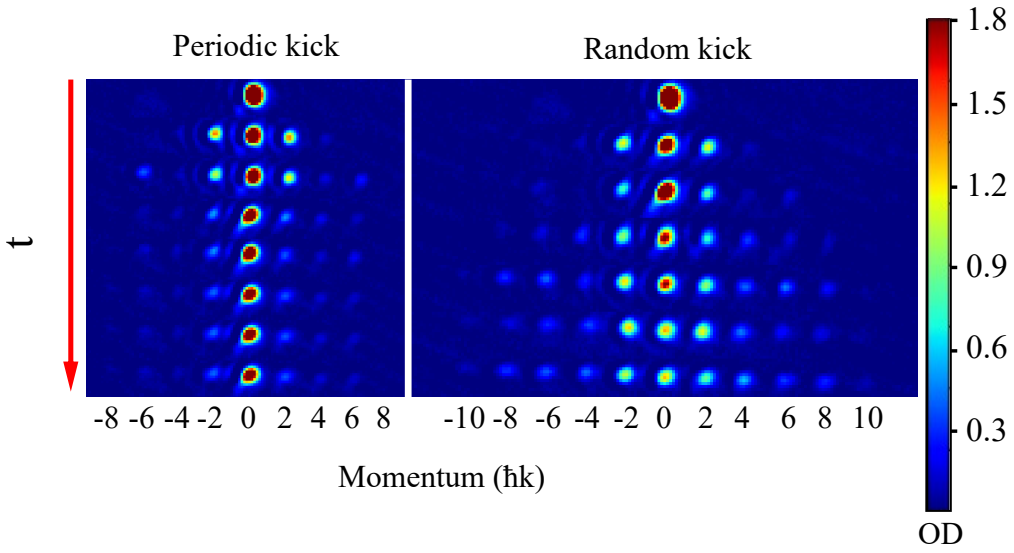

Figure 1.5: Dynamical localization. The left image shows the dynamical localization with periodic kicks and the right image shows the diffusive nature with random kicks.

For a example, see the Fig. 1.5 right image, it shows the Dynamical Localization (DL) with periodic kicks on a BEC. The left image shows the exponential loss of coherence and diffusive behavior by applying random kick (not periodic). BEC based QKR system provides the tunable interaction between the atoms by Feshbach resonance and interaction effect on dynamical localization. The effect of interaction on DL is recently observed in BEC based system [63,64]. It shows that Interaction driven dynamically localized to delocalized state are sub-diffusive in nature and this behavior is not classical chaos but quantum anomalous diffusion. Further imprinting the phase of the lattice on BEC also provides the different type of effect like on resonance quantum ratchet [65,66] and quantum boomerang effect (QBE) [67–69]. On resonance quantum ratchets can be controlled by preparing different initial superposition state of BEC and the phase difference [70]. Atomic current in such quantum ratchets is completely phase dependent between superposition states. Similarly in the QBE, the time-parity reversal symmetry determines the presence or absence of QBE in localized system [68, 71]. QBE also describes the quantum nature of dynamical localization in highly disordered system. BEC based QKR system also has been utilized in coupled quantum rotors [61] where two incommensurate optical lattices drive a quantum to classical transition by breaking dy-

namical localization and the emergence of classical diffusion. Very narrow momentum width of BEC also shows early time quantum diffusion because of strong quantum correlation in time evolution [72]. A discrete time quantum walk has been also observed in BEC based quantum kicked rotor [44]. Numerous studies have explored dynamical localization and its breakdown in the quantum kicked rotor, but coherent control of dynamical localization without disruption has received limited attention. As dynamical localization relies on destructive quantum interference, achieving control necessitates manipulating this interference. Theoretical proposals for controlling quantum chaos exist [5, 73], but experimental implementation is challenging. Given the classical chaos of the quantum kicked rotor, coherent control must be meticulously engineered using external parameters to prevent the system from behaving classically. The main focus of this thesis is to delve into this challenge, discussing coherent control over dynamical localization without disruption, in subsequent chapters.

1.4.4 Ultra-cold Atoms in Optical Lattices:Quantum Simulator

Ultra-cold atoms trapped in optical lattices represent a powerful and versatile platform for quantum simulation [8], an approach that harnesses one quantum system to emulate the behavior of another. This emerging field has huge potential to address complex quantum many-body problems, simulate condensed matter phenomena, and uncover novel insights into fundamental physics [74]. In this context, ultra-cold atoms confined in optical lattices serve as quantum simulators, offering unprecedented control over parameters and enabling the emulation of diverse quantum systems in a highly controllable environment [75, 76]. Let's take a simple example of the Bose-Hubbard model,

$$\hat{H}_{\text{BH}} = -J \sum_{\langle i,j \rangle} (\hat{a}_i^\dagger \hat{a}_j) + \frac{U}{2} \sum_i \hat{n}_i(\hat{n}_i - 1) - \mu \sum_i \hat{n}_i, \tag{1.2}$$

Here, $a_i^\dagger$ and a_j are the creation and annihilation operators, respectively, at the i-th site, and $\hat{n}_i(\hat{n}_i - 1)$ represents the number operator at the i-th site. J is the hopping parameter for nearest neighbor, it describes the kinetic energy, U is on-site potential and μ is the chemical potential [77]. To mimic this Hamiltonian in an atom-optics system, optical lattices are formed by superimposing laser beams to create a periodic potentials

that traps ultra-cold atoms. The resulting lattice structure mimics the periodicity found in crystalline solids, allowing researchers to investigate quantum phenomena associated with Bose-Hubbard model. When $U/J \ll 1$, the system exhibits a super-fluid state, characterized by the dominance of kinetic energy over interaction energy. This occurs when the strength of interactions (U) is much smaller compared to the hopping parameter (J), and a Bose-Einstein Condensate (BEC) in a 3D optical lattice displays coherent flow without significant localization. Conversely, in the limit $U/J \gg 1$, achieved by adiabatically increasing the lattice depth, the system undergoes a transition to a Mott insulator phase. Here, strong interactions prevail over kinetic energy, leading to localized atoms with a fixed number at each lattice site. In this phase, phase uncertainty is high, causing a blurred interference pattern due to overlapping wave-packets from different sites during free evolution. This contrasts with the super-fluid state, where phase correlations result in a well-defined interference pattern under similar conditions. It was first realized by the I. Bloch group [78]. Super-fluid to mott-insulator transition has extensively studied till single atomic level [79–81]. Furthermore, BEC loaded into a 1D optical lattice also provide a great opportunity to study periodically driven Hamiltonian. This platform is suitable for simulating tunneling and transport phenomena, as well as shortcuts to adiabaticity for quantum optimal control and optimal Floquet engineering [82, 83].

One more advancement in quantum simulator is the momentum-space lattice based on ultra-cold atoms and multiple Bragg diffraction, first proposed by B. Gadway in this paper [13, 84]. Arbitrary control over phases on each lattice site and individual hopping parameters make the momentum-space lattice a great tool for simulating the Bose-Hubbard model and exploring new topological materials. Momentum-space lattice are based on multiple Bragg diffraction [85], each Bragg diffraction provide one momentum synthesize lattice point and by using many Bragg diffraction, one can form many lattices point. The phase and Rabi oscillation of each Bragg diffraction gives control over phases and hopping parameter over individual lattice sites. Momentum-space lattice is robust and easy to construct in ultra-cold atoms. In this field, most of the experiment is done by Gadway group. Their observation reveals the topological soliton state in the Su-Schrieffer-Heeger model [86], Anderson insulator transition [87], Non-linear

transport, generalized Aubry-Andre model [88] and other phenomena related to tight binding model can be simulated.

1.4.5 Precision Measurement: Atom Interferometer as Quantum Sensor

Laser-cooled atoms represent a groundbreaking advancement in precision measurement technologies [89]. The precise control over atomic motion allows for unprecedented levels of accuracy in measurements, particularly in the realm of atom interferometer, timekeeping and frequency standards. The ability to manipulate and study ultra-cold atoms paves the way for improved atomic clocks, gravimeters, and other high-precision instruments that are vital for a diverse range of scientific and technological applications. This remarkable precision, contributing to advancements in fields like metrology and fundamental physics.

Atom interferometry is one of the application for precision measurement using laser cooled atoms. As we know that wave-like properties of matter emerges as we go down in temperature, like the light. Atoms, unlike light, are massive so theoretically, the atom interferometer sensitivity is about 10 orders of magnitude larger than the optical interferometer due to the mass of the interfering atoms compared to photons [90]. For a simple understanding of an atom interferometry, first we will go through the optical interferometer. In optical interferometry, first we split the laser beam for two different path, light waves travel separate paths. Depending on the phase accumulation along the two paths, either the light interferes constructively and gives a bright fringe or may interfere destructively giving a dark fringe. In atom interferometry, atoms are laser-cooled to just 100 nK away from absolute zero temperature. After the creation of matter wave with laser cooling, one uses laser light to coherently manipulate the atoms. By manipulating the state of the atoms, either in different momentum state through Bragg diffraction [91] or in different internal state with Raman transition [92], one can split, reflect and recombine the matter waves similar to light waves. Before the measurement, atoms will be in superposition of the two states.

Phase associated with the matter waves in an atom interferometer is given by [93]:

$$\Phi = n(\phi_1 - 2\phi_2 + \phi_3) = 2n\mathbf{k} \cdot \mathbf{g}T^2, \tag{1.3}$$

where n is the order of diffraction in Bragg case. Φ is total phase gathered during interferometer. T is interferogram time, $\mathbf{k}$ and $\mathbf{g}$ are wave-vector and gravity respectively. The fundamental concept of measuring gravity is to balance the phase difference imparted on the atoms by gravitational acceleration. As freely falling atoms experience a time-dependent Doppler shift for the laser beam, by chirping the laser frequency to balance the Doppler shift [94]. The overall phase shift can be obtained by scanning the lattice acceleration around the local gravity, which becomes:

$$\Phi = n(2\mathbf{k} \cdot \mathbf{g} - 2\pi\alpha)T^2, \tag{1.4}$$

where α is sweep rate. To determine the value of $\mathbf{g}$, the value of α (say, $\alpha 0$) will balance the gravity, and the overall phase shift Φ will be zero, thus providing $\alpha 0 = \frac{1}{\pi(\mathbf{k}\cdot\mathbf{g})}$. To determine the value of $\alpha 0$, one has to observe the interferometric signal for at least three different interferogram time (T), and all those interferometric signals have a common minima at $\alpha 0$ [95]. The technological advancement of the quantum gravimeter is mature enough for field operations now, achieving a sensitivity of $50\,\mu\text{Gal}/\sqrt{\text{Hz}}$, with a measurement frequency of 2 Hz. One such system is commercially available from Muquans SAS.

1.4.6 Quantum Computation in Atom-optics System

To build a viable quantum processor, researchers are exploring diverse physical platforms [96, 97]. Among these, manipulating arrays of single neutral atoms with light beams [98] emerges as a potent and scalable technology for quantum registers, accommodating up to several thousand qubits possibilities [99]. Each qubit is encoded in the two electronic states of an atoms [100]. The key advantage of a neutral atom quantum processor lies in the inherent uniformity of these atoms, in contrast to artificial atoms like superconducting circuits or Silicon spin qubits that demand meticulous manufacturing for minimal heterogeneity. This intrinsic uniformity offers a notable advantage,

enhancing the potential for achieving low error rates during computations. Neutral atom devices also present advantages such as extensive connectivity [101], flexible and dynamically re-configurable architecture and the native ability to implement multi-qubit gates [98].

In neutral atoms based quantum computing, the advantage of controlling the interaction strength between the atoms with the help of Rydberg atoms. Rydberg atoms are like super excited atoms, reaching really high excited states with principle quantum numbers as high as 100 [102]. These states are characterized by electrons orbiting the nucleus at a much greater distance than in lower energy states. Named after Swedish physicist Johannes Rydberg, who extensively studied the spectral lines of hydrogen, Rydberg atoms exhibit unique and intriguing properties. The large principal quantum number of Rydberg atoms, which determines the size of their orbit. This leads to an enormous atomic size, making these atoms highly sensitive to external electric and magnetic fields. The long-range interactions between Rydberg atoms enables the creation of exotic quantum phenomena, such as Rydberg blockade [103] and Rydberg dressing [104]. Rydberg blockade occurs when the excitation of one Rydberg atom prevents the excitation of neighboring atoms, paving the way for applications in quantum computing and quantum simulation [98]. Rydberg dressing involves modifying the atomic energy levels through external fields, offering opportunities for engineering new quantum states and enhancing control over atomic interactions. The current state of the art two qubit gate fidelity is 99.5% on 60 neutral atom qubit [101]. Neutral atom based quantum simulators are also leading in the field [8]. A significant industrial effort is underway in the field of neutral atom quantum computers and simulators, with notable contributions from companies such as QUERA, Pasqal, and Atom Computing.

1.5 Motivation and Objective of the Thesis

1.5.1 Motivation

As discussed earlier, numerous experimental and theoretical studies have been conducted on dynamical localization and its destruction in the quantum kicked rotor. However, coherent control of dynamical localization without its destruction has received

relatively limited attention. Since dynamical localization is a phenomenon rooted in destructive quantum interference, achieving control over dynamical localization requires the ability to manipulate and modify these quantum interference. There are few theoretical proposal for control over quantum chaos, but direct implementation in experiments are challenging. It's important to remember that since the classical counterpart of the quantum kicked rotor is entirely chaotic, any attempt at coherent control over dynamical localization in the quantum system must be carefully engineered using external control parameters. Otherwise, making adjustments during the evolution may disrupt the system, causing it to behave classically.

Quantum dynamics is also get affected by small motion, called micromotion of initial wave-function (BEC), it's not get considered often in calculations. But the effect of micromotion is inherently hidden in output of the dynamics. As micromotion plays crucial role in precision measurement and imprint unwanted offset in the result for e.g. in atom interferometry, developing a precise method to measure micromotion by observing features of the quantum kicked rotor would be a valuable tool. This motivation provides a clear ground for investigating coherent control over dynamical localization in the quantum kicked rotor system and utilizing it's feature for precision measurements sets the stage for the research that follows in the thesis.

1.5.2 Objective

One part of the present thesis focuses on addressing methods for controlling dynamical localization and delves into the underlying physics of this control, using the periodically kicked ultra-cold atoms with 1-d optical lattice. The first approach is a periodic modulation of a control parameter during entire dynamical evolution. This periodic modulation is selected in such a way that it creates a competition between quantum diffusion and dynamical localization, causing the system to localize at higher localization length and providing a control over it. Similarly, in our extended study, we introduce a simple and more intuitive method for controlling dynamical localization using only a single parameter. This single knob coherent control facilitates linear control over dynamical localization across a broad range without introducing any decoherence into the system.

Further in this thesis, we focus on the asymmetric dynamical localization and it's

stability, by launching the initial wave-function with varying velocity. The initial wave-function (BEC) is launched with varying recoil velocities within periodically kicked optical lattices. Our observations reveal an asymmetric dynamically localized profile characterized by a small initial current. We conduct our investigation in two scenarios: when the BEC is in motion within the laboratory frame and when the optical lattice is in motion in the laboratory frame. We found some interesting velocity-dependent features. Furthermore, we utilize these velocity-dependent features for quantifying the micromotion of the BEC. Our approach provides a direct measurement of the micromotion of the BEC rather than relying on a long wait time to measure the displacement on a camera sensor with the time-of-flight method, which is not reliable in the experimental setup. The micromotion velocity within a Bose-Einstein condensate (BEC) is typically around 20 to 80 times smaller than the momentum of a single-photon recoil . This velocity is orders of magnitude smaller than the mean velocity associated with the BEC temperature. Our method enables precise measurement of this micromotion velocity, unaffected by Doppler broadening coming from the BEC temperature, a common challenge in spectroscopy techniques. Accurate knowledge of micromotion is crucial in precision measurements, as it helps nullify any unknown shifts in the measurements. In short, the objectives of the thesis are as follows:

1. Interplay between quantum diffusion and localization in the atom-optics kicked rotor.

2. Single knob coherent control of dynamical localization.

3. An asymmetric localization in BEC launched with varying recoil velocity in periodically kicked optical lattice.

4. Measurement of micromotion of BEC below single recoil photon momentum by quantum kicked rotor

I also led the reconstruction of our Rb setup. The experimental apparatus used for my research underwent development and reconstruction by both myself and our team as it experienced a shutdown after the COVID pandemic. We also improved the rate

of the production of Bose-Einstein Condensate (BEC) by optimizing evaporation sequence through machine learning. However, I won't go into the details of the experimental setup. Instead, the thesis is more centered on the experiments conducted with the established and robust BEC producing setup.

1.6 Organization of the Thesis

Chapter 2 discusses the theory of classical and quantum kicked rotor, important for this thesis.

Chapter 3 presents the experimental setup used for production of laser cooled atoms and interaction with optical standing wave.

Chapter 4 reports the observation of coherent control of dynamical localization and explain the physics based on the competition between diffusion and localization.

Chapter 5 reports the single knob coherent control of quantum system and a linear control over dynamical localization.

Chapter 6 observation of an asymmetric momentum distribution by launching the BEC with a varying velocity and its utilization in the measurement of micro-motion.

Chapter 7 presents the conclusions and future outlook.

Chapter 2

The Classical and Quantum Kicked Rotor

In this chapter we will explore the classical and quantum kicked rotor. The classical kicked rotor is a simple foundational model for understanding chaotic dynamics, while its quantum counterpart dwells into the intriguing interplay between quantum mechanics and chaos theory, shedding light on the transition from classical to quantum behavior in a periodically driven system. The chapter aims to explain the key principles and highlights the distinctive features characterizing these two realms of dynamical systems.

2.1 Hamiltonian for the Kicked Rotor

The 1-d kicked rotor (KR) is a textbook model system for studying chaos in classical and quantum system [105, 106]. Lets take a very simple system, a pendulum attached to a free rigid rod, periodically kicked with certain kick strength K. Now the coordinate to describe dynamics, like position can be described by the angle x (defined by modulo 2π) and the associated momentum p, so the time dependent Hamiltonian for this system can be written as follows,

$$\hat{H} = \frac{\hat{p}^2}{2} + K\cos(\hat{x})\sum_{n=1}^{N}\delta(t-n)\,, \tag{2.1}$$

where, n is the number of kick. Although, it is a strictly deterministic Hamiltonian system, it shows chaotic motion after certain parameter range (especially K). Controlling the chaos with an external parameter makes this Hamiltonian system popular for studying chaos in classical and quantum system [39].

2.2 The Classical Kicked Rotor and Phase Space

The dynamics of the classical kicked rotor can be evaluated using the standard map:

$$p_{n+1} = p_n + K\sin(x_n)$$
$$x_{n+1} = x_n + p_{n+1}\ .$$

The map described by the equations above is commonly known as the Chirikov map [107]. These equations of motion may be slightly modified for an angular or linear kicked rotor, but the underlying physical interpretation remains the same. The dynamics of the classical kicked rotor is defined by a single stochastic parameter K. Changing the range of K gives interesting phase-space diagrams. If $K < 5$, the trajectories in the phase space are regular with well defined trajectories. For $K > 5$, the phase space becomes fully chaotic [108]. Most of the research looks into the chaotic regime where $K > 5$ for the study of classical and quantum chaos [39]. Fig. 2.1 shows the classical phase space for $K = 0.97$ and for $K = 5$.

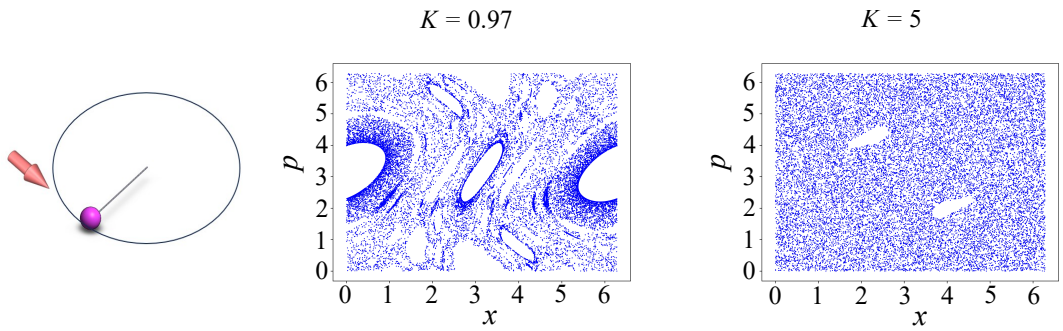

Figure 2.1: Phase space. Classical Phase space for stochastic parameters $K = 0.97$ and $K = 5$

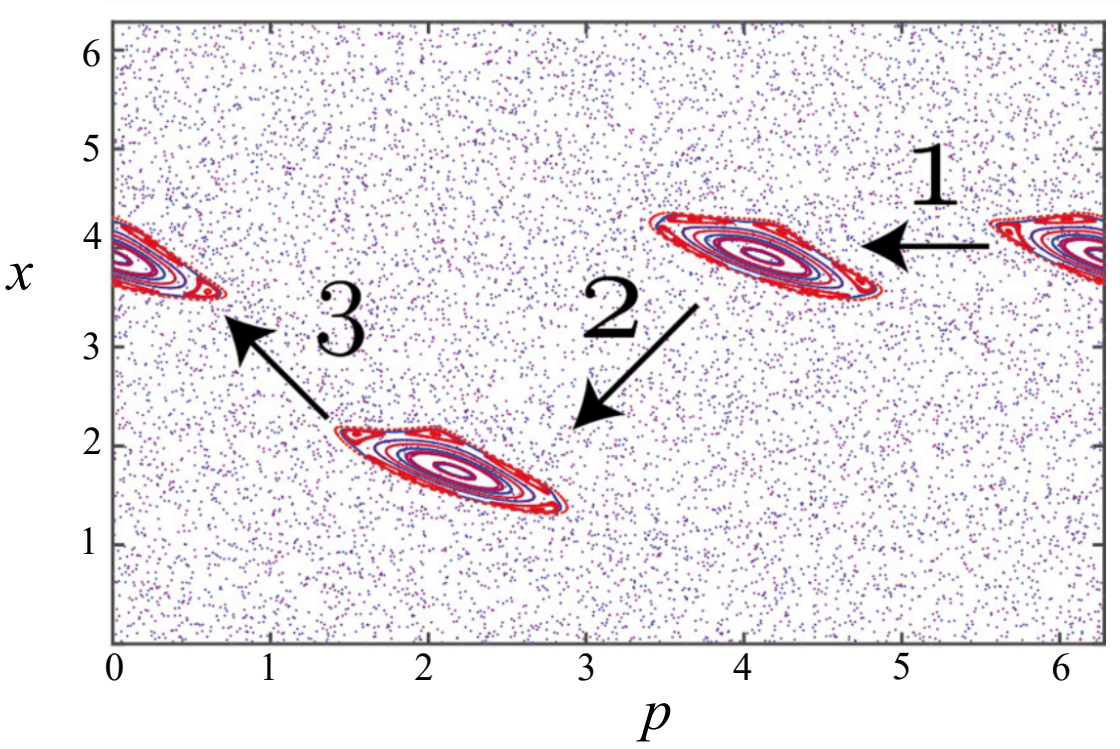

Figure 2.2: Modified phase space. A moving island is generated by an appropriate phase modulation for $K \approx 3$.

2.2.1 The Classical Diffusion and It's Manipulation in Phase-Space

In the case of fully chaotic system, the classical kicked rotor shows a random walk in momentum space, even though it's deterministic in nature. The diffusion rate, $D = K^2/2$, it only depends on the value K. The mean-square value of the momentum grows as $\langle p^2 \rangle = 2Dn$ where n is the number of kicks [108,109]. Further, average energy grows linearly with the kicks imparted on the system, $\langle E \rangle \propto n$. The growth of the average energy of the system can be controlled by manipulating the classical phase space. By manipulating the classical phase space by means of generating transporting islands or accelerators mode in chaotic phase space [110]. This can be done by modulating the phase or stochastic parameter (K) as the dynamics evolve. Here, we have shown two example of such phase space. In first case, a periodic phase change in $cos(\hat{x} + a_n)$: $a_n = \phi_n \,(\mathrm{mod}\, 3), \quad \{\phi_1, \phi_2, \phi_3\} = \{0, \frac{2\pi}{3}, 0\}$, generates a particular islands [111] as shown in Fig. 2.2. The system moves along these transporting islands faster in phase

space and helps the rapid energy growth of the system. Energy growth of this system with kicks as $\langle E \rangle \propto n^{1.3}$ and it follows the power law. The effect of this classical phase space in quantum kicked rotor is observed and well studied in reference [111]. In the second example, a change of sign of stochastic parameter K to $-K$ after every 2, 3 or 4 kicks creates transporting islands and help in faster energy growth. The corresponding classical phase space is shown in Fig. 2.3. These transporting islands are small in phase space and difficult to probe experimentally, but effect of these transporting islands can be seen in energy growth [112].

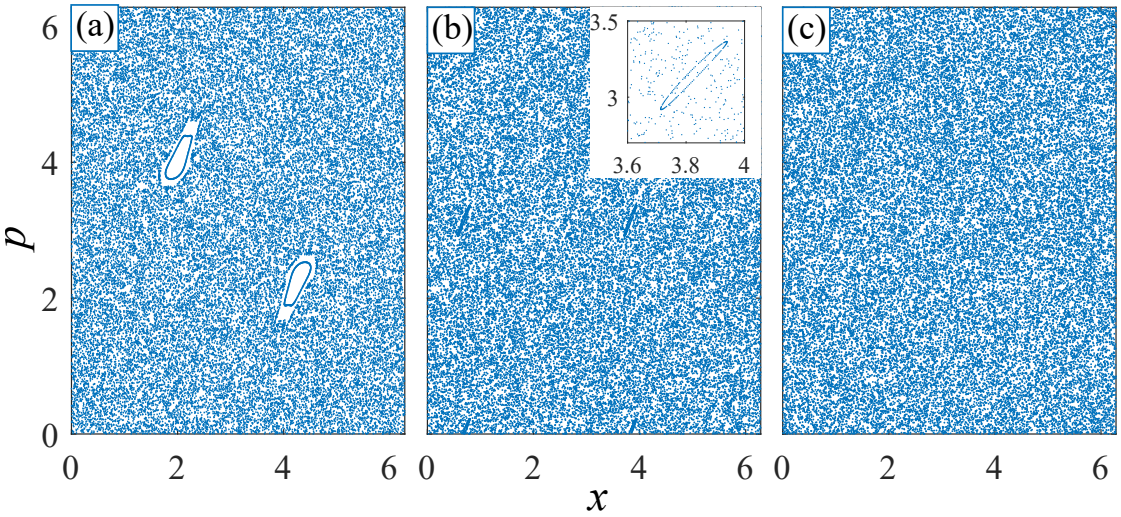

Figure 2.3: Modified phase space. (a) Standard phase space (b) Transporting island by change of sign of parameter K to -K after every 2 kick (c) Very small transporting island (not visible) in case of a modulation after every 3 kick, in all cases, $K = 5$.

2.3 Quantum Kicked Rotor

Considerable focus has been directed towards investigating the quantum mechanical counterparts of classically chaotic systems [113], to understand the quantum phenomena within chaotic frameworks. People are interested in studying the quantum kicked rotor (QKR) because it helps us in understanding how a transition to quantum domain affects its chaotic behavior. This area of study is called ”quantum chaos.” In this thesis, we’re mostly looking at the chaotic regime where things are unpredictable everywhere unless we mention otherwise.

Model Hamiltonian for quantum kicked rotor is same as classical kicked rotor [49,

114], only imposing the commutation relation for quantization. Let's take a simple example from experimental point of view, a laser cooled cloud of atoms are periodically getting perturbed by 1D optical lattice. The full Hamiltonian for this system is:

$$\mathcal{H} = \frac{P^2}{2M} + \frac{\hbar\Omega^2\tau}{8\Delta_L}\cos(2kX)\sum_{n=1}^{N}\delta_\tau(t_0 - nT)\ , \tag{2.2}$$

Where, Ω is Rabi frequency, τ is pulse time, Δ_L is detuning and k is wave-vector. After scaling it to dimensionless parameter as discussed here in details [108], we get same Hamiltonian as discussed in previous section:

$$\hat{H} = \frac{\hat{p}^2}{2} + K\cos(\hat{x})\sum_{n=1}^{N}\delta(t-n)\ , \tag{2.3}$$

$$[x, p] = i\hbar_{\text{eff}}\ , \tag{2.4}$$

Here, $\hbar_{\text{eff}} = 8\omega_r T$ and $K = \Phi_d\hbar_{\text{eff}}$, where ω_r is recoil frequency, T is period between the kick and $\Phi_d = \frac{\Omega^2\tau}{8\Delta_L}$. As this Hamiltonian is invariant under time translation $t \to t+T$, so this is a time-periodic $H(t) = H(t+T)$ problem and Floquet formalism can be utilized [115, 116]. This Hamiltonian can also be transformed into tight bonding model to make a connection with Anderson localization, this analogue will be discussed later in this section. A schematic of periodically kicked cloud of cold atoms, use to simulate the QKR, is shown in Fig. 2.4.

2.3.1 Floquet Analysis and Floquet Engineering

The time evolution of the wave-function $\psi(t)$, which is characterized by the Hamiltonian H, is determined by the time-dependent Schrödinger equation:

$$H(t)\psi(t) = i\hbar_{\text{eff}}\frac{\partial\psi(t)}{\partial t}\ . \tag{2.5}$$

So the time evolution operator for Eqn. 2.3 can be written by the Floquet operator [112, 117]:

$$U = U(T,0) = \exp\left(-i\frac{p^2}{2\hbar_{\text{eff}}}\right)\exp\left[-i\frac{K}{\hbar_{\text{eff}}}\cos(x)\right]\ , \tag{2.6}$$

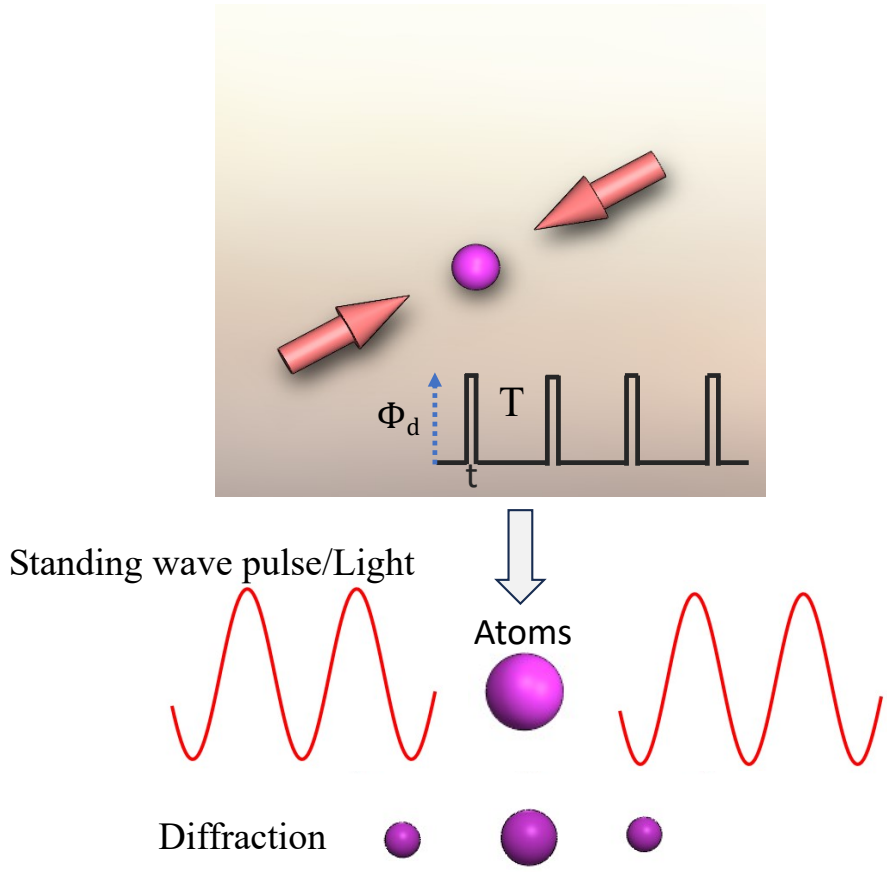

Figure 2.4: Experimental schematic for QKR. A periodically kicked cloud of cold atoms with standing wave for experimental realization of quantum kicked rotor. The periodic turning on and turning off of the optical lattice acts like strong periodic perturbations-leading to application of kicks

by replacing: p to $-i\hbar_{\text{eff}}\frac{\partial}{\partial x}$, we get:

$$F^{KR} = \exp\left(\frac{i\hbar_{\text{eff}}}{2}\frac{\partial^2}{\partial x^2}\right)\exp\left[-i\frac{K}{\hbar_{\text{eff}}}\cos(x)\right] \quad . \tag{2.7}$$

The Floquet operator, as represented by Equation 2.6, is a fundamental concept in the study of periodically driven quantum systems. It comprises two main components: the kick operator and the free evolution operator.

Kick Operator: This term, $\exp\left[-i\frac{K}{\hbar_{\text{eff}}}\cos(x)\right]$, represents the effect of the external perturbation or "kick" applied to the system. In the context of atom optics kicked rotor systems, this kick typically arises from periodically switching on and off the optical

potential, which affects the dynamics of the quantum particles.

Free Evolution Operator: The other term, $\exp\left(-i\frac{p^2}{2\hbar_{\text{eff}}}\right)$, describes the free evolution of the quantum state over a period T. This component represents the dynamical evolution of the system in the absence of external perturbations.

Floquet engineering involves manipulating the parameters K and T to achieve specific desired outcomes in the dynamics of the system [5,118]. By adjusting these parameters, one can control the behavior of quantum systems and engineer various quantum phenomena.

For instance, by varying the strength of perturbation K, one can influence the degree of chaos or regularity in the system's dynamics. Similarly, changing the free evolution time T allows for the tuning of dynamical phases between different momentum states of the system [53,56]. Overall, Floquet engineering provides a powerful framework for understanding and controlling the behavior of periodically driven quantum systems.

For Floquet engineering, we can express Eqn. 2.6 for n steps, where each step provides control to modify the parameters, in the case of control over free evolution, $\hbar_{\text{eff}}$ is not a good parameter to define, so we can just write in different free evolution for simplicity:

$$\begin{aligned} U &= U(T, nT) \\ &= \left\{\exp\left[f(T_1)\right]\exp\left[-i\frac{K_1}{\hbar_{\text{eff}}}\cos(x)\right]\right\} \\ &\quad\times\left\{\exp\left[f(T_2)\right]\exp\left[-i\frac{K_2}{\hbar_{\text{eff}}}\cos(x)\right]\right\} \\ &\quad\times\ldots \\ &\quad\times\left\{\exp\left[f(T_n)\right]\exp\left[-i\frac{K_n}{\hbar_{\text{eff}}}\cos(x)\right]\right\}\ , \end{aligned} \tag{2.8}$$

Here $(T_1, T_2 ... T_n)$ and $(K_1, K_2 ... K_n)$ are control parameters. Particularly from an experimental standpoint, the control over the free evolution(T) in a periodically kicked rotor system provides very precise control, with a precision of nanoseconds. However, control over K introduces an error of more than 5% [56]. So throughout this thesis, I will be exploring the control over T, whether it involves periodic changes or single changes. Further, multiple features are associated with T in quantum dynamics. Select-

ing the value of T can provide resonances, anti-resonances, and irrational phase evolution (causing dynamical localization), which makes this parameter suitable for control. I will discuss these features in the next section

2.3.2 Quantum Resonance and Quantum Anti-resonance

The time evolution described by the Floquet operator Eqn. 2.6, display many features with T. To understand this, Consider a wave function of the system $\psi(x,t)$ at any time t. This can be expanded in the momentum basis as: $\psi(x,t) = \sum_m A_m \langle x|m\rangle$, with A_m being the expansion coefficients. Now, we can apply free evolution Floquet operator on momentum state $|m\rangle$:

$$\exp\left(\frac{-ip^2}{2\hbar_{\text{eff}}}\right)|m\rangle = \exp\left(\frac{-im^2\hbar_{\text{eff}}}{2}\right)|m\rangle \ . \tag{2.9}$$

We replace, $p = m\hbar_{\text{eff}}$, where m is integer. This is true because of periodicity of potential or Bloch theory.

Now for resonance condition, a phase evolution of 2π is required because it's recreate the initial wave-function [119]. We can calculate the time required for a phase evolution of 2π:

$$\exp\left(\frac{-im^2\hbar_{\text{eff}}}{2}\right) = \exp(-i2\pi) = 1 \ . \tag{2.10}$$

From solution of above equation: $\hbar_{\text{eff}} = 4\pi$, where, $\hbar_{\text{eff}} = 8\omega_r T$. So, $T = T_T = \frac{\pi}{2\omega_r} = \frac{\hbar\pi}{2E_r}$, where, $2E_r$ is recoil energy. This time is called the Talbot time [117] and it's related to temporal Talbot effect, which is explained in detail in this section below.

Let's take an example of a plane wave state with zero momentum denoted as $|0\rangle$. The wave-function immediately after the application of the first kicked rotor pulse:

$$|\psi(t=0^+)\rangle = \exp\left[-i\frac{K}{\hbar_{\text{eff}}}\cos(x)\right]|0\rangle = \sum_{m=-\infty}^{\infty}(-i)^m J_m\left(\frac{K}{\hbar_{\text{eff}}}\right)|m\rangle \ . \tag{2.11}$$

Bessel function comes from Bessel identity after solving the equation. For a evolution

of pulse period of T_T, the wave-function just before the second pulse is:

$$|\psi(t = T_T)\rangle = \sum_{m=-\infty}^{\infty} (-i)^m e^{-i2\pi m} J_m \left(\frac{K}{\hbar_{\text{eff}}}\right) |m\rangle \,. \tag{2.12}$$

From the above equation, it's clear that the free propagation is unitary as m is an integer for Talbot time evolution. This Talbot time evolution recreates the wave-function that was just after the pulse.

$$|\psi(t = T_T)\rangle = \sum_{m=-\infty}^{\infty} (-i)^m e^{-i2\pi m} J_m \left(\frac{K}{\hbar_{\text{eff}}}\right) |m\rangle = |\psi(t = 0^+)\rangle \,. \tag{2.13}$$

The phenomenon of wave-function revival following a period of free propagation is recognized as the matter-wave Talbot effect [120]. It's analogues to the optical Talbot effect [121], where a similar revival of the interference pattern is observed in the vicinity of a diffraction grating. Introducing a second pulse with equal kick strength amplifies the phase modulation induced by the previous pulse, leading to a further increase in the population of states. Applying two kick with Talbot time evolution is like adding kick strength and replacing with single pulse.

$$|\psi(t = {T_T}^+)\rangle = \sum_{m=-\infty}^{\infty} (-i)^m J_m \left(\frac{2K}{\hbar_{\text{eff}}}\right) |m\rangle \,. \tag{2.14}$$

Similarly for N kicks:

$$|\psi(t = (N-1){T_T}^+)\rangle = \sum_{m=-\infty}^{\infty} (-i)^m J_m \left(\frac{NK}{\hbar_{\text{eff}}}\right) |m\rangle \,. \tag{2.15}$$

Now, the average energy growth of the system at Talbot time evolution with the kick is quadratic:

$$\langle E\rangle \propto n^2. \tag{2.16}$$

A plot of a simulation is shown in Fig.2.5a, considering an initial state as a plane wave. Similarly, the distribution after 40 kicks is also shown in Fig. 2.5b, it shows

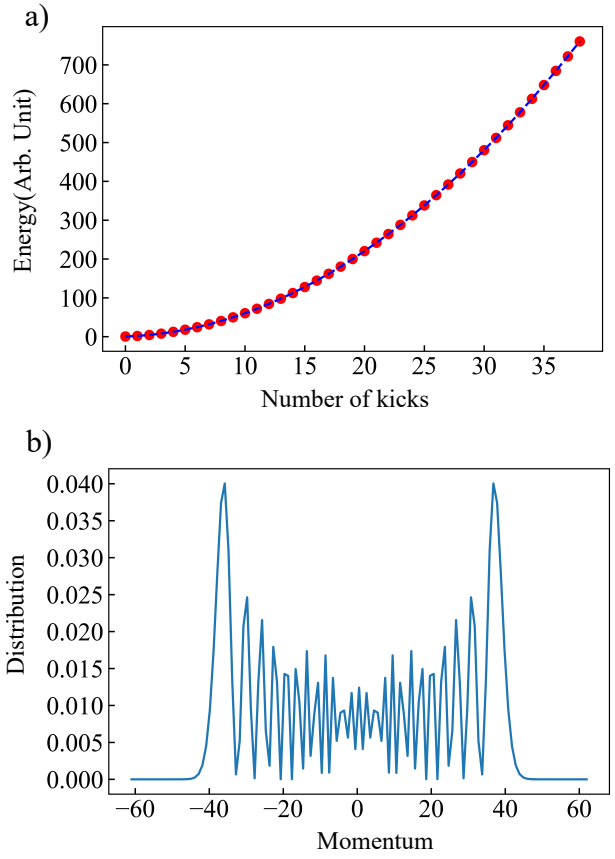

Figure 2.5: Resonance in QKR. Quadratic energy growth at resonance and the momentum distribution after 40 kicks

that the distribution grows symmetrically towards higher momentum states. This is analogous to a quantum random walk [122].

Similar calculation can be done for anti-resonance [117, 123], where a phase evolution of π takes place between the neighboring states. From the solution of Eqn. 2.10: $T_{\frac{T}{2}} = \frac{\pi}{4\omega_r} = \frac{\hbar\pi}{4E_r}$. This time is called the half-Talbot time. The solution just after first kicks will be the same as Eqn. 2.10. Solution just after two kicks is:

$$|\psi(t = T_{\frac{T}{2}})\rangle = \exp\left[i\frac{K}{\hbar_{\text{eff}}}\cos(x)\right]\exp\left[-i\frac{K}{\hbar_{\text{eff}}}\cos(x)\right]|0\rangle = |0\rangle\,. \tag{2.17}$$

In the case of a perfect plane wave with no external noise, a complete revival of the wave-function occurs. An odd number of kicks will reproduce the wave-function exactly as it was after one kick. Similarly, an even number of kicks will produce a distri-

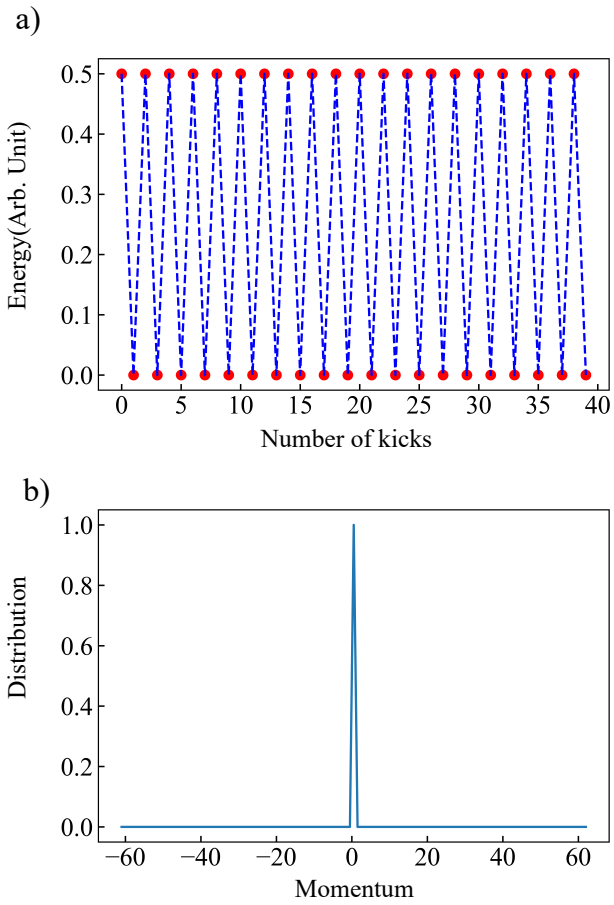

Figure 2.6: Anti-resonance in QKR. A energy growth showing the revival after even number of kicks and the distribution after 40 kicks.

bution identical to the initial wave-function without any kick. An energy growth and a distribution after 40 kicks is shown in Fig. 2.6a and Fig. 2.6b. Revival after even kick can be seen in energy as well as in distribution after 40 kick. Till this point, it's quite clear that by tuning the parameters of free evolution, we can manipulate the dynamical interference and the corresponding energy growth of the system. Such control is highly precise in experiments, making it one of the most effective parameters for controlling quantum systems. Also, to explain above theory, we have taken a zero momentum-width of the initial wave-function. Results will change, if you consider finite momentum width [123]. Further, as discussed in classical phase space, the creation of different types of transporting islands can indeed influence the dynamics of a system, potentially leading to the growth of energy. However, these transporting islands are highly sensi-

tive to parameters, and their presence can result in uncontrolled energy growth, leading to decoherence in the system [111, 124]. Therefore, they are not ideal parameters for quantum control.

2.3.3 Dynamical Localization in Quantum Kicked Rotor System

In the quantum mechanical treatment of the kicked rotor, resonance and anti-resonance arise when the time evolution matches 2π or π, respectively. A straightforward question emerges: what happens when this phase evolution corresponds to an irrational multiple of 2π? Let's write a Floquet operator for this:

$$U = U(T, 0) = \exp\left[-i\frac{p^2}{2\hbar_{\text{eff}}}\right] \exp\left[i\frac{K}{\hbar_{\text{eff}}}\cos(x)\right] , \tag{2.18}$$

Here, $T = \frac{\sqrt{3}+1}{2}T_T$, for this time evolution the phase difference between momentum states will not be π or 2π but it will be quasi-random phase evolution. Interesting dynamics emerge from this system for this irrational phase evolution when the stochastic parameter K is greater than 5. As we discussed before, the classical phase space is fully chaotic for $K > 5$ and energy growth is linear. The quantum counterpart exhibits a fundamentally distinct behavior. For a given stochastic parameter$(K, \hbar_{\text{eff}})$, initially, the average energy of the system increases linearly, resembling classical behavior. However, after a certain period, it reaches a saturation point [125, 126]. Regardless of the strength or number of kicks of external perturbations, the energy does not continue to increase. This critical time, at which energy growth ceases, is termed the "quantum break time," marking the onset of dynamic localization within the system. The momentum distribution after dynamical localization shows exponential distribution, shown in Fig. 2.7. The quantum break time and localization length [127] can be calculated for given parameters $(K, \hbar_{\text{eff}})$,

$$T_{\text{break\_time}} \simeq \frac{K^2}{4\hbar_{\text{eff}}^2},\ P_{\text{break\_time}} \simeq \frac{K^2}{4\hbar_{\text{eff}}} \tag{2.19}$$

In contrast to classical systems, where chaotic behavior is prevalent, quantum systems follow the linear evolution dictated by the equations of quantum mechanics. Consequently, chaos in the classical sense is not directly observable in quantum systems.

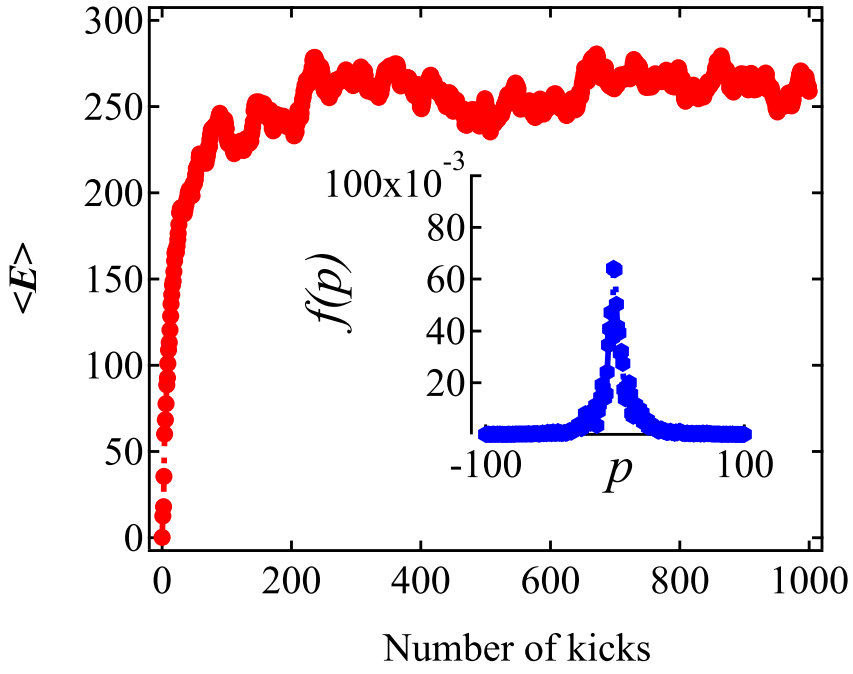

Figure 2.7: Dynamical localization in QKR: Energy growth for K = 5.5 exhibiting the characteristics of dynamical localization, with an inset showing an exponentially localized momentum distribution after 1000 kicks.

Instead, the manifestation of chaos occurs through a phenomenon known as dynamical localization [126], which shares strong connections with Anderson localization. Following the initial period of apparent classical motion (referred to as the "quantum break time"), momentum diffusion becomes constrained, leading the system to reach a steady state where no additional energy is absorbed. The first experimental demonstration of dynamical localization was done by M. Raizen in 1995 [49] with atoms and optical lattice. Simply, the dynamical localization occurs due to destructive quantum interference, which arises from the periodic nature of the kicking potential and the discreteness of quantum states. As the number of kicks increases, the quantum wave-function evolves in a manner where destructive quantum interference takes place. Eventually, a strong quantum correlation builds up [72], canceling out classical diffusion.

2.3.4 Coherent Control of Quantum Chaos

As discussed above, a periodic kick with certain stochastic parameter, can lead to a dynamical localization of a quantum system. Dynamical localization is defined by the localization energy and localization length for a given fixed strength of perturbation, and fixed period of the kick. The idea behind coherent control of quantum chaos is to manipulate the final localized state, achieving desired energy and localization length, solely through the manipulation of the dynamical phase, without introducing decoherence into the system, for a given parameter K. Such an idea was briefly discussed in this paper [5, 118]. An example is shown in Fig. 2.8. Starting with an initial state (shown in blue on the left), periodic driving will lead to an exponentially localized distribution (also shown in blue on the right). Coherent control involves finding a method to achieve a desired state with higher energy and localization length while maintaining an exponential localized distribution, as shown in green and red. Such control is achieved solely through the manipulation of dynamical phases, without increasing the strength of perturbation or adding more energy to the system, while maintaining quantum coherence. This makes it quite interesting. It's important to note that as the classical phase space for

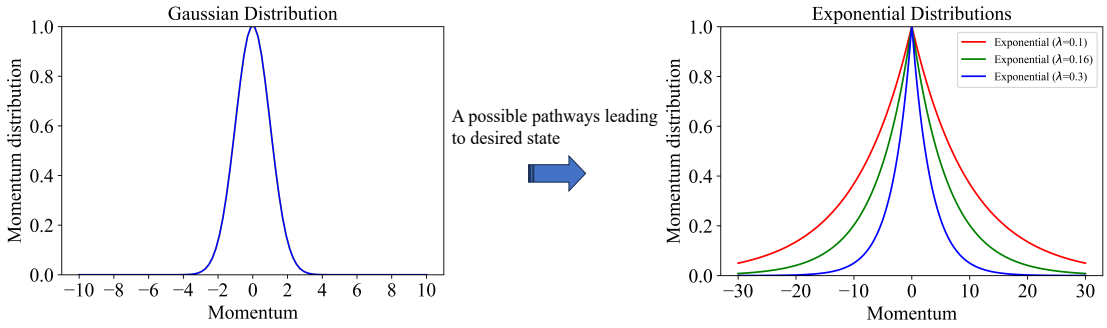

Figure 2.8: Coherent control of DL. A simple illustration demonstrating the concept of coherent control of quantum chaos.

the Hamiltonian is fully chaotic, any alteration may not yield the desired state. Chaos is highly parameter-sensitive, and any random external change may eventually lead to decoherence in the system, resulting in the loss of dynamical localization. Many proposed scheme for coherent control explored either by initial state preparation or by periodic phase modulation [128–130]. One experimental demonstration of coherent control was

demonstrated in ref. [42] with molecular kicked rotor. We have explored the coherent control through periodic phase modulation and through manipulation of initial state for coherent control experimentally.

2.3.5 Anderson Localization vs Dynamical Localization

Let's recall the Anderson model [27], the Hamiltonian for the Anderson model is:

$$H = t\sum_{\langle ij\rangle} \hat{a}_i^\dagger \hat{a}_j + w\sum_{\langle i\rangle} c_i \hat{a}_i^\dagger \hat{a}_i \ , \tag{2.20}$$

Here, t is hopping parameter and w is strength of disorder, c_i uniform random distribution. This proposed model by Anderson, exhibits complete localization in position space for one and two dimensions, for any finite disorder strength. In three dimensions, it shows a transition from localized to delocalized state, also called Anderson insulator-metal transition [34]. The localized wave-function will be $\psi(x) \sim e^{-\frac{x}{\ell}}$. A simple illustration is shown in Fig. 2.9 (left), the red one shows the random disorder on each lattice site and corresponding localized wave-function. Now let's revisit the quantum kicked rotor Hamiltonian:

$$\hat{H} = \frac{\hat{p}^2}{2} + K\cos(\hat{x})\sum_{n=1}^{N}\delta(t-n) \ . \tag{2.21}$$

The Floquet operator is:

$$U = \exp\left[-i\frac{K}{\hbar_{\text{eff}}}\cos(x)\right]\exp\left[-i\frac{p^2}{2\hbar_{\text{eff}}}\right] = \exp\left[-iV(x)\right]\exp\left[-iH_0\right] \tag{2.22}$$

After a transform through Hermitian operator J:

$$e^{-iV(x)} = \frac{1-iJ(x)}{1+iJ(x)}, \quad J(x) = \tan\left[\frac{V(x)}{2}\right] \tag{2.23}$$

and applying the operator: $F|\phi\rangle = e^{-i\phi}|\phi\rangle$ gives

$$(1-iJ)e^{i\phi} - iH_0|\phi\rangle = (1+iJ)|\phi\rangle \ , \tag{2.24}$$

Further solving it, we get

$$\tan\phi - \frac{H_0}{2}|\phi\rangle - J|\phi\rangle = 0\ . \tag{2.25}$$

Now, using the momentum (p) representation (eigenvectors of the unperturbed system, $H_0|n\rangle = \frac{n^2}{2M}|n\rangle$), further: $J_n = \frac{1}{2\pi}\int_0^{2\pi} dx \tan\left(\frac{k\cos x}{2}\right) e^{-inx}$, $\epsilon_n = \tan\left[\frac{\phi}{2} - \frac{n^2}{4M}\right]$, $\varphi_n = \langle n|\varphi\rangle$, we get the following:

$$\epsilon_n\varphi_n - \sum_{m\neq n} W_{n-m}\varphi_m = E\varphi_n\ , \tag{2.26}$$

with $E = J_0$.

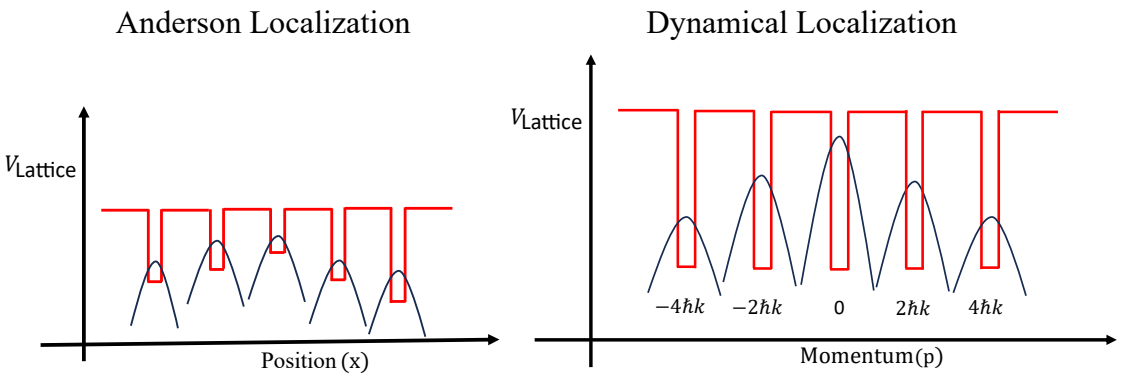

Figure 2.9: Anderson vs dynamical localization . A graphical representation of Anderson and dynamical localization

Eqn. 2.25 shows that the quantum kicked rotor Hamiltonian is exactly analogous to the Anderson model, but in momentum space. A exact theory can be found in reference [48]. In quantum kicked rotor, the randomness arises from the dynamical phases originating from irrational phase evolution. Fig. 2.9 (right) depicts a graphical representation where there is no randomness in the strength of the perturbation.

In short, the randomness appears in the diagonal elements for both the Anderson model and quantum kicked rotor Hamiltonian, causing them to behave in a similar way. The quantum kicked rotor system is quite flexible for simulating the 1D, 2D, and 3D Anderson model, allowing for experimental observation of Anderson transitions and critical states [53, 131].

2.4 Quantum Kicked Rotor in Moving Frame of Reference

In the kicked rotor Hamiltonian, either the lattice or the initial wave-function can be moved from the laboratory frame to model the quantum kicked rotor in a moving frame of reference. Let's consider when lattice is in motion, the Hamiltonian of quantum kicked rotor is expressed as follows in the laboratory frame [111, 132]:

$$H = \frac{\widehat{p}^2}{2} + K\cos(2k\widehat{x} - 2\pi\alpha t)\sum_{n=1}^{N}\delta(t-n)\ , \tag{2.27}$$

where p represents momentum and x denotes the position coordinate, K is the stochastic parameter, k is wave vector and α is a frequency difference between two lattice beams that imparts a constant velocity to the optical lattice. Similarly, we can write the initial wave-function as follows:

$$\psi(x) = \frac{1}{\sqrt{2\pi}\sigma_w}\exp(-\frac{x^2}{2\sigma_w^2})\exp(-ip_0x)\ , \tag{2.28}$$

Here, σ_w is the width of the wave-function and p_0 is the initial launch velocity. If the wave-function is in motion in the Hamiltonian with velocity p_0 in lab frame, α = 0 in that case and if lattice is moving in lab frame, p_0 = 0 in the wave-function. We consider this for making things simple. As it's clear that lattice potential and initial wave function has point symmetry around some center. Consequently, either a moving lattice or atoms with the same velocity in the lab frame should induce similar effects [65, 66].

Just for further clarification, in this section, we consider the initial wavepacket as a Bose-Einstein condensate (BEC), where the momentum width of the BEC is two orders of magnitude smaller than that of two-photon recoil momentum. The narrow initial momentum distribution is helpful in resolving different momentum eigen states, easy to quantifying many observables precisely, which is necessary for our idea [65–67, 123]. To develop the basic idea for numerical approach, we are taking an example of the lattice moving in lab frame in our ease. Kicked rotor potential when lattice is moving in lab

frame is written as,

$$V(x) = K\cos(2kx - 2\pi\alpha t)\ , \quad \text{where } K \text{ is constant.} \tag{2.29}$$

For a given α, the velocity (v) of the lattice is, v = $\frac{\lambda\alpha}{2}$, where λ is the wavelength of the optical lattice. A lattice moving with constant velocity creates a constant phase difference in fixed interval. For a periodically kicked rotor with a kicking period of T, phase difference between each kick is given by:

$$\phi = 2\pi\alpha T\ . \tag{2.30}$$

and the phase evolution for any kick is given by,

$$\phi = (2\pi\alpha T)(n-1)\ , \tag{2.31}$$

where n is the number of kicks and considering the phase is zero for the first kick. Through this straightforward calculation, it becomes evident that a constant phase difference exists between each kick. To understand the long term dynamics, we can analyze early time features for this system. To illustrate, considering the first two kicks as an example, the phase difference between them is given by $2\pi.\alpha$.T. This phase difference creates an in-homogeneity in position space and it causes an asymmetric momentum distribution in early time [66]. To quantify this asymmetry, we measure the $\langle p\rangle$, The $\langle p\rangle$ just after two kicks is given by:

$$\langle p(t = 2T)\rangle = c\ \sin[4\pi(vT/\lambda)]\ , \tag{2.32}$$

where c is constant. This is oscillatory in nature as a function of the velocity of lattice. It also shows that, any finite velocity jitter in lattice will give us an observable $\langle p\rangle$ for quantifying those little velocity jitter.

2.4.1 Micromotion in Bose-Einstein Condensates

What we mean by micromotion of BEC in this system is the very small initial velocity of BEC in the direction of lattice. This small velocity is challenging to measure accurately

through conventional time-of-flight methods [133]. The quantum kicked rotor provides us a technique to measure this small velocity which is of the order of $100\,\mu$m/s. Going through the same idea as moving lattice, a similar asymmetry in average momentum will occur when the wave-function is in motion. Such asymmetry is quite interesting for quantifying the initial micromotion of the wave-function. Let's consider there is a very small velocity jitter in the Bose-Einstein Condensate (BEC) in the direction of the lattice. By applying two kicks, we should observe some asymmetric features in the momentum distribution, as quantified in Eqn. 2.32. However, there is an unknown constant parameter c present. It's quite challenging to provide a tunable constant velocity to the BEC to fit it with Eqn. 2.32.

To overcome this challenge, we implemented a simple idea: since we know that the velocity jitter of the BEC is small and fixed, we can precisely scan the lattice velocity by adjusting the frequency difference (a feasible control in experiments). As soon as the lattice velocity matches that of the BEC, we will observe a zero asymmetry in the average momentum $\langle p \rangle$. This method is quite helpful as it provides the zero-crossing point by scanning around the BEC velocity. A detailed discussion with experimental data and a broad motivation behind this work will be provided in the following chapter.

2.4.2 Asymmetric Dynamical Localization

As discussed above, oscillatory early time dynamics emerges when we move the lattice or the atomic wave-function. This asymmetry also affects the long term dynamics. To conclude the long-term dynamics, we know that phase difference between consecutive kicks remains constant for a fixed lattice velocity, so whatever the asymmetry comes, it from a given velocity in early time dynamics. This asymmetry settles down at some value in long time dynamics due to dynamical localization and the nature of asymmetry established by early time dynamics. An interesting observation is that, for certain values of v, for a given kicking period T, if, $vT/\lambda = n/4$ (where n is an integer), $\langle p \rangle = 0$ implying an absence of asymmetry for specific choice of initial velocity and kick period. To conclude, in the quantum kicked rotor in a moving frame, the nature of long-term dynamics will be analogous to the early-time dynamics. If there is an asymmetry in the early-time dynamics, it will also manifest in dynamical localization, avoiding some

special cases like quantum boomerang effect [67], further asymmetry with cold atoms is well studied [134–136].

2.4.3 Numerical Simulations

For numerical simulations, the standard split-operator method using discrete Fourier transform [137] is commonly used to evolve the Hamiltonian of the kicked rotor [138–140]. With the assumption that there is no dynamical phase evolution during a delta kick, implementation of the Floquet operator makes the simulations easier. This method involves two main components:

1. The kicked operator, which is diagonalized in position space.
2. The free evolution operator, which is diagonalized in momentum space.

Both of these have already been discussed in the theory section. Now, for a time dependent Hamiltonian, we define evolution operator with a quite small time step, $\exp\left(-i\hat{H}\frac{\Delta t}{\hbar}\right)$, further we can split it in momentum and position operator, $\hat{U}_p(\Delta t) = \exp\left(\frac{i\hat{p}^2\Delta t}{2m\hbar}\right)$ and $\hat{U}_x(\Delta t) = \exp\left(\frac{iV(\hat{x})\Delta t}{\hbar}\right)$. After this, we apply this operator on an initial wave-function and switch back and forth from momentum to position with the help of discrete Fourier transform [141]. As operator $\hat{x}$ and $\hat{p}$ don't commute, so an error accumulates with the time of order of Δt^2 [142], such error can be reduced by applying Baker-Campbell-Hausdorff theorem. For delta pulses, we can safely drop the time dependent part in potential which make simulation slightly easier. This technique is a widely used approach for simulating the dynamics of the quantum kicked rotor.

To simulate the system when lattice is in motion in lab frame, we adjust the phase before each kick. As we know the phase evolution with lattice velocity, and this assumption is valid for delta pulse. Similarly, to simulate where the Bose-Einstein Condensate (BEC) is in motion in the laboratory frame, we initialize the simulation with a wave-function that already accounts for the motion from the beginning.

2.5 Conclusions

This chapter described the theoretical description of the classical and quantum kicked rotor. The role of classical phase space in energy growth, as well as the free evolution pa-

rameter in quantum systems for similar control, is discussed. Furthermore, we explored how this parameter can be utilized for controlling dynamical localization, eventually influencing quantum chaos. We also investigate the Hamiltonian in a moving frame and develop a method to measure micromotion and cause of asymmetric dynamical localization.

Chapter 3

Experimental Setup

I will present the experimental setup used for the kicked rotor. The initial setup was constructed by former students in the years 2012 and 2013 [143, 144]. However, during the COVID-19 pandemic, the oven had passed its lifetime and the vacuum system needed to be reconstructed with some modifications for enabling faster production of BEC and better optimization.

I'll provide a brief overview of each component, physics and techniques associated with them, which serves as the foundation for conducting the kicked rotor experiments. Finally, a brief discussion the implementation of machine learning and a novel cooling technique that we demonstrated experimentally.

3.1 Laser Cooling and Trapping

Laser cooling is a sub-field of atomic physics for slowing down the motion of atoms to extremely low temperatures [10, 145], typically just a 100 pK away from absolute zero [19]. This process is crucial for various experiments, including the creation of BEC and the study of quantum phenomena, matter-wave interference and new quantum states.

The principle behind laser cooling relies on the interaction between atoms and laser light. Atoms absorb and emit photons, which are packets of light energy. In laser cooling, specialized lasers are used to target the electronic transition of atoms. As we know, the absorption of photons by atoms is directional, but spontaneous emissions

is random [146]. The momentum of atoms can be balanced by absorption, slowing them down, and over many cycles of absorption and emission, the momentum through spontaneous processes averages to zero. By carefully controlling the parameters of the laser beams, such as their frequency, polarization, intensity and direction, one can slow down atoms [147]. Atoms are slowed down in all directions, akin to the way molasses slows down moving objects immersed in it. As a result, the temperature of the atoms decreases [148]. Laser cooling techniques have several variations, including Doppler cooling, magneto-optical trapping (MOT), and evaporative cooling. Doppler cooling is the initial stage where atoms are first cooled down using laser light. Magneto-optical trapping involves additional magnetic fields to confine the cooled atoms in a small region of space. Evaporative cooling, on the other hand, is a subsequent step used to further reduce the temperature of the trapped atoms by selectively removing the hottest atoms from the sample. The basic principle of laser cooling remains consistent across most atoms. However, experimental difficulties arise depending on factors such as wavelength requirements, line-width of the transition, and the electronic structure, like whether the atom has one or two electrons in its outer shell. Due to these difficulties, laser cooling techniques are only applicable to a limited number of atoms. Rubidium (Rb), Sodium (Na), Potassium (K), Lithium (Li), Cesium (Cs), Strontium (Sr), Ytterbium (Yb), and Dysprosium (Dy) are famously used in laser cooling experiments.

I will go through the scattering force considering two level system, magneto-optical trap and evaporation cooling for production of BEC.

3.2 Scattering Force

In a two-level system, such as atoms with simplified electronic structure, the scattering force arises due to the interaction between atoms and the incident photons. This interaction can be understood through the process of absorption and emission.

When an incident photon interacts with atoms in the ground state (lower energy level), it can induce a transition of the electron to an excited state (higher energy level) through absorption. During this process, the photon imparts momentum to the system, which leads to a change in its velocity [10, 148]. This change in velocity corresponds to a force acting on the system, known as the scattering force.

The scattering force is given by:

$$F_{\text{scatt}} = \frac{\hbar\vec{k}}{2}\frac{\Gamma}{2}\frac{I/I_{\text{sat}}}{1+\frac{I}{I_{\text{sat}}}+4\left(\frac{\delta}{2\Gamma}\right)^2}\,, \tag{3.1}$$

Here, $\hbar$ represents the reduced Planck constant, $\vec{k}$ denotes the wave-vector of the incident light, Γ stands for the line-width of the atomic transition, I represents the intensity of the incident light, I_{sat} is the saturation intensity, and δ signifies the detuning of the incident light from the resonance.

The magnitude and direction of the scattering force depends on various factors, including the intensity and polarization of the incident light, the transition probability between the energy levels involved, and the detuning of the incident light from the atomic transition frequency.

3.2.1 Zeeman Slower

The utilization of the scattering force comes into play during the initial stage of slowing down the velocity of atoms. Let's take an example of Rubidium (Rb) atoms, first we will go through the electronic structure of Rubidium. Rubidium has two isotopes naturally, ^{85}Rb and ^{87}Rb with a natural abundance of 72.2% and 27.8% respectively. Rubidium has an electronic configuration of [Kr] $5s^1$. This means that it has one valence electron in its outermost shell. The most common isotope of Rubidium is ^{85}Rb, which has a nuclear spin of $I = \frac{5}{2}$. Another stable isotope, ^{87}Rb, has a nuclear spin of $I = \frac{3}{2}$. A detailed electronic structure can be found in reference [149]. In our experimental setup, we cool ^{87}Rb for production of BEC.

Fig. 3.1, a Russel-Saunders plot for ^{87}Rb which shows the quantum energy levels of single valence electron. It gives the idea of frequency requirement to drive the transition, also polarization requirements with selection rule. Now for slowing down the atoms which are coming from a hot oven of temperature $120°$C and well-collimated. A counter-propagating laser beam, large red-detuning from $|F = 2\rangle \rightarrow |F' = 3\rangle$, shown in figure 3.1 as ZS is used. To maintain the resonance condition by balancing Doppler shift, as atoms undergo the process of deceleration through opposite scattering force, a spatially varying magnetic field [150] is maintained to keep the atoms on resonance

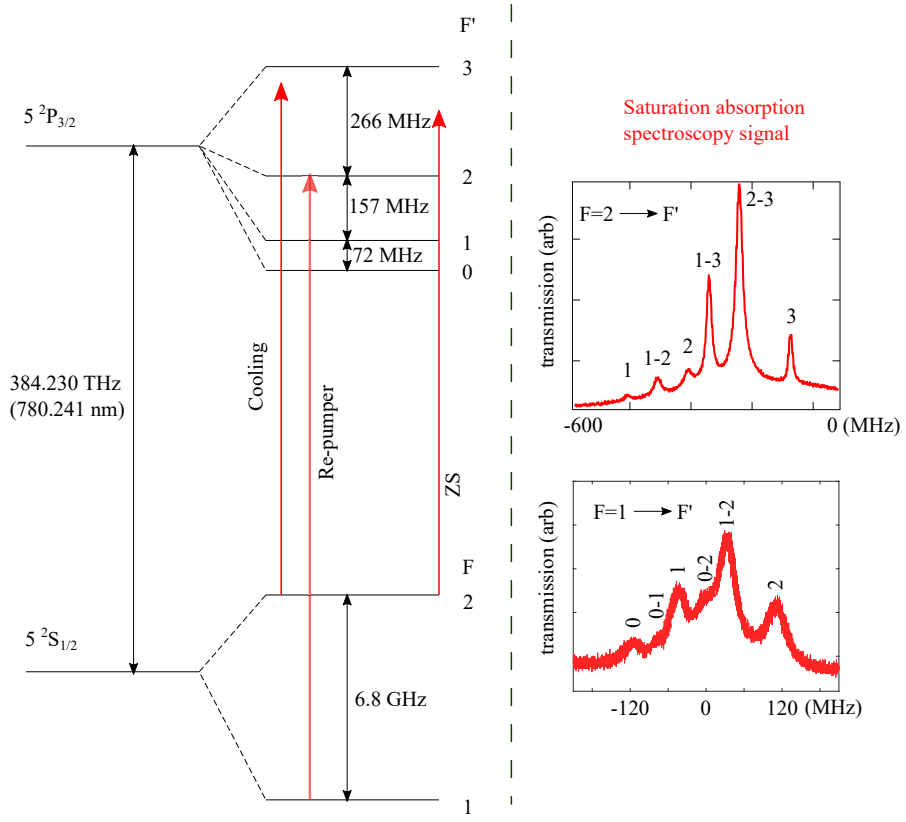

Figure 3.1: Energy level diagram. A schematic representation of the energy level diagram for the D2 line of ^{87}Rb, featuring cooling and repumping lasers alongside the Zeeman slower (ZS). The spectroscopy signal from saturation absorption spectroscopy is also shown, illustrating its role in stabilizing the laser.

by using the Zeeman effect. Particularly, this setup is called a Zeeman slower(ZS). This step effectively reduces the velocity of atoms from several 100 m/s to less than 20 m/s [151]. As we have taken example of ^{87}Rb, a scattering force calculation can be done by equation 3.1, for different laser beam intensity and detuning. More details about this is available in previous thesis from our group [143]

3.3 Magneto-Optical Trap

The basic principle of a magneto-optical trap involves using six laser beams and magnetic fields to slow down and trap atoms [146, 152]. The process begins with a beam of atoms, typically slowed by Zeeman slower [153], a good background vapor of atoms is also used for MOT [154]. Particularly in our setup, Zeeman slowed atoms are intro-

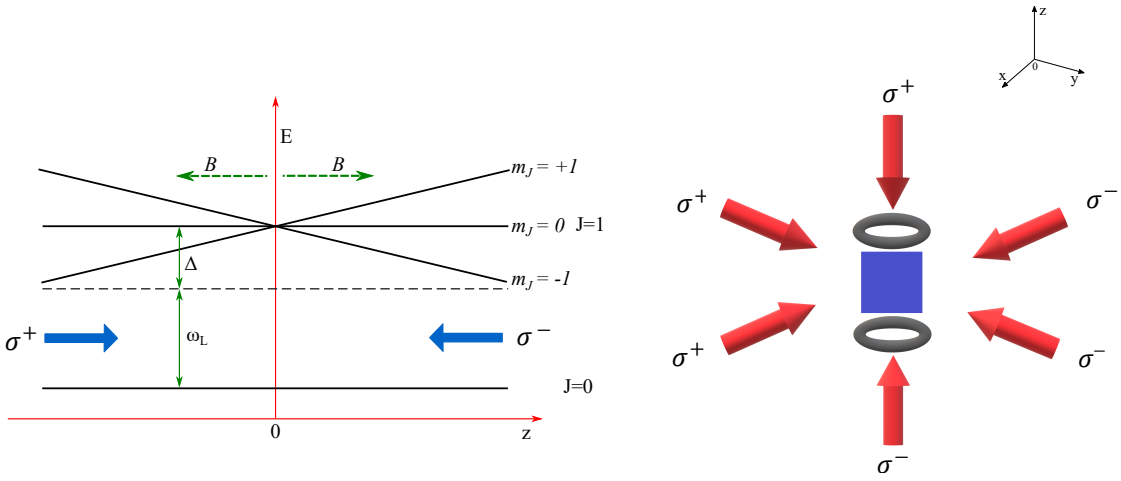

Figure 3.2: MOT. **(Left)** Working principle of MOT. **(Right)** Schematic for confining atoms using six laser beams. The blue square in the middle of the laser beams is the glass cell maintaining UHV.

duced into the MOT chamber.

In a magneto-optical trap (MOT), we use a magnetic quadrupole field and laser beams with σ^+- σ^- polarization to create a situation where the energy level of atoms changes depending on their position. This energy shift helps in trapping the atoms. An illustration is shown in Fig. 3.2 (right).

We now elaborate on this mechanism for a simplified $|J = 0\rangle \rightarrow |J = 1\rangle$ transition considering 1D scenario. As depicted in Fig. 3.2(left), the degeneracy of the excited state $|J = 1\rangle$ is perturbed by the magnetic field gradient, resulting in the splitting of the state into three magnetic sub-levels: $m_J = -1, 0, +1$. Now using laser beams that are "red-detuned" on an atomic transition where the energy levels get closer as the magnetic field increases. To achieve selective absorption in the transitions $|J = 0, m_J = 0\rangle \rightarrow |J = 1, m_J = \pm 1\rangle$, pairs of orthogonal beams consisting of circularly polarized light with opposite helicity are used. For simplification, consider a 1D scenario, if atoms try to move to the right side of the $B = 0$ axis, the beam with σ^- polarization is preferentially absorbed and scattered compared to the σ^+ beam, primarily due to the detuning of the σ^- beam being closer to the laser frequency as well as full-filling the criteria of selection rule. This provides a force in the opposite direction of motion, similarly if atoms try to move to the left, the force will push them back to the center of magnetic field. The combination of these laser beams and the magnetic fields creates a

force that slows down the velocity of atoms as well as provide a spatial confinement [10]. The total force in MOT system is:

$$F_{\text{MOT}} = -\alpha v - \frac{\alpha}{k}\frac{g\mu_B}{\hbar}\frac{\partial B}{\partial z}z, \quad \text{where:} \quad \alpha = 4\hbar k^2 \frac{I}{I_{\text{sat}}} \frac{-\left(\frac{2\delta}{\Gamma}\right)}{\left[1+\left(\frac{2\delta}{\Gamma}\right)^2\right]^2} \tag{3.2}$$

For our experiment, The cooling transition $|F = 2\rangle \rightarrow |F' = 3\rangle$ is used. From Eqn. 3.2, laser beams are kept red-detuned by -2Γ, where Γ is the natural linewidth of the cooling transition (approximately $2\pi \times 6$ MHz), and $\frac{\partial B}{\partial z}$ is about 15 Gauss/cm. The Doppler limited temperature comes from natural line-width (Γ) which is given by:

$$k_B T_D = \frac{\hbar\Gamma}{2}\,. \tag{3.3}$$

As our cooling cycle is not fully closed, atoms also undergo transitions to $|F = 1\rangle$ through finite spontaneous emission. Therefore, we also utilize an additional laser known as the repumping laser. This laser beam brings the atoms back into the cooling cycle through the $|F = 1\rangle \rightarrow |F' = 2\rangle$ transition [144]. The typical loading process for a Magneto-Optical Trap (MOT) runs for a duration of 3 to 5 seconds to capture approximately 2×10^8 atoms.

To further cool and increase the phase space density of atomic cloud, we go through a process called compressed MOT [155]. Ramping the magnetic field strength from 15 Gauss/cm to 20 Gauss/cm, also increasing the detuning linearly from -2Γ to -11Γ, we reach a temperature of approximate $50\,\mu$K and just loosing less than 15% of atoms.

3.4 Dipole Trap and It's Evaporation

To further cool the atoms for producing the Bose-Einstein condensate, we transfer the atoms in a tightly focused far-detuned optical dipole traps. Two single mode laser beams of 1064nm in a crossed beam geometry, in a plane perpendicular to gravity is used to confine the atoms in this potential [10, 156]. A schematic is shown in figure 3.3 of our setup. For a Gaussian beam with waist w_0 and peak intensity I_0, the dipole trap potential is given by:

$$U_{\text{dipole}} = -\frac{\hbar\Gamma^2}{8\delta}\frac{I}{I_s}e^{-\frac{2r^2}{w_0^2}} \ . \tag{3.4}$$

The optical system of the dipole traps starts with a high-power laser, the Azurlight-1064nm-50W, which is a single-mode laser. We utilize 20W from this laser, split by a polarizing beam splitter and directed through two acousto-optic modulators (AOMs) operating at frequencies of 110 MHz and 120 MHz, respectively. This setup allows us to independently control the power and switching of each beam. Additionally, this configuration prevents interference between the two beams, which could otherwise lead to loss of atoms [157]. The beam size of the laser is initially 1mm. We expand it to ap-

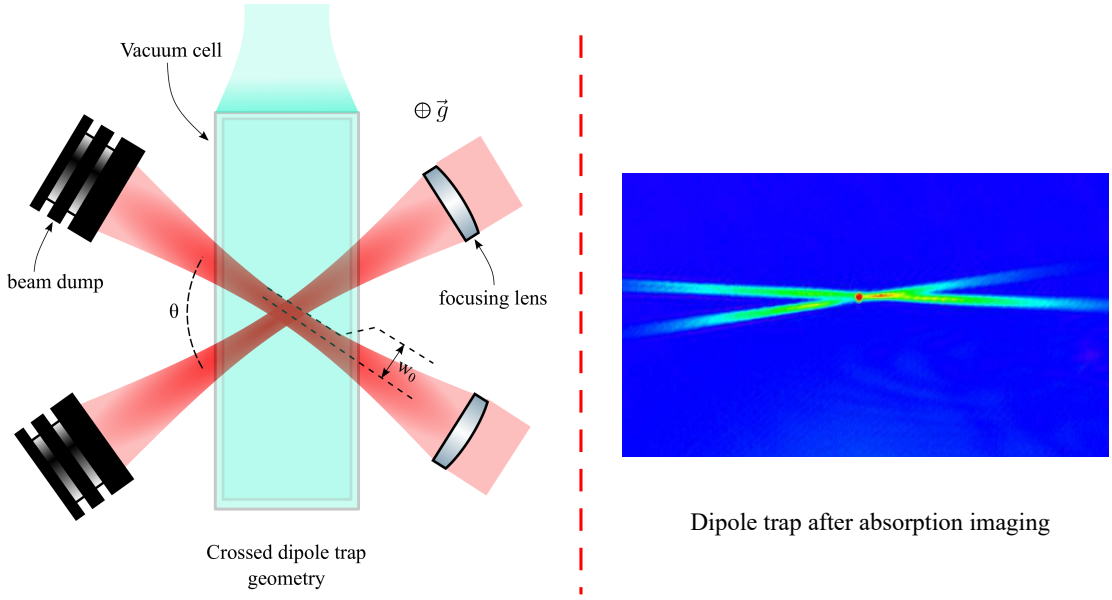

Figure 3.3: Schematic of the dipole trap. **(Left)** Tightly focussed crossed dipole trap in glass cell. **(Right)** An absorption image of atoms captured in this trap

proximately 6 mm to create a tight trap at the focal point, achieved by passing it through a 200 mm focal length lens. The trap depth is approximate 200 μK in our setup, enough to capture more than 2×10^6 atoms together in dipole trap. An absorption image of atoms captured in dipole trap is shown in Fig. 3.3, after holding it for 50ms. The lifetime of atoms in dipole trap is more than 10 s, it provides enough time to evaporate to reach BEC. Once the atoms are in the optical dipole trap, precisely lowering the potential energy of the dipole traps, the hottest atoms, typically those with the highest kinetic

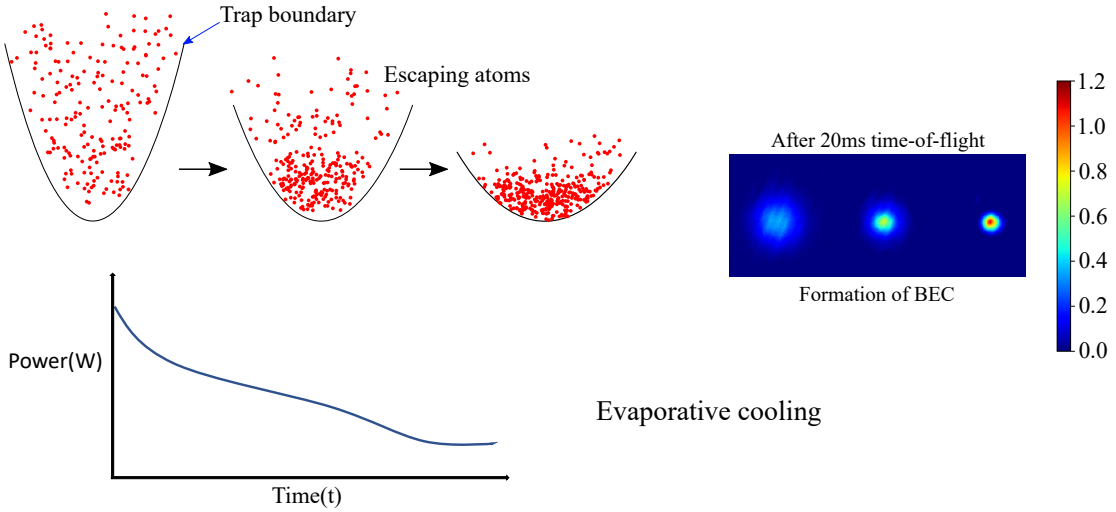

Figure 3.4: Evaporative cooling. **(Left)** Lowering potential adiabatically for evaporation. **(Right)** A transition to BEC

energy escape from the trap [158, 159]. This selective removal process leads to a redistribution of the remaining atoms' energies, resulting in a lower average kinetic energy because of continuous elastic collision and, consequently, a colder sample as shown in top of the Fig. 3.4. To gain a deeper understanding of evaporation, one can adopt a statistical perspective. Consider the analogy of many cycles of elastic collisions among atoms: some atoms gain kinetic energy while others lose it. Continuously reducing the potential depth is akin to lowering the threshold for escape. Consequently, atoms with higher kinetic energy are more likely to surpass this threshold and "evaporate" from the system, while those with lower kinetic energy remain trapped, effectively leading to cooling [160].

The key parameter controlling the efficiency of evaporative cooling is the trap depth, which determines the energy threshold for atoms to escape the trap. By gradually reducing the trap depth over time, typically through reducing the laser power as shown in Fig. 3.4, the temperature of the atomic ensemble can be progressively lowered. For monitoring the cooling and optimizing the evaporation, we measure the temperature and phase space density after each time-step evaporation. This reduction in temperature can eventually lead to the formation of Bose-Einstein condensate (BEC) or quantum-degenerate gas. In Fig. 3.4 (right), a time-of-flight image of our lab's Bose-Einstein condensate (BEC) is presented. The image distinctly shows the evolution from a thermal distribu-

tion to a bimodal distribution, ultimately revealing the pure BEC state, the details are available in this thesis [144].

3.4.1 Machine Learning for Production of BEC and Pulse-Width Modulation for Evaporative Cooling

We used machine learning [161] to speed up the process of achieving Bose-Einstein condensation (BEC) through evaporation cooling. After reconstructing our setup and installation of a new high power laser, we managed to achieve BEC after few weeks of manual optimization, but this didn't guarantee the fastest production or finding the best settings. Initially, manually optimizing evaporation took about 8-9 seconds to produce the BEC. To improve this, we implemented machine learning by giving the control of the system to machine learning. Basically, machine learning used to control the shape of the evaporation cycle by controlling the laser power used for dipole trap, and took the absorption image after 8 ms time-of-flight to process further and move to next parameter. We fed data from these processes to the machine learning algorithm. Knowing that the power reduction over time follows a higher-order polynomial equation, the machine learning model adjusted the coefficients of this equation, essentially shaping the evaporation curve within a specified time frame [162, 163]. We provide a cost function to machine learning which is related to higher optical density. By monitoring the optical density of atoms during the time of flight and adjusting parameters using Gaussian optimization, the machine learning system learned and optimized the evaporation process. Eventually, we achieved BEC with an evaporation time of just 5 seconds, reducing the cycle time by more than 35%.

More detailed information about the algorithms and implementation of machine learning on the experimental setup can be found in this paper, where we implemented machine learning to increase the number of atoms in a strontium MOT [164].

We also implemented a new technique to cool the atoms during the evaporation process using a time-averaged potential. As mentioned earlier, by decreasing the trap depth through the reduction of laser power, one can effectively cool the atoms. This reduction in laser power is achieved through the voltage variable attenuator (VVA) of the acousto-optic modulators (AOMs) drivers. By adjusting two analog outputs corresponding to

the VVAs and reducing the voltage, we can lower the power output. This is a traditional method to implement for evaporation. We came up with an idea where we keep the laser power fixed at its maximum available power, and we switch the laser on and off at a rate of 1 MHz using a fast RF switch. Atoms perceive this rapidly switching potential as static. By adjusting the duty cycle, which is achievable through pulse-width modulation, we can control the average potential experienced by the atoms. Implementing this technique involves controlling the duty cycle to gradually decrease the average potential over time, thereby cooling the atoms until they reach a temperature of 2 μK. The time-averaged cooling process is quite rapid, capable of cooling the atoms from over 100 μK to 2 μK. However, reaching the BEC state using this method presents challenges due to certain constraints. A detailed analysis of this method can be found in our paper[cite later].

3.5 BEC Machine

A general overview of the experimental steps involved in making the BEC is shown in Fig. 3.5.

After undergoing through this steps, where each step is crucial, we produce Bose-Einstein condensate of ^{87}Rb atoms, with over 75,000 atoms in the BEC. The production rate ranges from 8 to 10 s, with MOT loading varying from 3 to 5 s, and evaporation taking 5 s. A BEC setup without laser system and an image of fluorescent from MOT loading is shown in Fig. 3.6.

3.5.1 Experiments with BEC Machine in Our Lab

We investigate the quantum kicked rotor Hamiltonian using cold atoms, where the cloud temperature ranges from (2-8) μK . This study includes dynamical localization, control over quantum chaos, and the investigation of exponential and non-exponential loss of coherence in quantum systems [56, 112, 165]. Additionally, we utilize Bose-Einstein condensates (BEC) to explore dynamical localization due to several advantages they offer. The narrow initial momentum width of the wave function provided by BEC aids in resolving different momentum states, facilitating precise calculations of sensitive observable. Furthermore, precise phase imprinting of lattices on BEC enables the study of

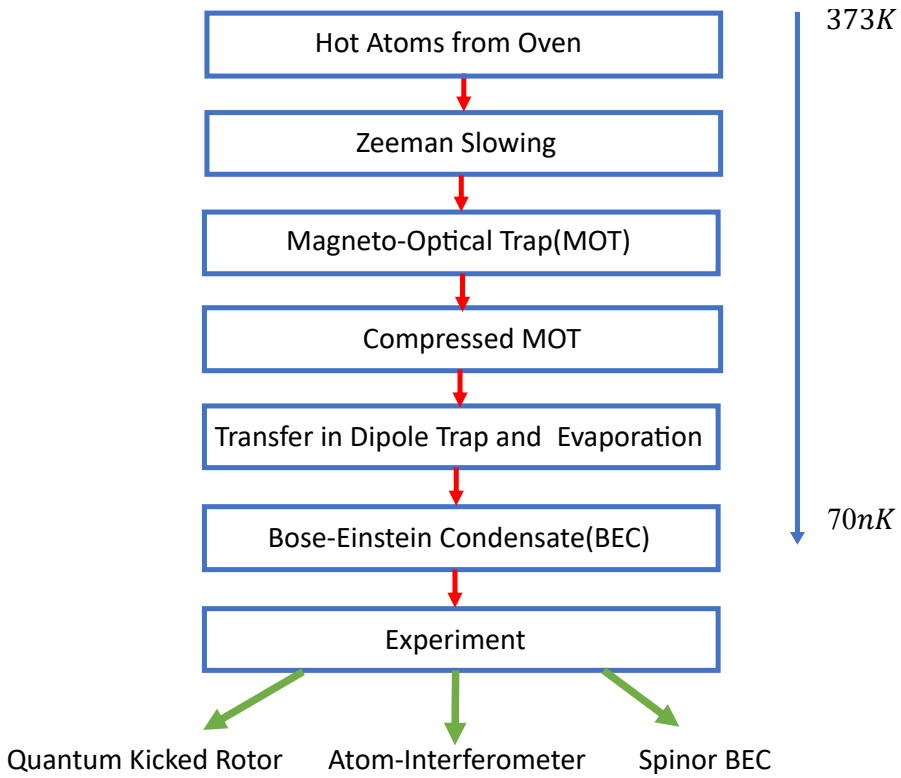

Figure 3.5: Experimental sequence. A general overview of the steps involve in production of BEC

phase-sensitive Hamiltonian and the observation of early-time quantum correlations.

Further, we utilize BEC for precision measurements by implementing atom interferometry (AI) to measure gravity [95, 166]. Additionally, we study the formation of atom lasers and their diffraction [167], investigate Talbot revival phenomena, and examine the role of momentum width in BEC [123]. Our setup is also capable of producing spinor BEC where spin collision and conservation can be studied under different conditions.

For this thesis, my main focus is on dynamical localization with cold atoms and BEC. I'll be presenting how we can control quantum systems coherently, especially in relation to dynamical localization or quantum chaos. Additionally, I'll present the investigations on asymmetric dynamical localization by launching BEC with initial velocity in periodically kicked potential and developing a method to measure micromotion using a sensitive observable.

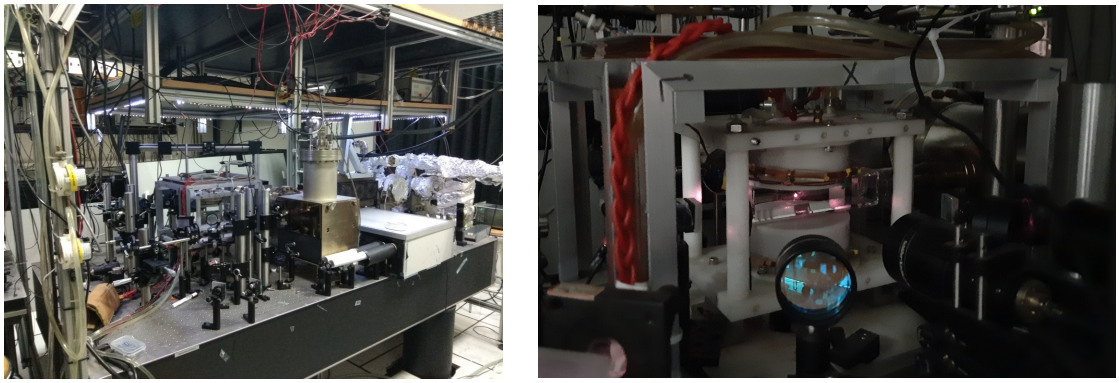

Figure 3.6: Experimental setup. BEC machine and a bright ^{87}Rb MOT

3.6 Optical Lattice and It's Interaction with Cold Atoms

A 1-D optical lattice is formed by two counter-propagating laser beams, where the interference between the lasers forms a standing wave with a periodic intensity modulation. The period of the optical lattice can be tuned by the wavelength or by changing the angle between the beams' wave-vectors. A detailed description of optical lattices can be found in references [168, 169, 169]. In our experiment, we utilize two counter-propagating laser beams with a wavelength of 780 nm. The cooled atoms reside in the state $|F = 1\rangle$. Our lattice laser is locked to $|F = 2\rangle \rightarrow |F' = 2\rangle$ transition, resulting in a detuning of 6.8 GHz. With the assistance of the optical lattice, a coherent momentum transfer to the atoms becomes feasible. By periodically switching the lattice on and off, we can transfer energy to the atoms to periodically perturb them, effectively making a system for simulating the quantum kicked rotor. Now to characterize the interaction of optical lattice with atoms, we consider a two level system, the Hamiltonian of the system in the rotating wave approximation (RWA) [169–171] is given by,

$$H = \frac{p^2}{2M} - \hbar\delta|e\rangle\langle e| + \hbar\Omega(t)\cos(2kx)(|e\rangle\langle g| + \text{H.c.}) \,, \tag{3.5}$$

Here, k is the wave-vector, δ is the detuning and $\Omega(t)$ is the Rabi frequency, here we consider it as time independent as we are not doing any pulse shaping. Substituting a linear solution $|\psi(t)\rangle = e(x,t)|e\rangle + g(x,t)|g\rangle$ in Eqn. 3.5, we get two coupled equations of ground state and excited state. But under some realistic assumption, like the

detuning being very large compared to the line-width of the transition, we can eliminate the excited state safely, so the final equation is:

$$-i\hbar\dot{g}(x,t) = -\frac{\hbar^2}{2M}\frac{\partial^2 g(x,t)}{\partial x^2} + \frac{\hbar\Omega^2}{\delta}\cos^2(kx)g(x,t)\ . \tag{3.6}$$

Now after simplification, we can see the Hamiltonian of Eqn. 3.6 is periodic and we can use Bloch theorem, and for constant Ω the solution will be Mathieu equation:

$$g(x,t) = \sum_{m=-\infty}^{\infty} g_m(t)e^{imkx}\ , \tag{3.7}$$

m is the momentum state, further solving Eqn. 3.6 by introducing Eqn. 3.7, we get a final equation:

$$-i\hbar\dot{g}_m = \hbar(\omega_r m^2 + \Omega_0)g_m + \hbar\frac{\Omega_0}{2}(g_{m+2} + g_{m-2})\ , \tag{3.8}$$

Here, ω_r is recoil frequency $\omega_r = \frac{\hbar k^2}{2M}$ and $\Omega_0 = \frac{\Omega^2}{2\delta}$. It's clear from this equation that it couples only even or odd momentum, we can continue with any one of them. A detailed calculation is done in reference [170, 172]. Now we discuss about different regime in Kapitza-dirac or Raman-Nath diffraction.

3.6.1 The Raman-Nath Regime

In the Raman-Nath regime, the interaction is for a very short time of the optical lattice with atoms, during which we assume no movement of atoms. Therefore, we can safely drop the kinetic energy term in Eqn. 3.8 and shifting the constant energy scale:

$$-i\hbar\dot{g}_m = \hbar\frac{\Omega}{2}(g_{m+2} + g_{m-2})\ . \tag{3.9}$$

The solution of the above equation is a Bessel function:

$$g_{2m} = -i^m \cdot J_m(\Omega t)\ . \tag{3.10}$$

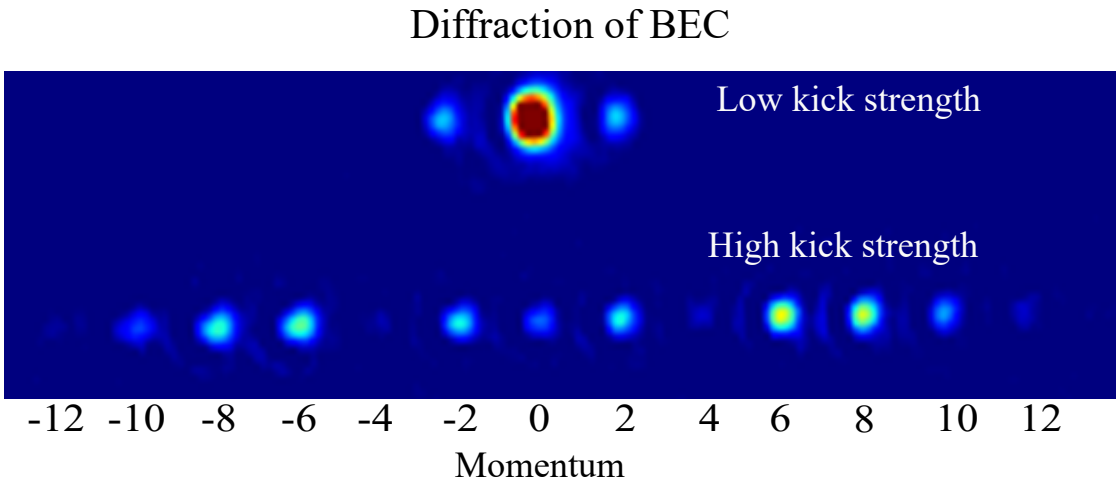

Figure 3.7: Diffraction of a BEC in different momentum states. Diffraction of BEC with a pulsed optical lattice ^{87}Rb MOT

Now the probability of finding the atoms in different momentum states $2m\hbar k$ where, m = ..-3,-2,-1,0,1,2,3..., is given by,

$$P_{2m}(t) = J_m^2(\Omega t) \ . \tag{3.11}$$

At time $t = 0$, all the atoms will be in zero momentum state. With interaction time and laser power, atoms will move to higher momentum states. By applying a short pulse (less than 500 ns to maintain the condition for delta-kicked rotor in our system) and measuring the atom's distribution in different momentum states, we quantify the strength of perturbation. An experimental distribution of BEC after applying a 500 ns optical pulse with different laser power is shown in Fig. 3.7. Using this technique, we coherently transfer energy to the system to simulate the quantum kicked rotor type Hamiltonian. For the BEC, these momentum states get resolved due to quasi-momentum being approximately 100 times less compared to the momentum of two recoil photons. However, with cold atoms, the momentum wave packets will not get resolved.

3.6.2 The Bragg Regime

In the Bragg regime, the interaction time is comparatively long, and we can not neglect the kinetic energy term in Eqn. 3.8. Just to clarify, Bragg diffraction also requires a strict resonance condition. To satisfy this resonance condition, we move the lattice with the

momentum we want to populate, or such resonance is also possible if we can move the atoms. Further if the atoms are initially at rest and the lattice is also static, it represents just a phenomenon beyond the Raman-Nath regime [170]. A detailed mathematical analysis is given in reference [172]. For the resonance condition to transfer atoms in m^{th} momentum state, we can write a simple equation from energy-momentum conservation:

$$m\hbar\Delta\omega = \frac{q^2}{2M} + \frac{\hbar}{M}\vec{k}_i \cdot \vec{q}\,, \tag{3.12}$$

Here, $q = 2m\hbar k$ and $\Delta\omega$ comes from frequency difference between lattice. By satisfying the desired resonance condition and properly creating a frequency difference between two lattices, we can induce Rabi cycles between momentum states. Bragg diffraction proves to be a useful method for generating π (mirror pulse) and $\frac{\pi}{2}$ (beam-splitter pulse) pulses for atom interferometry with a Bose-Einstein condensate (BEC). We utilize Bragg diffraction to launch the BEC with different recoil momentum into a periodically kicked optical lattice, which will be discussed further. For a stationary BEC

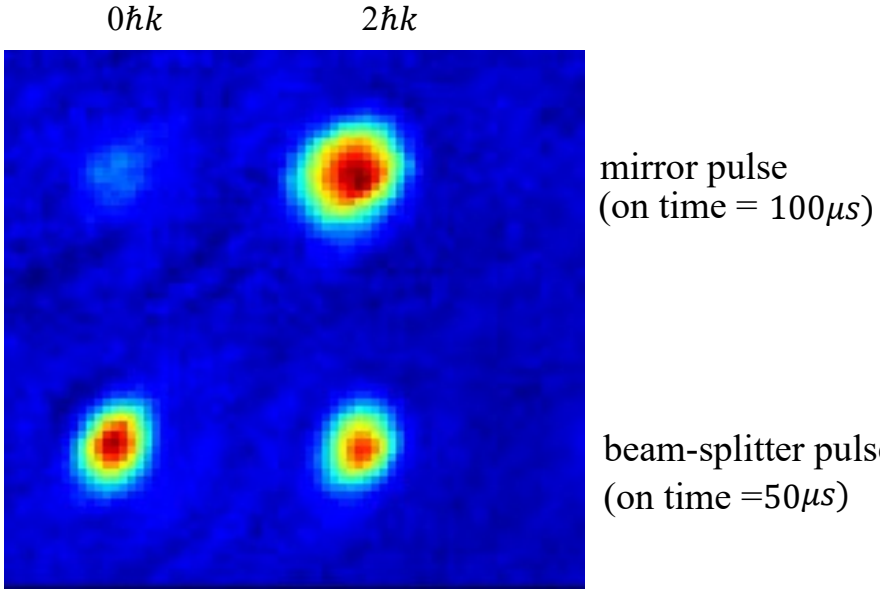

Figure 3.8: Bragg Diffraction. Bragg Diffraction of ^{87}Rb BEC between $0\hbar k$ and $2\hbar k$ with pulsed optical lattice

in the lab frame, $\vec{k}_i = 0$. Thus, for first-order Bragg diffraction, the frequency difference turns out to be $\Delta\omega = 2\pi \times 15.07$ kHz. In the experiment, we provide a frequency differ-

ence between lattice beams of 15.07 kHz for the first order and 30.14 kHz for the second order, and continue. A Bragg diffraction with 15.07 kHz frequency difference is shown in Fig. 3.8, controlling the on-time of pulse we can either completely transfer the atoms to the other momentum state or we can equally split depending on the requirements.

3.7 Conclusions

This chapter briefly described our experimental setup, which we reconstructed with a few advancements following the COVID-19 pandemic. We incorporated machine learning techniques for BEC production and developed a novel time-averaged cooling method for evaporative cooling. After running the BEC setup for six years, I can say it's one of the most reliable setups out there with flexibility of experiments. It consistently produces BECs without needing daily optical alignment or running into frequent problems.

Chapter 4

Demonstration of Coherent Control of Dynamical Localization in Quantum Chaotic System

This chapter has been published as:

"Interplay between quantum diffusion and localization in the atom-optics kicked rotor" ***S. Sagar Maurya****, J. Bharathi Kannan, Kushal Patel, Pranab Dutta, Korak Biswas, Jay Mangaonkar, M. S. Santhanam, and Umakant D. Rapol,* Phys. Rev. E*,* ***106, 034207 (2022)***

In this chapter, we present a modification to the kicked rotor model, both through experimental investigation and numerical analysis. By introducing half Talbot time delays in the kicking sequence which is equivalent to reversing the kick strength, we establish a modified atom-optics kicked rotor system. Notably, the modified system exhibits increased quantum mean energies with higher localization length in comparison to the standard kicked rotor model. These results not only contribute to our understanding of quantum chaos in the kicked rotor paradigm but also hold significant implications in coherent control over quantum phenomena. The scheme also provides another route to quantum control in the kicked rotor class of systems, particularly when such a control arises from a competition between quantum diffusion and localization.

4.1 Background and Definition of the Problem

The kicked rotor (KR) model has been extensively investigated as a paradigmatic model of both classical and quantum chaos [39, 173]. The atom-optics based kicked rotor (AOKR) is an experimentally realizable analog of the KR model in which an ensemble of cold atoms are periodically kicked by sinusoidal potentials formed by a counter-propagating standing wave of light [49, 52, 59, 114]. The classical limit of AOKR is chaotic for sufficiently strong kick strengths and exhibits intrinsic stochasticity in its dynamics. In this limit, KR behaves similar to a random walk. As the kicks impart energy to the system, diffusive growth of mean energy is observed. In contrast, the quantum regime entirely suppresses the classical diffusive growth beyond a short break-time due to destructive quantum interference [39]. This is the regime of dynamical localization and is the momentum-space analogue of Anderson localization in real space. This shows up as wave-functions localize in the momentum space, $\psi_p \sim e^{-p/\xi}$, where p labels discrete momentum basis states and ξ is the localization length. Further, AOKR and its variants are studied in other fields – condensed matter physics [48, 174], molecular physics [175, 176], and quantum information [177, 178] – to explore quantum correlations to many-body localization. See Ref. [39] for a recent review of variants and applications of kicked rotor system.

For many applications in the emerging areas of quantum technologies, it is important to be able to control the quantum effects. In the context of AOKR, the ability to control localization length and the energy of localized states can be useful [42]. Dynamical localization is generally destroyed by the addition of noise through decoherence processes and does not provide a means of quantum control. For example, it has been shown that decoherence in the form of noise [179–181], coupling with rotor [182], and quantum measurements [177] can destroy dynamical localization. However, surprisingly, it was shown experimentally that Levy noise added to kick sequences of AOKR could control the decoherence rate and even the mean energy of localization, the Levy parameter in the noise distribution acting as the control parameter [56]. More conventional routes to exercise control is by manipulating the phases of the initial wave-function. For instance, it was shown previously that quantum-chaotic diffusion can be enhanced or suppressed

by controlling the phases of the initial states [128, 129]. However, in order to control the localization length, the unitary evolution operator that evolves the initial state needs to be changed and is not achievable by just controlling the phase of the initial state. In one such novel control scheme, introduced by Gong and Brumer [119], the phase of the kicking field is flipped periodically. By changing the sign of the kicking potential after M kicks (corresponds to introducing a phase shift among rotor momentum states), a significant change in the dynamical localization and quantum diffusion was observed. This variant of AOKR is different from the amplitude-modulated KR systems [125], in which the kick strength is varied. Quantum control in the context of AOKR has been experimentally realized by phase modulation [58, 111] and also in laser-kicked molecular rotors using time delay [42].

In the work, we experimentally realize a protocol of quantum control (similar in spirit to the one introduced in Ref. [119]) of diffusive and localized phases by appropriate modulation of the perturbations. Effectively, the sign of the kick strength in the KR system is periodically flipped. This is achieved using periodic time delayed kicks after a certain number of standard kicks that induce dynamical localization. Quite remarkably, this simple modification of kick sequences in AOKR does not destroy localization but leads to an enhancement of quantum energy at which localization takes place. In contrast to the earlier work [119] that depend on presence of classical transporting islands in phase space for energy enhancements, we show that enhancements arise from a competition between two time periodic sequences in the AOKR system.

4.2 Modified Atom-Optics Kicked Rotor

Just to point out, we emphasize the crucial differences between the standard KR and AOKR. AOKR is a system of kicked atoms moving on a line, while the standard KR can be visualized as rotors moving on a circle. With a sufficiently broad initial distribution of momenta, the dynamics of AOKR involves the play of different quasi-momenta β, while for the standard KR it is generally restricted to $\beta = 0$. Due to these differences, the modified kicked rotor (MKR) is presented as a motivation and a benchmark for the main ideas. All the experimental results are compared, not with MKR but, with the simulations of the floquet operator of the AOKR averaged over quasi-momenta β.

We start with the modified kicked rotor model (MKR), and the modified *atom-optics* kicked rotor (MAKR) presented at the end of this section. The experimental and simulation results are reported in subsequent sections.

The system of interest is a modified form of kicked rotor given by [119],

$$H = \frac{p^2}{2} + K\cos(x)\sum_n f_M(n)\,\delta(t-n), \tag{4.1}$$

where p and x denote the dimensionless momentum and position respectively, K is the chaos parameter, and time t is scaled by the pulse period T such that $t \to t/T$. If $f_M(n) = 1$, then Eqn. 4.1 is just the standard KR. In this work, $|f_M(n)| = 1$, and $f_M(n)$ changes sign after every M kicks. In rest of this paper, Eqn. 4.1 will be referred to as the modified kicked rotor (MKR) model, and it can be thought of as a specific realization of a generalized KR model in Ref. [183]. By discretizing the Hamilton's equation of motion corresponding to Eqn. 4.1, a formal map connecting the position and momentum variables at time n and $n + 2M$ with $M \geq 1$, can be written down as

$$x_{n+2M} = F_1(x_n, p_n), \qquad p_{n+2M} = F_2(x_n, p_n). \tag{4.2}$$

In this, $F_1(,)$ and $F_2(,)$ are the map functions. In general, these map functions are sufficiently simple for the standard kicked rotor, but can get increasingly cumbersome to write down explicitly for $M \geq 2$. However, numerical determination of the stroboscopic map is straightforward.

In Fig. 4.1 the classical stroboscopic section of KR (a), MKR with $M = 2$ (b) and with $M = 3$ (c) for kick strength $K = 5$ is shown. As evident in Fig. 4.1(a), the phase space is largely chaotic with a few regular islands. An ensemble of initial conditions launched from these islands will remain bound to these islands. In the case of MKR with $M = 2$, special non-chaotic structures called transporting trajectories exist in phase space, as seen in the inset of Fig. 4.1(b). Transporting islands are present in many periodically driven dynamical systems, *e.g.*, standard map [184], Hamiltonian ratchets [185], atomic KR [46, 186] and are usually referred to as the accelerator modes because they support ballistic classical diffusion, *i.e.*, $\langle E\rangle_n \propto n^2$, where n is the no of kicks. The quantum accelerator modes have been realized in cold atom experi-

ments [187–189]. In the MKR, anomalous diffusion is observed in which $\langle E\rangle_n \propto n^\gamma$ with $1 < \gamma < 2$. Physically, this situation arises due to the "stickiness" of the boundary between the transporting trajectories and the chaotic sea. In contrast, the phase space is chaotic for $M = 3$ (Fig. 4.1(c)) and leads to normal diffusion. The classical energy $\langle E\rangle_c$ growth versus the number of kicks is shown in Fig. 4.1 (d), for various M values. Due to the presence of transporting islands, it is clear that the classical energy growth is enhanced for $M = 2$ when compared to that for other values of M. It also exhibits anomalous diffusion compared to other values of M, which shows linear diffusion. The transporting islands play a significant role in quantum dynamics even though their area in the phase space is tiny [119]. The presence of these transporting trajectories is ambiguous for MKR with larger values of M [119]. Now let us explore the quantum dynamics of MKR in the parameter space where transporting trajectories are present in their classical phase space of MKR with $M = 2$ as seen in Fig. 4.1 (b) and compare it with the properties of KR. The quantum dynamics of MKR can be obtained by solving the time-dependent Schrödinger equation corresponding to the MKR Hamiltonian. The split evolution technique is implemented to evolve the initial state according to the Schrödinger equation [184].

To build the quantum dynamics of MKR, let us consider the period-1 Floquet operator corresponding to the standard kicked rotor $\widehat{F}^{\pm}_{\rm KR}$ for which $f_M(n)$ is a constant, *i.e.*, $f_M(n)$ is either $+1$ or -1 for all n.

Thus, the required operator is

$$\widehat{F}^{\pm}_{\rm KR} = \exp\left(i\frac{\hbar_{\rm eff}}{2}\frac{\partial^2}{\partial x^2}\right)\exp[\mp i\frac{K}{\hbar_{\rm eff}}\cos(x)], \tag{4.3}$$

where $\hbar_{\rm eff} = T\hbar$ is the scaled Planck's constant, $\Phi_d = K/\hbar_{\rm eff}$ denotes the strength of phase modulation imparted by the kicks. Using this as the building block, the Floquet operator for MKR can be constructed as M application of $\widehat{F}^{+}_{\rm KR}$ followed by M applications of $\widehat{F}^{+}_{\rm KR}$. Thus, for MKR, we obtain

$$\widehat{F}_{\rm MKR} = \left(\widehat{F}^{-}_{\rm KR}\right)^M \left(\widehat{F}^{+}_{\rm KR}\right)^M \tag{4.4}$$

To implement this Floquet Hamiltonian in an atom-optics experiment, the sign of

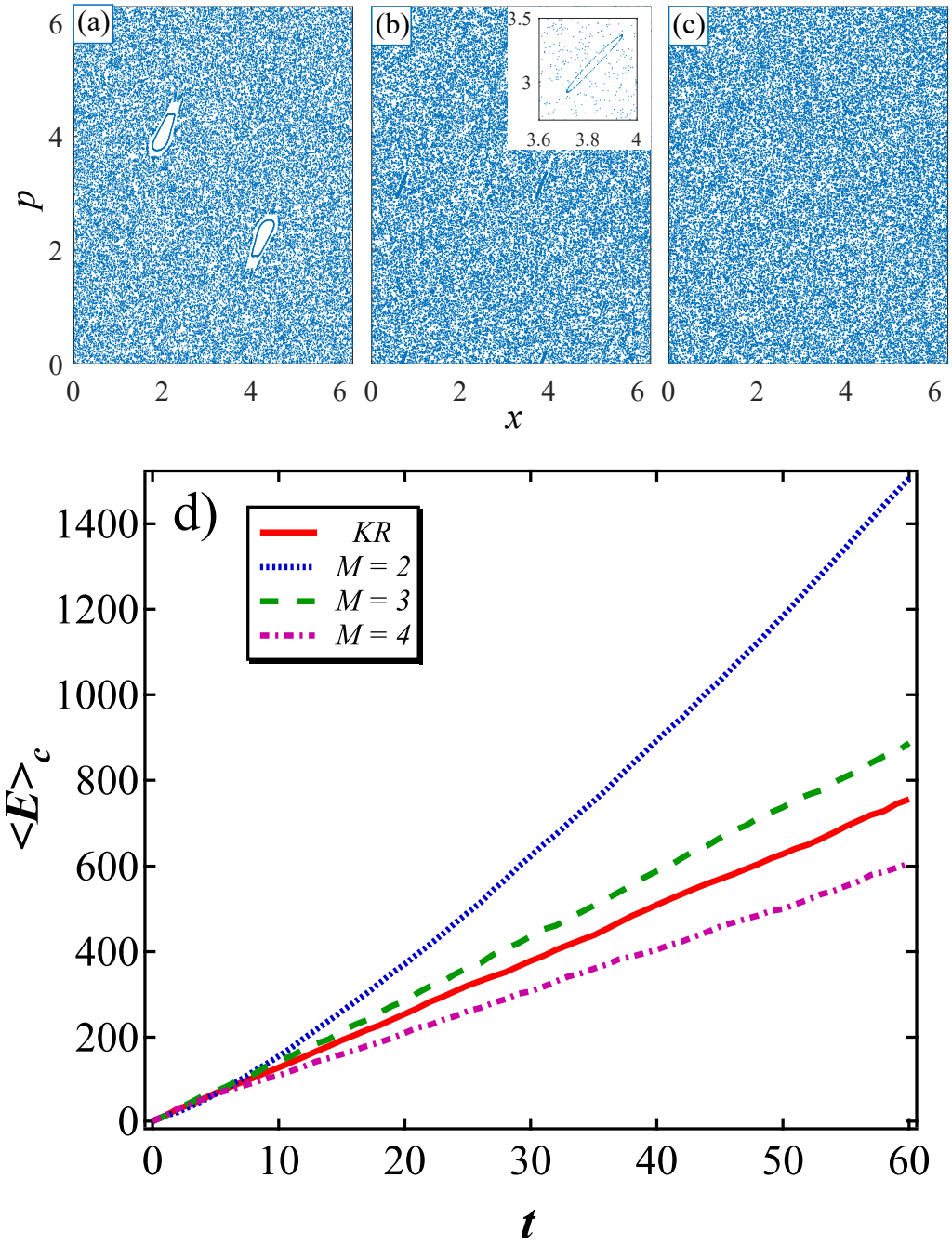

Figure 4.1: Phase portraits and classical energy growth. Phase portrait's of the standard ($M = 0$) and modified kicked rotor ($M > 0$). The parameters are kick strength $K = 5$ and (a) $M = 0$, (b) $M = 2$ and (c) $M = 3$. The regular islands in the chaotic sea in (a) are non-transporting whereas those in (b) are transporting in nature, albeit much smaller in size. The inset in (b) shows an enlarged view of one of these islands. No regular structures are visible in (c). The classical energy $\langle E \rangle_c$ growth for various vales of M at $K = 5$ is shown in (d).

the phase modulation must change with periodicity M as dictated by Eqn. 4.4. The kicking scheme of Eqn. 4.4 is shown in Fig. 4.2(a) and simulated time evolution of mean quantum energy $\langle E\rangle_q$ is shown in Fig. 4.2(b) for KR and MKR with $M = 2$. The inset in Fig. 4.2(b) represents the momentum distribution. However, this type of Hamiltonian is difficult to realize in experiments since it involves abrupt sign change of the kicking potential after M kicks. An alternative method to realize MKR is by introducing controlled time delays after every M kicks [119]. Consider a wave-function of the system $\Psi(x,t)$ at any time t. This can be expanded in the momentum basis as:

$$\Psi(x,t) = \sum_m A_m \langle x|m\rangle, \tag{4.5}$$

with A_m being the expansion coefficients. The flipping of sign of K can also be thought of as shift in spatial coordinate by π, since $K\cos(x+\pi) = -K\cos x$. Hence, it is convenient to use $x \to x+\pi$ instead of $K \to -K$. Now, to see its effect on the momentum basis states, let us consider

$$\Psi(x+\pi,t) = \sum_m A_m \langle x+\pi|m\rangle = \sum_m A_m \exp i(x+\pi)m = \sum_m (-1)^m A_m \langle x|m\rangle. \tag{4.6}$$

It is clear that the change of sign of kicking strength effectively introduces a phase difference of π between the neighboring states. This phase difference can also be generated by introducing time delays in the system. To see this, consider the action of a free-evolution operator of MKR for $t = T$ acting on a momentum state:

$$\exp\left(ip^2T/2\hbar\right)\ |m\rangle = \exp\left(im^2\hbar T/2\right)\ |m\rangle \tag{4.7}$$

From this, we can estimate the duration of free evolution T_d required to obtain a phase-difference of π between neighboring momentum states. For a phase difference of π, the condition to be satisfied is $\exp\{i\hbar T_d[(m+1)^2 - m^2]/2\} = \exp(i\pi)$, and from this we get the time duration to be

$$T_d = \frac{2\pi}{\hbar} = \frac{2\pi T}{\hbar_{\text{eff}}}. \tag{4.8}$$

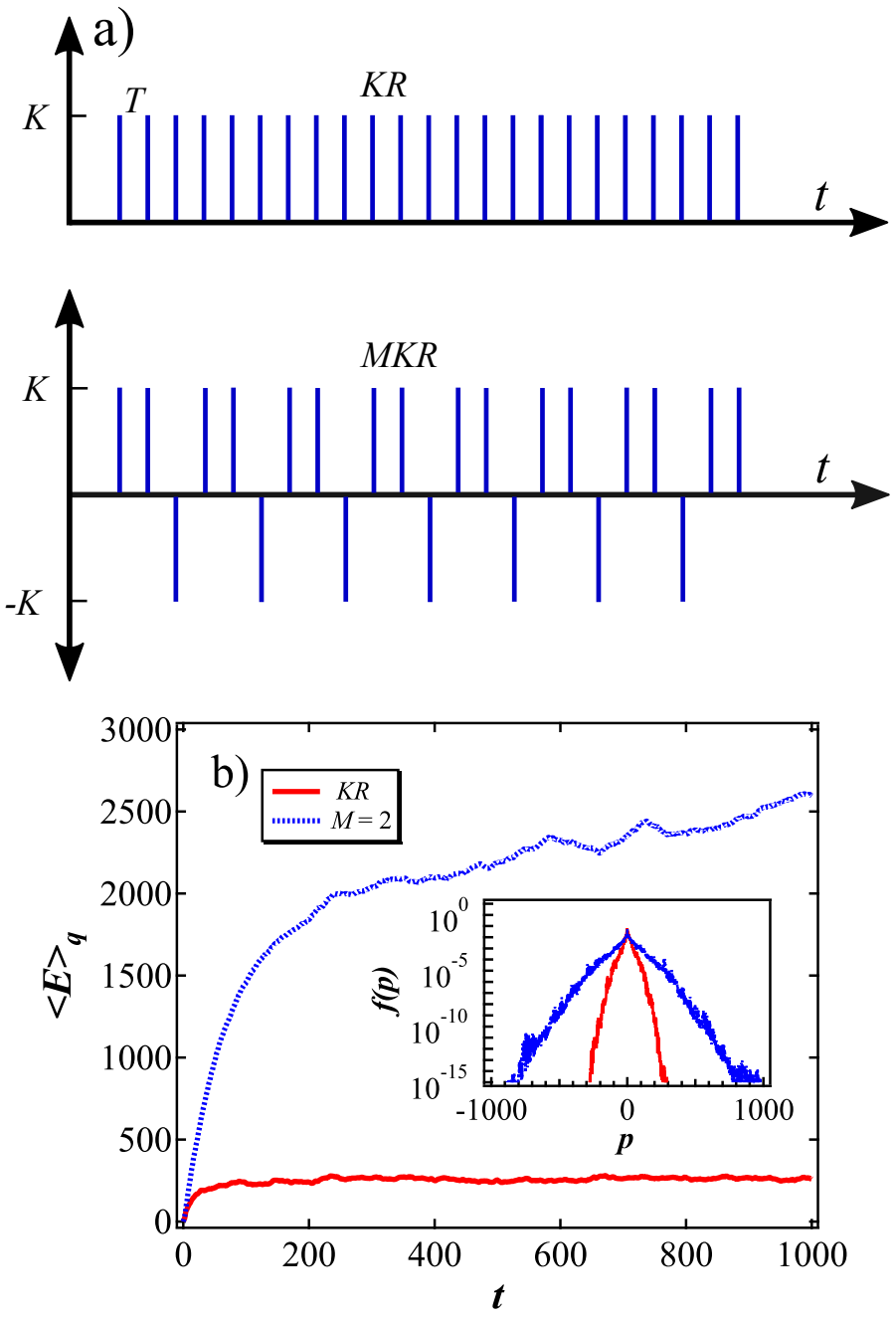

Figure 4.2: Kicking scheme and quantum energy growth. (a) Pulse scheme for the regular and modified kicked rotor at $k = 5$ and $\hbar_{eff} = 1$ ($K = 5$). For $M = 2$, the sign of K is flipped alternatively. (b) Simulated energy evolution of KR (dashed line) and MKR with $M = 2$ (solid line). The quantum energy $\langle E \rangle_q$ for $M = 2$ localizes at a higher energy. Inset plots (in a semi-log scale) the momentum distribution of for the same at $t = 1000$.

This delay corresponds to half Talbot time and has the same effect as flipping the sign of the kick strength between the pulses [119]. Fig. 4.4(a) shows the kicking scheme for MAKR with $M = 2, 3$ and 4. including the delay time T_d. Due to the presence of two periods, the system is no longer periodic with time period T, but has an effective period of $T(M-1)+T_d$. Thus, the Floquet operator for the modified *atom-optics* kicked rotor $\widehat{F}_{\mathrm{MAKR}}$ is given by:

$$\begin{aligned}\widehat{F}_{\text{MAKR}} &= \left\{\exp\left[-i\frac{\hbar T_d}{2}(\hat{p}+\beta)^2\right]\exp\left[-i\frac{K}{\hbar_{\text{eff}}}\cos(\hat{x})\right]\right\} \\ &\times\left\{\exp\left[-i\frac{\hbar_{\text{eff}}}{2}(\hat{p}+\beta)^2\right]\exp\left[-i\frac{K}{\hbar_{\text{eff}}}\cos(\hat{x})\right]\right\}^{M-1} \\ &= \widehat{\mathbf{F}}_{\text{KR}}\widehat{F}_{\text{KR}}^{M-1}.\end{aligned} \tag{4.9}$$

where $\hat{p} = -i\frac{\partial}{\partial x}$ and β is the quasi-momentum. In this, $\widehat{F}_{\mathrm{KR}}^{M-1}$ denotes $M-1$ applications of $\widehat{F}_{KR}$ for time duration T, and $\hat{\mathbf{F}}_{KR}$ denotes the application of kicked rotor Floquet operator with a free propagation time of T_d. The existence of two time periods, T and T_d in the atom-optics version of the kicked rotor system makes it different from the standard KR system.

It is worth pointing out that when studying resonance phenomena for a finite-temperature cloud, we should take into account $\beta \neq 0$ since all the quasi-momentum sub-spaces are initially populated. The Floquet operator governing the dynamics in each quasi-momentum subspace is explicitly dependent on β [see Eq.(4.9)]. This leads to the overall dynamics exhibiting significant differences when compared to the case of standard QKR in which case the dynamics are restricted to the $\beta = 0$ subspace. At anti-resonance AOKR exhibits a significant momentum spread and a diffusive growth of the particle energy, whereas the energy of the standard QKR is localized [117]. In a thermal cold atom cloud, atoms have a non-negligible initial velocity relative to the standing wave potential, and this non-integer "quasi-momentum" determines the behavior under half-Talbot time kicking. Before the results are discussed, a brief review of experimental procedure is in order. The experiment begins with a brief description of the optical lattice formation, achieved through the precise arrangement of counter-propagating laser beams. This lattice serves as the foundational framework for the subsequent interactions with

atoms considering it's detuning from resonance transition and it's power. Mainly, I will discuss the Kapitza-Dirac diffraction in Raman-Nath regime, this is the way we transfer the energy to the atoms. Moreover, a critical aspect of the experimental process involves quantifying the strength of perturbation directly related to K. Measuring K properly in experiment is important, K suffers from approximately 10% error in experiment, we also discuss the measurement of K utilizing BEC.

4.3 Atom-Optics Experimental Setup

First, we discuss the experimental setup. The variables and parameters of kicked rotor system and AOKR are related as follows: $x \rightarrow 2kx$, $p \rightarrow 2kTp/m$, and $\hbar_{\text{eff}} = 8\omega_r T$ where k, m and ω_r are the wavenumber of the optical lattice beam, mass of the atoms and recoil frequency respectively. The amplitude modulation depth or the kick strength is $\Phi_d = \Omega^2\tau/8\Delta$, where Ω, Δ and τ are the resonant Rabi frequency, the detuning of the light used to create the optical lattice potential and the pulse duration respectively. The experimental setup is the same as described in Ref. [56]. We create a cold thermal ensemble of ^{87}Rb consisting of 2×10^5 atoms every 12 seconds (our old setup) in a crossed optical dipole trap. The temperature of the thermal cloud is about $5\ \mu K$. The optical standing wave is formed with two counter propagating laser beam(shown in Fig. 4.3) as the atoms are present in $|F = 1, m_F = -1\rangle$ state. The laser used for realizing the standing wave is locked to the $|5\ S_{1/2}, F = 2\rangle \rightarrow |5\ S_{3/2}, F' = 2\rangle$ D2 transition at 780 nm and is thus 6.8 GHz red-detuned from the atom's accessible transition. With the help of optical lattice, we transfer the energy to the atoms by switching it on and off according to model Hamiltonian. To synthesize the MKR Hamiltonian, the off-time between the delta pulses is adjusted. The on-time τ of the standing wave is kept as 100 ns.

The quantum AOKR is governed by two dimensionless parameters: $\hbar_{\text{eff}}$ and K. The scaled Planck constant ($\hbar_{\text{eff}}$) is directly proportional to period of the kicks and $K = \Phi_d\hbar_{\text{eff}}$. To keep K fixed, Φ_d is adjusted for different values of $\hbar_{\text{eff}}$. To calibrate the kick strength Φ_d, we use Raman-Nath diffraction (as discussed in Section 3.6.1) on an almost ideal zero-momentum state *i.e.*, a Bose-Einstein Condensate. The number of atoms in the m^{th} momentum state after undergoing diffraction is a Bessel function

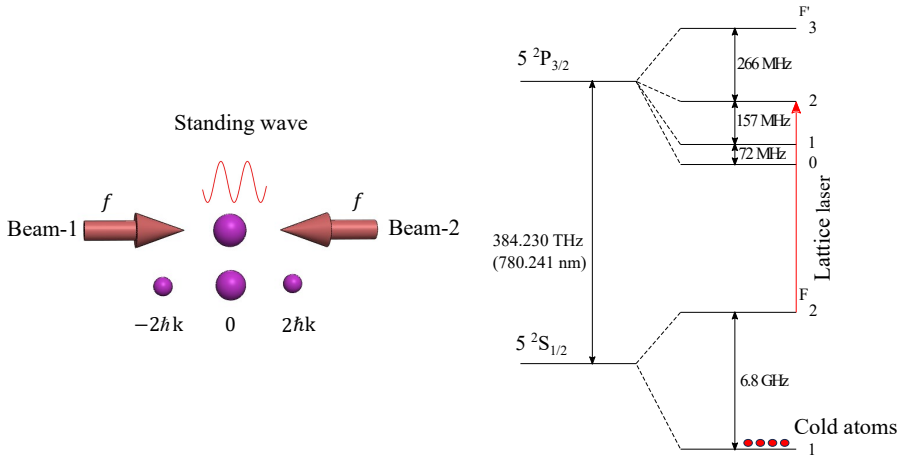

Figure 4.3: Standing wave and lattice laser. The left image is showing the optical lattice formed by two counter propagating laser beam and diffraction of the atoms. The right image is showing the lattice laser frequency and it's detuning from atoms energy level

$J_m^2(\Phi_d)$. Thus, Φ_d can be accurately determined by measuring the distribution and fitting it to this Bessel distribution [123]. As mentioned before, for MKR, we use a time delay of half Talbot time ($\sim 33.17\ \mu s$ for ^{87}Rb and $2\pi/k = 780$ nm) to introduce appropriate phase relations between the diffracted wave-packets.The timing error fluctuations are of the order of picoseconds ensuring good control over tuning this phase according to Hamiltonian. The optical lattice is arranged in a retro-reflected configuration, making it more stable against vibrational phase noise.

4.4 Evolution of Mean Energy

In experiments, the initial state consists of an ensemble of atoms with a finite momentum spread. In order to model a thermal cloud of cold atoms, numerical simulations are performed using Eqn. 4.9 operating on a Gaussian distributed momentum state.

$$|\psi(t=0)\rangle = \int_{-1/2}^{1/2} d\beta \sum_{p=-\infty}^{\infty} D_p(\beta)^{1/2} |p+\beta\rangle, \tag{4.10}$$

where $p \in \mathbb{Z}$, and $D_p(\beta) = \frac{1}{w\sqrt{2\pi}} \exp\left[-\frac{(p+\beta)^2}{2w^2}\right]$ is the Gaussian momentum distribution with zero mean and standard deviation w as a function of quasi-momenta $\beta \in (-1/2, 1/2)$ [117]. In practice, the summation over p in this equation is carried

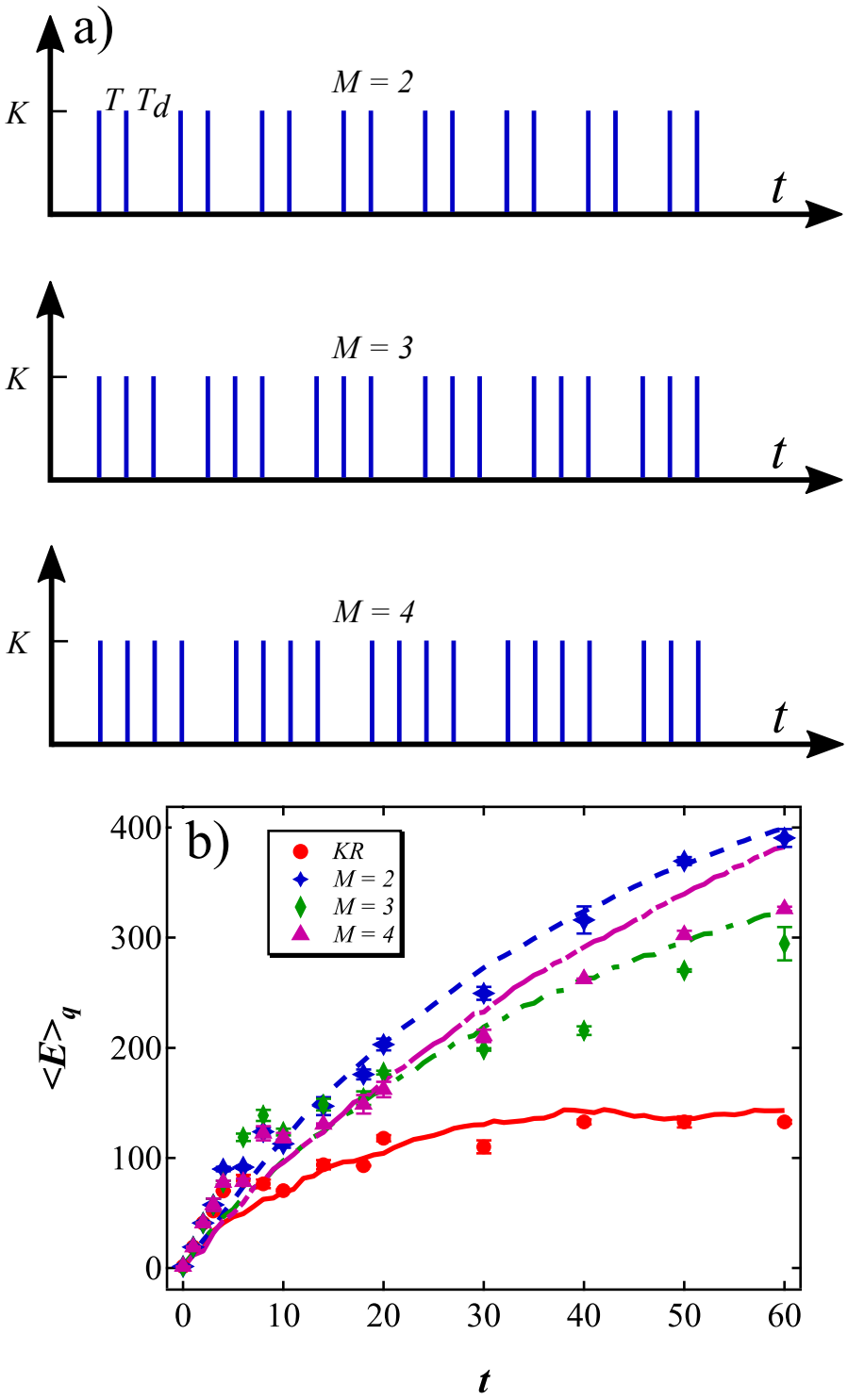

Figure 4.4: Kicking scheme of MKR and mean energy growth. (a) Kicking scheme for MAKR with $M = 2, 3, 4$. This scheme also shows the delay time T_d. (b) Mean quantum energy $\langle E \rangle_q$ evolution for different values of M at $K = 5$ and $\hbar_{\text{eff}} = 1$. The solid lines and markers indicate the numerical simulation and the experimental data respectively.

out over only a finite set of momentum basis states.

4.4.1 $M = 2$ case

The kicking scheme for MKR is shown in Fig. 4.4(a). The time evolution of mean quantum energy from the numerical simulations of MKR using Eqn. 4.4 is shown in Fig. 4.4(b). For the standard KR, the mean energy displays the expected linear increase for short times (within break-time t_b of order $K^2/2$). For $t > t_b$, the quantum effects become significant and dynamical localization is realized. For the same set of parameters as that for KR, except that $M = 2$, a pronounced enhancement in the saturated energy is evident in this figure. Dynamical localization occurs for $M = 2$ as well. In case of MKR, with $M = 2$ and $K = 5$, transporting trajectories are present in phase space as seen in Fig. 4.1(b). Thus, as argued in Ref. [119], in the quantum regime, the mean energy corresponding to MKR is enhanced with respect to the standard KR. Further, the width of momentum distribution (shown as inset in Fig. 4.2(b)) is also significantly enhanced for MKR compared with KR. For other parameters as well, transporting islands lead to an enhancement in quantum energy upon depending on the size of the island [119]. In this paper, due to experimental constraints, we will work with the parameters used in Fig 4.2 along with $M = 3, 4$.

Now, we will compare this phenomenon with the experimental results. Fig. 4.4(a) shows the kicking scheme for MAKR with $M = 2, 3, 4$ including the delay times T_d. Figure 4.4(b) displays the corresponding results for mean energy evolution from our atom-optics experiment. This figure shows both the experimental data (solid symbols) as well as the numerical simulations (lines) of MAKR obtained using the Floquet operator in Eq. 4.9. A good agreement is observed between the experimental and numerical simulations. At first sight, it is tempting to attribute the energy enhancement seen in the experiment to entirely the presence of transporting islands. However, these islands exist in phase space only over a small range of K. In the experiment, the value of kick strength K suffers from approximately 10% error that washes out most of the contribution arising from transporting islands. Further, the quantum contribution depends on the value of effective Plancks constant $\hbar_{\text{eff}}$ relative to the classical phase space structure whose effect is being probed [190]. In our case, the values chosen for $\hbar_{\text{eff}}$ are large

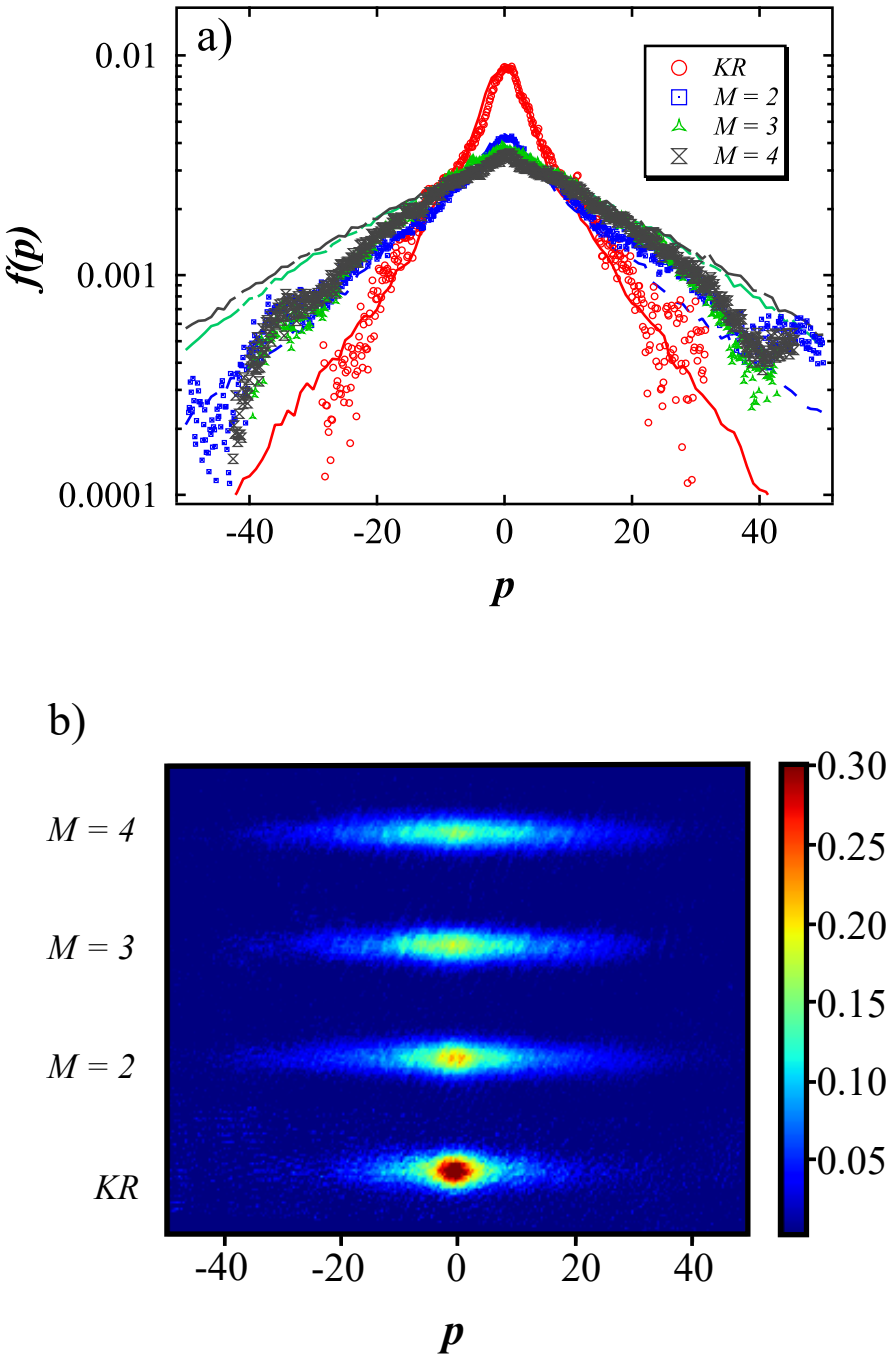

Figure 4.5: Momentum distribution and absorption image. (a) Momentum distribution profiles for $M = 0, 2, 3$ and 4 at the parameters $K = 5$ and $\hbar_{\text{eff}} = 1$. The markers and solid lines denote experimental and simulated momentum profiles respectively. $M = 2$ clearly shows enhanced localization length. (b) Absorption images for different values of M with $\hbar_{\text{eff}} = 1$ and $K = 5$.

relative to the small area of transporting islands. Hence, the quantum contribution of these island structures is not very significant. Bulk of the enhancement arises due to the presence of two time scales T and T_d in the MAKR system. An interesting interplay between the two time periods T and T_d is seen. The time evolution with a pulse period of T along with the kick strength Φ_d is arranged such that it induces localization in the system. For an initial state with significant momentum spread ($w \gtrsim 1$) a pulse period corresponding to half Talbot time T_d leads to a linear diffusive growth in energy [114, 117]. The dynamics of MAKR is governed by the competition between these contrasting behaviors of localization and diffusion.

In our experiments, the MAKR system can be evolved only up to 60 kicks due to constraints of the experimental arrangement. For a finite number of total kicks N applied to the atomic cloud, the number of (diffusion inducing) free evolution phase with time period T_d is $N_d = N/M$. Number N_l of localization-inducing evolution phase with time period T is $N_l = (M-1)N_d$. Thus, if $M \gg 1$, then $N_l \gg N_d$. In this scenario, localization effects dominate and diffusion is suppressed. This corresponds to the standard KR limit (the lowermost curve (red curve) in Fig. 4.4(b)). In the other limit, as $M \to 1$, diffusive growth of energy is strongly favoured over localization. The competition between these processes determines the enhancement of saturated energy in MAKR system. In a short time scale, the localization is destroyed by anti-resonance, but eventually localization sets into the system due to destructive interference in the momentum space. In particular, the contribution of classical transporting islands is not very significant. For $M = 1$, diffusion is dominant and localization is completely suppressed. For $M = 2$, we get $N_d = N_l$. Hence, we can anticipate localization as well as diffusive phase. Consistent with this constraint, both the experiment and numerics (blue color in Fig. 4.4(b)) show an enhancement induced by the diffusive phase as well as localization in the form of saturated mean energy.

In particular, we emphasize that the contribution of classical transporting islands is not very significant for $M = 2$. This argument presented above also implies that the enhancement in saturated energy should be seen for $M = 3, 4$ as well even though classically no transporting islands are present in phase space (see Fig. 4.1(c)). We shall consider these cases in the next section.

4.4.2 case of $M > 2$

For $M > 2$, $N_l > N_d$. This guarantees that localization can be seen for all $M > 2$. However, since N_d decays as M increases, the diffusive phase weakens. Hence, at any given number of kicks, the highest energy reached for $M > 2$ will always be lesser than that for $M = 2$. Figure 4.4(b) displays quantum energy $\langle E \rangle_q$ against the number of kicks for $K = 5$ and $\hbar_{\text{eff}} = 1$ for MAKR for $M = 3$ and $M = 4$. Even for $M = 3, 4$, a significant enhancement in the energy is seen. This is purely attributed to the half Talbot time evolution's T_d in the kicking sequence, as the classical phase space is completely chaotic. As argued in the previous section, two competing effects are at play – localization induced by the evolution over time-period T and diffusion due to time delay T_d. The long-time behavior of MKR would exhibit complete localization [119], even though it is not apparent in Fig. 4.4(b) due to the small number of kicks in the experiment.

From Fig. 4.5(a) of the momentum distribution in semi-log scale for KR and MAKR with $M = 2, 3, 4$ deduced from absorption images shown in Fig. 4.5(b). It is clear that the width of the distribution is larger for $M = 2, 3, 4$ as compared to that of standard KR. a This is also visible in the absorption images that carry more weight in the higher momentum states. After many kicks, numerical simulations begin to deviate from experimental data in Fig. 4.5 due to errors in deducing the number of atoms in the higher momentum states via absorption imaging. The experimental momentum distribution for $M = 2, 3, 4$ are qualitatively similar and show a non-exponential profile. Hence, the localization length is not a good measure to quantify the extent of localization.

For a wave-function (in momentum representation) $\langle m|\psi\rangle$, one of the commonly used localization measures is the inverse participation ratio (IPR), define as [191, 192]

$$I_D = \sum_{m=1}^{D} |\langle m|\psi\rangle|^4, \tag{4.11}$$

where D is the dimension of the Hilbert space in which $\langle m|\psi\rangle$ resides. A localized wave-function will have $I_D \sim 1$, while for a completely delocalized wave-function $I_D \propto 1/D$. Smaller values of I_D correspond to wave-functions spread over larger

set of basis states. As evident in Fig. 4.6, the IPR for $M = 2, 3, 4$ all have a much

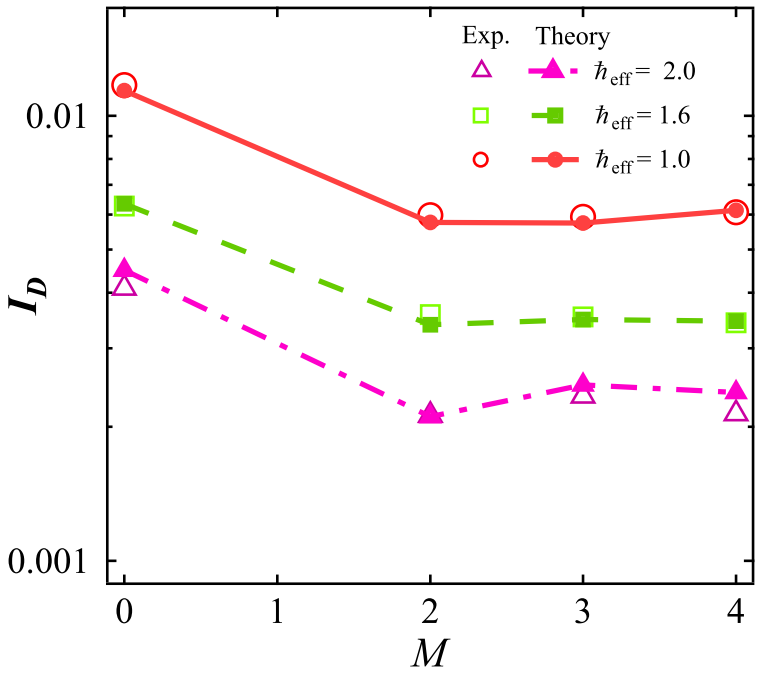

Figure 4.6: Calculation of IPR. IPR for experimental data as a function of M for different values of $\hbar_{\text{eff}}$ while maintaining the kick strength constant at $K = 5$. Errors bars for experimental data lie within the marker, hence, they are not shown here.

lower value compared to the KR, implying the spread in the momentum distribution and energy enhancement compared to KR. But I_D for $M = 2, 3, 4$ are very close to each other, indicating that the spread is almost the same for all of them. As transporting islands of significant size are only present in the case of MKR with $M = 2$ ($K = 5$), one would expect to have a maximum energy enhancement and momentum distribution spread for $M = 2$ [119]. But in our case, we observe the momentum distribution to be very close to each other for all the $M = 2, 3, 4$. This implies that the enhancement in the localization length or momentum distribution spread arising from transporting islands for $M = 2$ is less significant in MAKR. The dynamics is largely determined through the interplay of two time periods in the system. It has been shown that very small changes to the system parameters (Φ_d and $\hbar_{\text{eff}}$) can lead to the destruction of transporting islands present in the classical phase space and non-exponential shape of quantum momentum distribution [119]. This change in the line shape for dynamical localization even occurs

without causing an obvious difference in energy absorption behavior. A similar type of enhancement of dynamical localization length and energy absorption is observed for various values of M and for a range of parameters Φ_d and $\hbar_{\text{eff}}$ in the MKR model. The only requirement being that Φ_d should be sufficiently large for dynamical localization to take place in the system. As in the standard KR, the experimental data in Fig. 4.5 shows that for a fixed M, a decrease in $\hbar_{\text{eff}}$ is associated with broadening of the wave-function profile. Hence, I_D increases as $\hbar_{\text{eff}} \to 0$.

4.5 Conclusions

In this work, we have studied a modified kicked rotor model as well as its experimental implementation in an equivalent atom-optics based testbed. The model considered here is the modified atom-optics kicked rotor model, in which the sign of the kick strength (in the standard KR) is flipped after every M kicks. In the experiment, the modified atomic kicked rotor is realized by introducing appropriate time delays (equal to half Talbot time) in the kicking sequence, which is equivalent to flipping the sign of the kick strength. Introduction of periodic time delays in the KR system creates drastic changes in the dynamics as a result of two competing effects – one is the localization effects induced by periodic kick sequences of time period T and the other is the diffusive effects induced by sequences with delay time T_d equal to the half Talbot time. It is shown that the modified atom-optics kicked rotor system with $M = 2, 3, 4$ shows enhanced quantum mean energies when compared to the standard kicked rotor model. The competition between the two time periods, T and T_d, explains the observed mean energy dynamics and it is not dependent on the presence or absence of the transporting islands in classical phase space. While quantum mean energy enhancement can be engineered by taking advantage of the presence of transporting islands in classical phase space, it provides a somewhat restrictive framework. In contrast, this work emphasizes that quantum mean energy enhancement is possible without replying on classical features in atom-optics kicked rotor. This is shown through numerical simulations of AOKR and in the experiments.

These results are of intrinsic interest in the quantum chaos of kicked rotor, but also in the broader context of quantum control. Techniques to control the quantum systems

with classically chaotic behavior has become an active area of research interest over the years. Through this work, we have demonstrated a control over the best-known phenomenon experimentally in quantum chaos. The dynamical localization can be enhanced over a wide range of parameters provided the system is classically chaotic. Apart from the atom optics realization of KR and MKR, it would also be interesting to explore the dynamics of a molecular version of KR and MKR, *i.e.*, diatomic cloud periodically kicked by strong microwave fields. Another promising direction to look at is the experimental realization of KR and MKR in a square-well potential [193]. Along this direction, an interesting model (which is very different from the one discussed here) has been proposed for the study of classical and quantum anomalous diffusion [194]. These efforts might lead to a broader understanding of diffusion and localization in time-dependent chaotic quantum systems.

Chapter 5

A single Knob Coherent Control of Dynamical Localization

Coherent control over any quantum system opens a vast area of applications which include quantum computation, quantum communication, control over reactants in quantum chemistry, coherent control of semiconductor's properties and molecular rotation. Motivated by some recent works [42, 73, 195], we focused on coherent control over dynamical localization by tuning a single dynamical phase of the system as dynamical localization is a phenomena based on quantum interference. By adjusting a single dynamical phase, we achieve systematic control over the localization length of the quantum system without introducing decoherence. This control mechanism is effective both at the beginning of the dynamics and in deeply localized states. Our findings demonstrate that if the system maintains high coherence, any alteration in the dynamical phase propagates throughout the system, facilitating control over quantum interference.

5.1 Theory and Scheme for Single Knob Coherent Control

The theoretical description follows what was described in Section 2.3.1. It's like starting with the Talbot effect to control how the wave-function spreads out in the beginning. By doing this, we can see how it affects dynamical localization. This helps us to control the behavior of localized systems. As we discussed in the theory section for anti-resonance

and resonance, where a phase difference between alternative momentum states is either π or 2π, creates a revival or spread of initial wave-function. Revival is now almost identical to the initial wave-function for anti-resonance with limitations primarily arising from the momentum width of the BEC. However, the spread becomes extreme in a resonance condition. By scanning the time delay from anti-resonance to resonance, we can create different initial wave-function where the phase between alternative momentum states can be scanned from π or 2π. Such differing initial states will affect the final localized state due to the high phase coherence between momentum states. This initial phase difference propagates thoughout the dynamics during periodic kicking where the kick period is an irrational multiple of Talbot-time. It provides a good systematic control by imprinting the initial phase from π or 2π.

We explored two schemes: The first one is about preparation of the initial wave-function to control the dynamical localization. For the second method, the system is in a localized state with a good phase coherence and we add an external control-phase to restart the dynamics and to shift it to a new desired localized state. First scheme for the pulse sequence is as shown in Fig. 5.1.

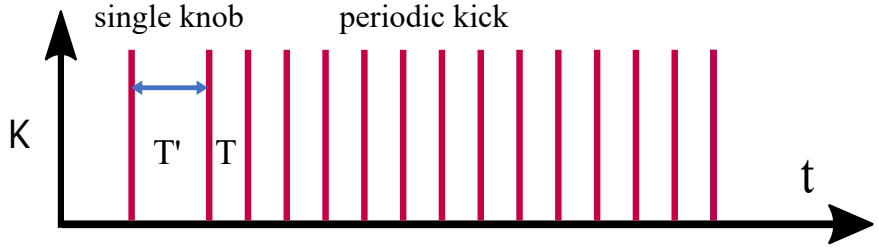

Figure 5.1: Pulse scheme. Kick sequence for single knob coherent control

With this kick sequence, we can write the Floquet operator for the first two kicks and the evolution with a control period T' followed by periodic kicks of time interval T:

$$U = \left\{ \exp\left[f(T')\right] \exp\left[-i\frac{K}{\hbar_{\text{eff}}}\cos(x)\right] \right\} \times \left\{ \exp\left[f(T)\right] \exp\left[-i\frac{K}{\hbar_{\text{eff}}}\cos(x)\right] \right\} \tag{5.1}$$

The time delay between the first two kicks T', will imprint the control phase between

the momentum states. In detail, the wave-function after 1 kick, $\psi(x,t)$can be expanded in the momentum basis as: $\psi(x,t) = \sum_m A_m\langle x|m\rangle$, with A_m being the expansion coefficients. Now, we can free evolution Floquet operator on the momentum state $|m\rangle$:

$$\exp\left(\frac{-ip^2}{2\hbar_{\text{eff}}}\right)|m\rangle = \exp\left(-im^2 4\omega_r T'\right)|m\rangle\ . \tag{5.2}$$

From Eqn. 5.2, for the QKR, the initial wave-function will not be just zero momentum state ($|0\rangle$) but a comb with a control phase difference between them. It will work as an initial wave-function for QKR. To demonstrate the coherent control, we simulate the kicking scheme shown in Fig. 5.1.

Here, we measure the normalized population of the zeroth momentum state by varying the control parameter from π to 2π. In the periodic case, after dynamical localization, the normalized population of the zeroth momentum state saturates close to maximum level and and mean energy close to minimum level after a quantum break time. Since we are using Bose-Einstein condensates (BEC), where momentum states are well-defined, precise calculation of the population of the zeroth momentum state provides comprehensive information, eliminating the need for energy calculations. Moreover, as we are not exploring localized to diffusive phenomena, we can rely on the population of the zeroth momentum state. To control the localization length and the mean energy, we measure the population of the zeroth momentum state. Lower population implies higher energy and increased localization length, as atoms redistribute to higher momentum states, adhering to the conservation of atom numbers.

5.2 Demonstration of Single Knob Coherent Control of Dynamical Localization

As we have explored two schemes, first we will go through the initial observation where we manipulate the initial wave-function to control the dynamical localization. Further, we will control an already localized wave-function to achieve a desired new localized state with same scheme.

5.2.1 Coherent Control by Preparing Different Initial State

First, we show the simulation results of the first scheme shown in Fig. 5.1. We scan T' from (0 - 266 μs), which corresponds to a phase evolution of (0 - 8π). For simulation and experiment, the Talbot time (T_T) is 66.6 μs, providing a phase evolution of 2π. The time gap between the periodic kicks is 24.3 μs. The stochastic parameter(K, $\hbar_{\text{eff}}$) is (5, 4.6), fixed for this experiment to keep the system in deep chaotic regime. We apply 60 periodic kicks by changing the time gap of control knob for a long range to find the systematic control regime. Simulation results are shown in Fig. 5.2. From Fig. 5.2(a), we can clearly find a parameter regime where we can control the population of zeroth momentum state (denoted as f(0)) in turn the the dynamical localization. These regions lie on both sides of periodic kicks and we choose a range of T' = 33.3 μs to T' = 66.6 μs. A simulation result for this control region is shown in Fig. 5.2(b). Experimental results are shown in Fig. 5.3. Initially, we measure the population of

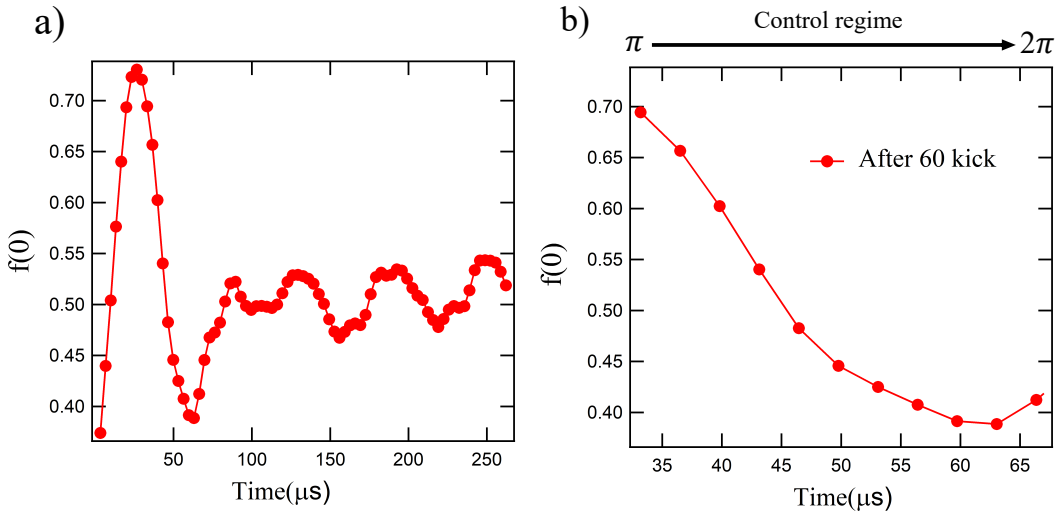

Figure 5.2: Simulation result. (a) The normalized population of the zeroth momentum state $f(0)$ is shown as a function of T' over an extended range (0-4π) after 60 kicks (b) Shows the actual control regime which lies in the π to 2π region or 0 to π region. Maximum population is when this time gap matches with periodic kick.

the zeroth momentum state with the number of applied kicks by varying the control parameter T' from π to 2π, it's shown in Fig. 5.3(a). A saturation in $f(0)$ is observed with increasing kicks after quantum break time, indicating dynamical localization and

maintaining phase coherence.

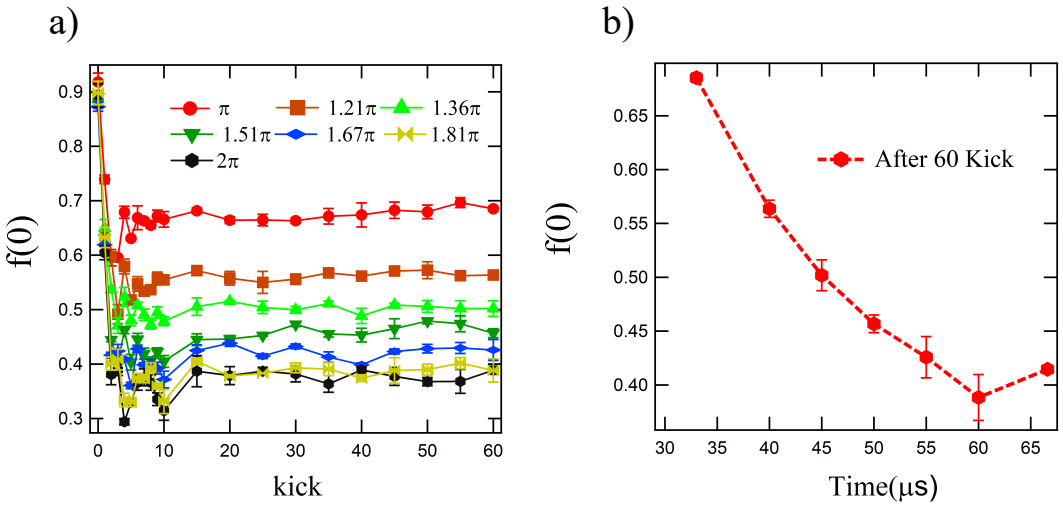

Figure 5.3: Experimental results. (a) The normalized population of the zeroth momentum state $f(0)$ is shown as s function of applied kicks, showing the feature of dynamical localization. (b) Demonstration of coherent control by varying single knob T'

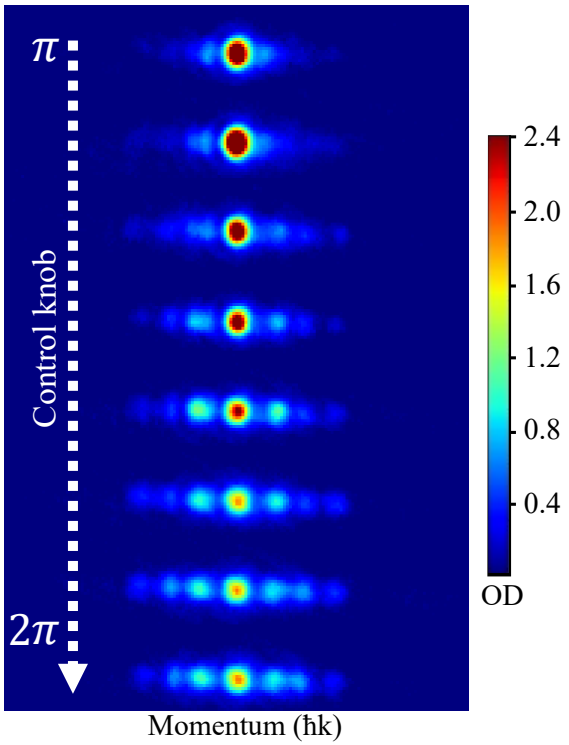

Figure 5.4: Localized distribution. Momentum distribution profile after 60 kick by varying the control knob from π to 2π. It clearly shows the control enhancement of localization length.

For each case, we get dynamically localized wave-packet with enhanced localization length and drop in the value of f(0). Value of f(0) is shown in Fig. 5.3(b) after 60 kicks for different control parameter T'. The behavior of the simulation results in Fig. 5.2(b) and experimental results in Fig. 5.3(b) are quite similar and show a similar control nature. Just the periodic kicks and or applying a delay of π shows quite similar behavior because of revival of wave-function by π delay. The choice of using a BEC helps us to observe a systematic large control over dynamical localization by simply changing a single knob with such a small step in phase of 0.15π.

Fig. 5.4 shows the momentum distribution after 60 kick with different control knob, taken from absorption images. It is clear that the width of the distribution is increasing from π to 2π. This is also visible in the absorption images that carry more weight in the higher momentum states. Our observations also reveal that after a time delay of

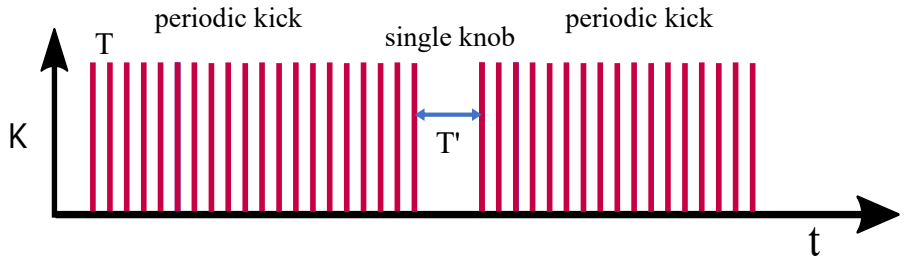

Figure 5.5: Kicking sequence. A pulse scheme for control over localized wave-function

2π, we lose systematic control as dephasing occurs during long periods of free evolution, making proper phase imprinting difficult. Here, there is an opportunity to explore how phase coherence is maintained when periodic kicks are applied, compared to the dephasing that occurs when the system is isolated and freely evolving.

5.2.2 Coherent Control of Dynamically Localized State

As we know a dynamically localized wave-function maintains it's phase coherence, our single knob coherent control scheme should work for such localized states as well. To explore this, first we apply 20 periodic kick to create a localized state, as break time is less than 10 kick for our parameter. A kick scheme is shown in Fig. 5.5

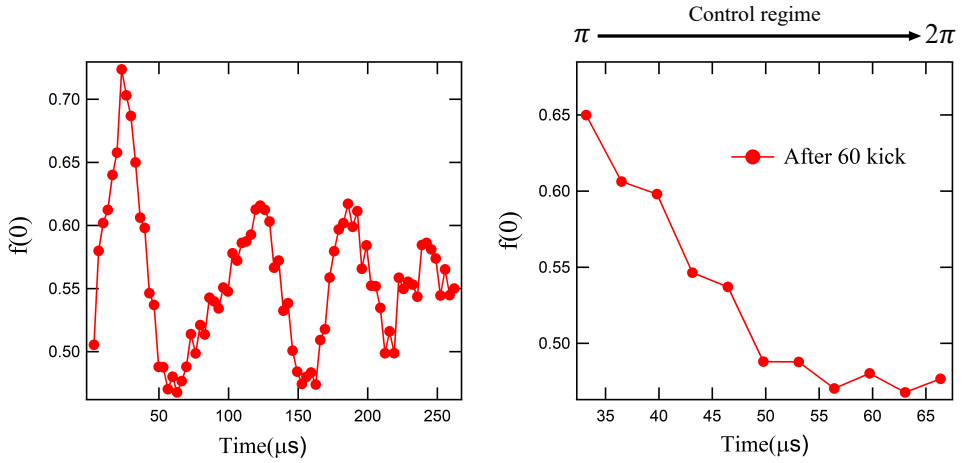

Figure 5.6: Simulation result. (a) The normalized population of the zeroth momentum state $f(0)$ is shown as a function of T' (b) Actual control regime which lies in the π to 2π region. Maximum population is when this time gap matches with periodic kick.

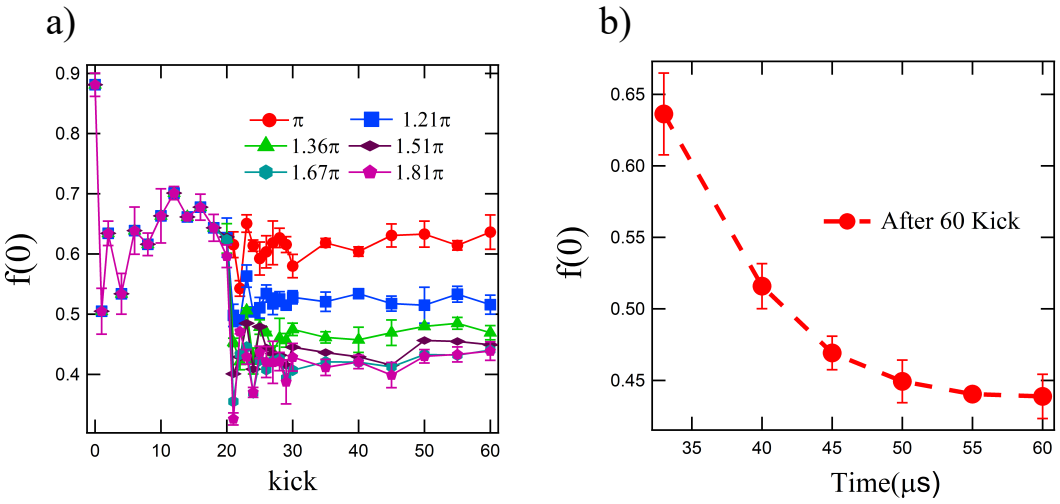

Figure 5.7: Experiment result. (a) The normalized population of the zeroth momentum state $f(0)$ is shown as a function of T' over an extended range (0-4π) after 60 kick, (b) It is showing the actual control regime which lie in π to 2π region or 0 to π region. Maximum population is when this time gap matches with periodic kick

Our simulation results are shown in Fig. 5.6, in same manner as discussed in previous section. Here too, we find quite a good control over $f(0)$ by tuning the control knob. The experimental results are shown in Fig. 5.7. We observe systematic control, but it saturates as we move from π to 2π. It is challenging to imprint phase on a localized wave-function where some momenta are already occupied and have gone through

dynamical localization. Therefore, the effectiveness of any control decays due to dephasing and which directly depends on the value of $f(0)$ before adjusting the control knob. Despite these challenges, our scheme remains effective, as the system maintains good coherence during dynamical localization. Moreover, our scheme demonstrates that we can control dynamical localization at any time during the dynamics simply by adding the desired phase to the system.

5.3 Conclusions

In summary, our utilization of Bose-Einstein condensates allowed us to demonstrate systematic and coherent control over dynamical localization. By encoding a relative phase between superposing momentum states through a single time evolution, acting as the initial wave-function, we effectively governed the QKR dynamics in the absence of noise and decoherence. This control enabled us to adjust a single parameter, leading to desired changes in the momentum distribution of the final dynamically localized state. As we quantify the control by measuring the normalized population ($f(0)$), the maximum degree of control in $f(0)$ is more than 90% with a freedom of tunability. We also showcase that such control is even effective for deeply localized states, because localized states also maintain a good coherence. It's worth noting the significance of our results, especially considering the fully chaotic nature of the classical phase space for our parameters and its highly sensitivity to initial conditions. Despite these conditions, our ability to control over quantum chaos shows the dominance of quantum coherence over chaotic dynamics. This suggests promising avenues for manipulating quantum systems with precision and efficacy.

Chapter 6

Asymmetric Dynamical Localization and Precision Measurement of the Micromotion of a Bose-Einstein Condensate

In this experimental investigation, we launch a Bose-Einstein condensate (BEC) with varying recoil velocity into a periodically kicked optical lattice to study its effect on dynamical localization. Our observations reveal an asymmetrically localized moving distribution with a small initial current. We conduct our investigation under two scenarios: when the BEC is in motion within the laboratory frame and when the optical lattice is in motion in the laboratory frame. Notably, we explain that such asymmetric features arise in early-time dynamics and settle down as dynamical localization stabilizes. By utilizing this asymmetric behavior in early-time dynamics, we measure the micromotion of a Bose-Einstein condensate (BEC). Micromotion, in this context, refers to the extremely low initial velocity of the BEC along the lattice direction. This small velocity originates from jitter during the turning off of the hybrid trap potential, and such micromotion adds systematic shift and uncertainty in light-pulse atom interferometer. By employing a quantum kicked rotor system with a BEC and a moving optical lattice, we measure the asymmetry in early-time dynamics to precisely characterize and quantify

the micromotion phenomena in the quantum system.

6.1 Background and Definition of the Problem

Precision measurement with light-pulse atom interferometers has opened nup tremendous applications in quantum sensing [91, 196, 197]. Atom interferometers are successfully utilized in gravimeters [91, 92, 94], rotation sensing [198, 199], and magnetometers [200], allowing for the determination of photon recoil [201]. Particularly for precision rotation sensing and gravimetry, nullifying systematic shifts and measurement errors coming from Coriolis effect [202] in phase shifts necessitates precise knowledge of the initial velocity [133, 198, 203]. This velocity may arise from external launch velocities or micromotion coming from small movements after turning off the trap potential. In the rotation sensor, such phase shift is called Sagnac phase shift: $\Delta\phi = 2\Omega(v_m \times k_{eff}) \cdot T^2$ [202]. The phase shift is in the range of tens of milliradians (mrad) for a velocity of 100 μm/s over an interferogram time of hundreds of milliseconds (ms). The velocity range of the micromotion can lie in the range of (100-1000) μm/s, which is much smaller compared to the velocity of a two-recoil photon ($\approx$ 1 cm/s). The measurement of such small velocities is challenging and requires huge time-of-flight in standard absorption imaging, or a very precise spectroscopy to measure the Doppler shift through Bragg or Raman spectroscopy [133, 204, 205].

Other aspects of this micromotion arise when atoms are trapped in periodically driven optical lattices [206, 207], the oscillation of atoms within lattice site. The micromotion is not considered in such cases because of a time-averaging performed on this degree of freedom, resulting in a time independent Hamiltonian [208, 209]. Finding a measurable observable, which gets affected by this micromotion is difficult and thus difficult in quantifying the micromotion. In the recent study, the feature of micromotion is revealed by measuring asymmetric momentum distribution [210, 211] in time-of-flight by modulation of the trap frequency of the optical lattice. In analogy to micromotions described by the oscillation of atoms in a trap, we present the measurement of micromotion described in velocity space [212, 213], which arises from turning off the trapping potential and which is very small in the experiment.

In recent years, there has been much interest in studying a quantum kicked ro-

tor (QKR) in Bose-Einstein condensate with and without tunable interaction [61–64]. Further the ease of imprinting the lattice phase on BEC also provides different types of effects like on-resonance quantum ratchet [65, 66] and quantum boomerang effect [67, 68, 214]. BEC based QKR system has also been utilized in coupled quantum rotors [61] where two incommensurate optical lattices drive a quantum to classical transition by breaking dynamical localization. A discrete time quantum walk has also been observed in BEC based system [44].

In the current chapter, we present the experimentally demonstrated localized momentum profile by launching the BEC with varying recoil velocity or by inducing lattice motion. A constant phase evolution of the launched wave-function or the lattice motion creates an asymmetric distribution. Furthermore, we illustrate that the asymmetric nature of the distribution can be easily controlled by adjusting the launch velocity, rather than altering the direction of the launch velocity. In contrast to previous studies [135] with cold atoms where such asymmetry arises from pulse-shape effects and are typically observed after long time, here we demonstrate that such asymmetry arises in early time dynamics [66, 67]. This asymmetry gets settled as the dynamical localization takes place. An asymmetry in localized states has been reported in BEC by a single phase change in the beginning and their reversal in reference [67]. By utilizing this asymmetric behavior in early time dynamics, we present a method to measure the micromotion of BEC in AOKR. The AOKR is already utilized for measurement of gravity through survival resonances [215, 216]. We demonstrate that even this micromotion of the Bose-Einstein condensate (BEC) can induce early-time asymmetry in the momentum distribution. This asymmetry directly quantifies the velocity of the micromotion, aligning with the primary focus of the current study [123, 210, 211].

6.2 QKR in Moving Frame of Reference

The QKR is a fundamental model of quantum chaos [184] extensively explored for its chaotic dynamics and for demonstration of dynamical localization [39, 40]. The classical kicked rotor, when strongly kicked by an external field, can display chaotic dynamics accompanied by diffusive growth of mean energy with time. Over extended time scales, quantum interference effects inhibit classical diffusive dynamics, a phenomenon in mo-

mentum space analogous to Anderson localization [48]. Since the first realization of the QKR using cold atoms [49], it has spurred numerous experimental investigations to explore a variety of scenarios that manipulate localization [112, 217, 218]. Physically, the standard kicked rotor describes a particle subjected to periodic kicks imparted by the stationary optical lattice created by counter-propagating laser beams. However, in this work, we consider a kicked rotor system in which the optical lattice moves at a constant velocity in the laboratory frame. The Hamiltonian of QKR in a moving lattice is given by [111]

$$H = \frac{\widehat{p}^2}{2} + K\cos(2k\widehat{x} - 2\pi\alpha t)\sum_{n=1}^{N}\delta(t-n), \tag{6.1}$$

where, $\widehat{p}$ and $\widehat{x}$ represent the momentum and position operators respectively. They obey canonical commutation relation $[\widehat{x},\widehat{p}] = i\hbar_{\text{eff}}$, where the effective Planck constant ($\hbar_{\text{eff}} = 8\omega_r T$) can be tuned in the experiment with pulse period T. Further, K is the stochastic parameter, k is the wave vector, ω_r is the recoil frequency, and α is the frequency difference between two lattice beams that make up the optical lattice. The lattice velocity arising from the frequency difference between the counter-propagating beams is $v = \frac{\lambda\alpha}{2}$, where λ is the wavelength of the optical lattice. Throughout this work, parameters will be chosen so that the classical analogue of QKR displays chaos, with $K \geq 5$. This parameter choice ensures that the localization effects we observe are of quantum origin.

As the quantum kicked rotor is time-periodic, the quantum dynamics can be conveniently analyzed through the period-1 Floquet operator

$$U = \exp\left(-i\frac{\widehat{p}^2}{2\hbar_{\text{eff}}}\right)\exp\left[-i\frac{K}{\hbar_{\text{eff}}}\cos(2k\widehat{x} - 2\pi\alpha t)\right] \tag{6.2}$$

This evolves an initial state $\psi(x, t=0)$ over one kick period T, *i.e.*, $\psi(x,T) = U\psi(x,0)$ with the initial state chosen as a coherent state in position space given by

$$\psi(x, t=0) = \frac{1}{\sqrt{2\pi}\sigma_w}\exp\left(-\frac{x^2}{2\sigma_w^2}\right)\exp(-ip_0 x), \tag{6.3}$$

and is consistent with the initial distribution of BEC. Here, σ_w characterizes the width of the wavefunction in position space, while p_0 is the initial velocity, typically arising

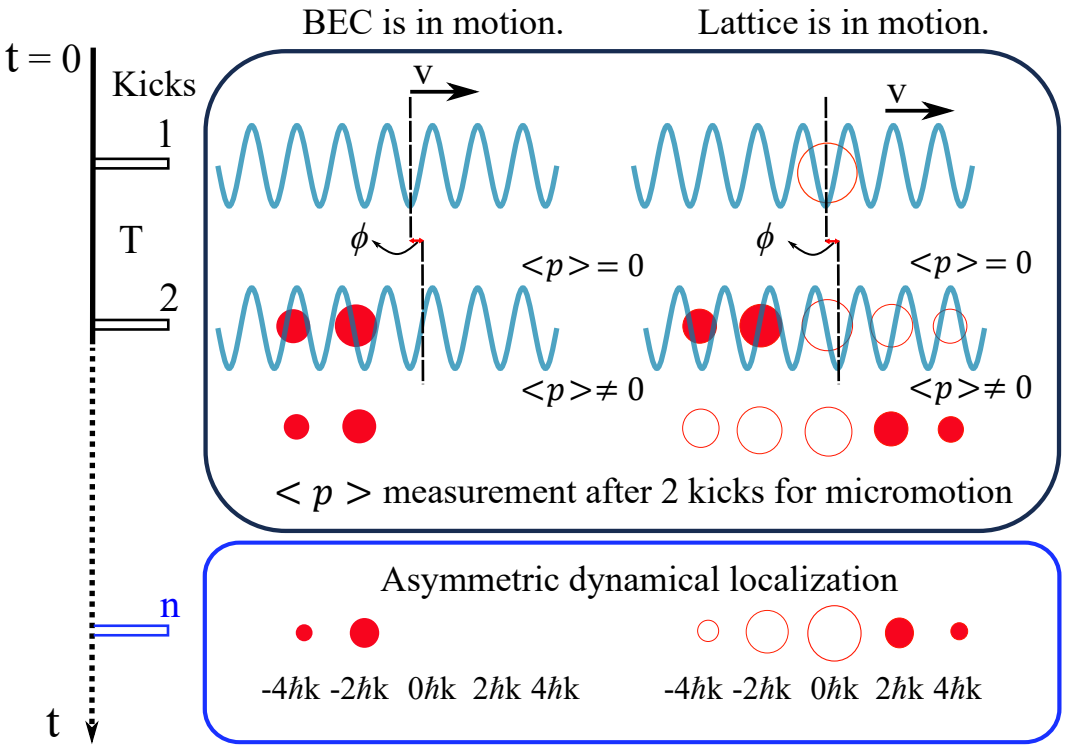

Figure 6.1: This experimental schematic shows the moving BEC (left side) with velocity v and periodically kicked 1D optical lattice. This relative motion between BEC and lattice provides asymmetry in momentum distribution which we quantify by measuring $\langle p \rangle$. Same asymmetry with opposite nature arises when lattice is in motion, shown in right side. Micromotion is measured by scanning lattice velocity (see Fig. 6.5 for details). Further, dynamical localization sets in for larger number of kicks.

from launched velocity or micromotion. Generally, in our experiments, when BEC is launched with initial momentum p_0, the lattice velocity is stationary and vice versa. In general, either moving the lattice or the BEC in same direction are expected to induce similar effects in early time dynamics with exactly opposite asymmetric momentum distribution [66, 219]. The experimental protocol is illustrated in Fig. 6.1.

For numerical simulations, we use the standard split-operator method to evolve an initial state of the kicked rotor. This method consists of two primary components: the kick operator, which is diagonal in position space, and the free evolution operator, which is diagonal in momentum space. To simulate scenarios where the lattice is in motion in the lab frame, we imprint the phase just before each kick. Similarly, to model the situation in which BEC moves in the laboratory frame, a wavefunction is initialized

incorporating the motion right from the outset.

Asymmetric Dynamical Localization and Micromotion

If the lattice is moved with constant velocity, then the kick potential (in the lab frame) $V(x) = K\cos(2kx - 2\pi\alpha t)$ induces a path difference at each kick. Consequently, the phase difference between successive kicks is $\phi = 2\pi\alpha T$ and this breaks the parity symmetry. The total phase difference accumulated after n kicks is $\phi_n = 2\pi\alpha T \times (n-1)$, assuming that the phase is initialized to zero for the first kick. The accumulated phase difference ϕ_n over short timescales induces an inhomogeneity in position space due to broken parity symmetry, leading to an asymmetric momentum distribution [66]. This asymmetry can be quantified through $\langle p(t = 2T)\rangle$ immediately following $n = 2$ kicks.

In the experiments, the lattice velocity v is controlled by tuning α and subsequently measuring $\langle p(t = 2T)\rangle$. Based on physical consideration and since phases are unique only upto 2π, we posit that the average momentum after two kicks to have a form

$$\langle p(t = 2T)\rangle = c\ \sin[4\pi(vT/\lambda)], \tag{6.4}$$

where c is a constant. Exactly the same expression holds good for moving BEC with opposite sign in average $\langle p\rangle$. Further, Eq. 6.4 implies that if $vT/\lambda = n/4$ (where n is an integer), $\langle p\rangle = 0$ implying an absence of asymmetry for specific choice of initial velocity and kick period. In the long time limit of $n \gg 1$, the initial asymmetry accumulated in the short-time limit eventually freezes due to the emergence of dynamical localization. Hence, the early-time dynamics dictates the long-term behavior and the onset of asymmetrical dynamical localization in the system.

To gauge micromotion accurately, the optical lattice is precisely moved with frequency difference of the order of 100Hz, aligning it with the scale of micromotion. Upon achieving a velocity for the lattice that corresponds precisely to the micromotion, we observe that $\langle p(t = 2T)\rangle$ equals to zero. This alignment establishes a direct correspondence between the velocity of the lattice and the velocity of micromotion.

6.3 Experimental Setup for QKR

The QKR setup we have used for this work is similar to the one described in Ref. [112]. However, instead of cold atoms, we utilize a BEC of ^{87}Rb every 8 seconds, through forced evaporative cooling. The atoms are initially prepared in the $|F = 1, m_F = -1\rangle$ state, with a BEC temperature of 80 nK and a population of approximately $40,000$ atoms. This BEC serves as the initial wave function for our experimental investigations. The optical standing wave is produced using two independent laser beams, which are generated by a single laser passing through two separate acousto-optic modulators. The frequency difference between lattice beams and their switching can also be controlled. Switching time and laser power provide us control over scaled Planck constant $\hbar_{\text{eff}}$ and stochastic parameter K.

This work comprises two main components: probing asymmetric dynamical localization and measuring micromotion. To investigate localization phenomena, we implement the Bragg diffraction technique to launch the Bose-Einstein condensate with varying recoil momentum, as outlined in Ref. [220]. By adjusting the frequency difference between the lattice beams and the on-time of the lattice beam, we achieve a good transfer of atoms to different momentum states. In our apparatus [95], a frequency difference of 15 kHz results in 2 photon recoil momenta, while a frequency difference of 30 kHz provides 4 photon recoil momenta to atoms, both have a fixed on-time of approximately ~ 66.6 μs. For a given frequency difference, optical lattice moves with half of the speed of diffracted wave-packets. After the creation of the initial wave function of BEC with different velocities, we apply the usual kicked rotor pulse sequence to study the dynamical localization. In our QKR experiments, we maintain the stochastic parameter at $K = 5$ and effective Planck constant at $\hbar_{\text{eff}} = 4.6$ to ensure that the corresponding classical dynamics remains in the chaotic regime [63].

For the motion of the optical lattice, we generate a frequency difference ranging from 0 to 75 kHz between the lattice beams. This frequency range corresponds to a velocity range:

$$v = \frac{\alpha}{15kHz}.\frac{\hbar k}{M_{\text{Rb}}}, \tag{6.5}$$

where, $\hbar$k is single photon recoil momentum. We ensure that the kick strength remains

constant across higher frequency regimes. The advantage of employing a moving lattice, rather than a moving BEC, lies in the flexibility to assign precise arbitrary velocities to the optical lattice from the laboratory frame. It also does not create any residual atoms in zeroth momentum state like in Bragg diffraction. Leveraging this control over micromotion, we scan the lattice velocity in a frequency range of -3 to 3 kHz with increments of 100 Hz, enabling precise measurement of micromotion BEC by balancing the relative motion.

6.4 Asymmetric Dynamical Localization in Moving Frame of Reference

In this section, we will consider two scenarios – (a) BEC launched with an initial momentum in a stationary lattice (called case-I), (b) BEC launched with zero initial momentum in a moving lattice (called case-II).

Case I: BEC Moving in Lab Frame

In our experiment, BEC is launched with various recoil velocity, $v_n = 2n\hbar k/M_{Rb}$ ($n \in \mathbb{Z}$), using Bragg diffraction, where $\hbar k/M_{Rb}$ is single photon recoil velocity. This is achieved by applying a pulse of length approximately 66.6 μs to transfer all the population to the required momentum state, and appropriately adjusting the lattice power. Subsequently, free evolution period of approximately 66.6 μs is allowed, corresponding to the Talbot time of the system [120]. This ensures recreation of the initial wavefunction without any unintended phase accumulation [70]. Once the wavefunction with different velocities is created, it is subjected to periodic kicks to observe dynamical localization. The period of these kicks is set at $T = 24.3$ μs, corresponding to a scaled Planck constant of $\hbar_{\text{eff}} = 4.6$. The stochastic parameter is $K = 5$ corresponding to a classical phase space that is almost fully chaotic [63, 112]. These parameters remain consistent throughout the paper unless stated otherwise.

Bose-Einstein Condensate is launched with initial velocity of $v_0 = 0, 2\hbar k/M_{Rb}$ and $4\hbar k/M_{Rb}$. The momentum distributions observed after $30, 40$, and 50 kicks are depicted in Fig. 6.2(a-c) respectively in the left panel. In Fig. 6.2(a), standard symmetric dynamical localization pattern is observed for initial velocity $v_0 = 0$. Figure 6.2(b), illustrates

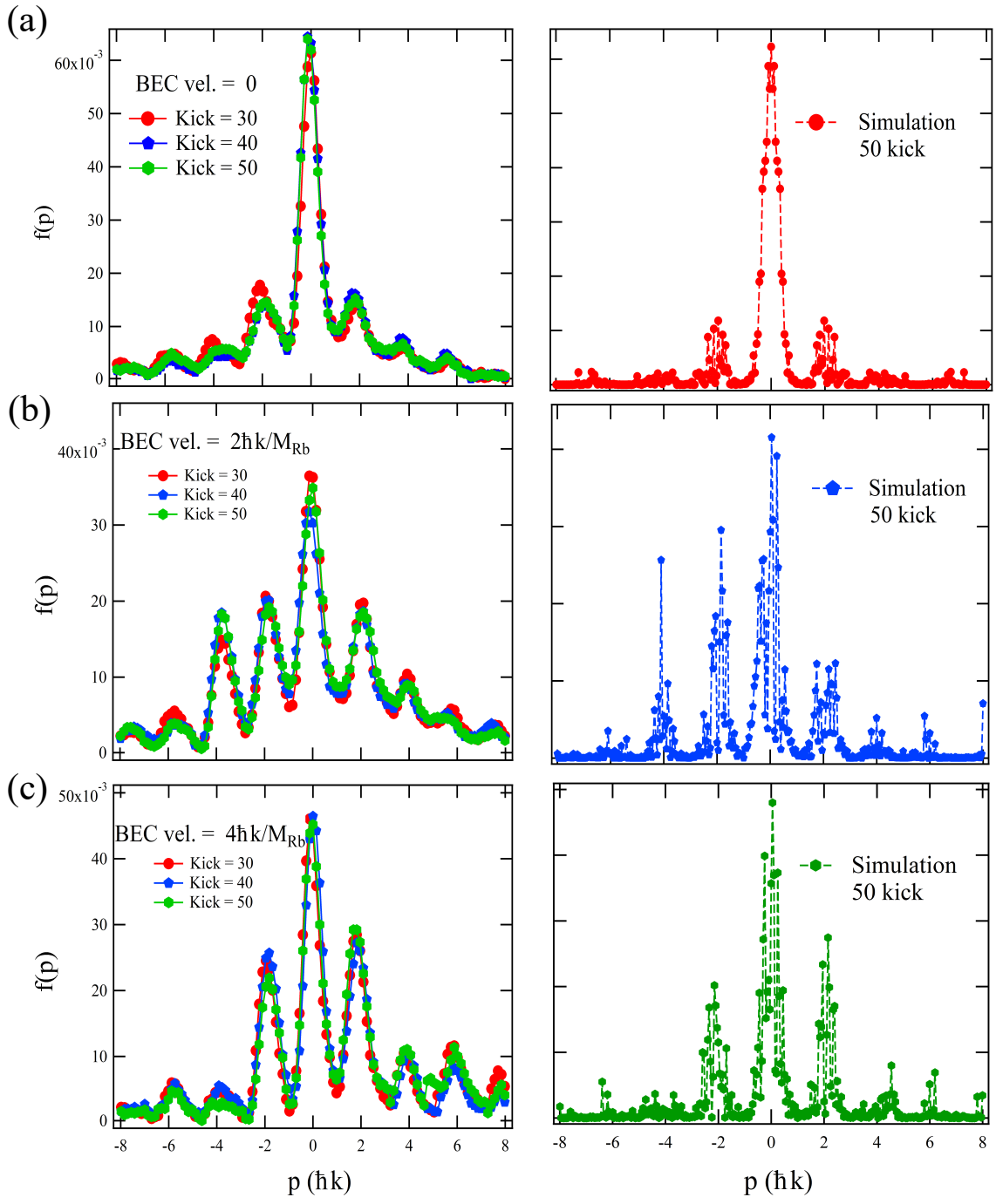

Figure 6.2: Wavefunction profile for different launch velocity shown at 30, 40 and 50 kicks. In all the cases, dynamical localization has set in for initial velocity corresponds to momenta (a) $0\hbar k/M_{Rb}$, (b) $2\hbar k/M_{Rb}$, and (c) $4\hbar k/M_{Rb}$. In all cases, in left side, symbols are obtained experimental data. In right side, symbols are obtained from kicked rotor simulations with 50 kicks.

an asymmetric dynamically localized momentum distribution when BEC is launched with $v_0 = 2\hbar k/M_{Rb}$ (peaked at $2\hbar k$, shifted to zero for better comparison). Similarly, in Fig. 6.2(c), dynamical localization is slightly asymmetric for a launch velocity of $v_0 = 4\hbar k/M_{Rb}$(peaked at $4\hbar k$, shifted to zero for better comparison). Asymptotically, as $n \gg 1$, the system remembers the initial velocity v_0 since the maxima of the steady-state distribution occurs at $p = |p_0|$. In Fig. 6.2(b), $\langle p \rangle$ with reference to initial given velocity v_0, is moving in the direction of the launched velocity (left direction), while in Fig. 6.2(c), small $\langle p \rangle$ is moving in the opposite direction of the launched velocity. As for the velocity of $v_0 = 4\hbar k/M_{Rb}$, $\langle p \rangle$ is small from the beginning, difficult to observe the asymmetry in localized state.

The right panel in Fig. 6.2 shows the corresponding results obtained from QKR simulations. The simulation results confirm the emergence of dynamical localization and evidently it is asymmetric for the case when BEC is launched with $v_0 = 2\hbar k/M_{Rb}$ and $v_0 = 4\hbar k/M_{Rb}$. For $v_0 = 2\hbar k/M_{Rb}$, the more population lies in the direction of the launched velocity and for $v_0 = 4\hbar k/M_{Rb}$, it lies in opposite direction with little asymmetry, matching with the experimental result. This asymmetry feature in early-time dynamics will be discussed further in upcoming section. The experimental profile in the vicinity of the peak value, in an average sense, is slightly elevated compared to simulation results (in both Figs. 6.2-6.3) in due to presence residual thermal atoms.

Case II: Optical Lattice Moving in Lab Frame

In this section, we discuss the dynamical localization by moving the lattice in the lab frame by inducing a constant frequency difference α in the range of $0 - 75$ kHz, which spans almost 5 recoil velocity. After creating the BEC, $100\mu s$ time-of-flight is allowed, and subsequently periodic kicks are applied. As seen in Figs. 6.3(a-c), dynamical localization is observed for various lattice velocities. For a direct comparison with case-I, the lattice has been moved in same direction, the observed distribution in this case has been flipped as discussed in Eq. 6.4 . The optical lattice is moved with velocity $\hbar k/M_{Rb}$ and $2\hbar k/M_{Rb}$ and $4\hbar k/M_{Rb}$ in the left direction. The resulting steady-state momentum distribution after 50, 60 and 70 kicks is displayed in Figs. 6.3 (a-c). The asymmetry induced by the lattice motion is visible for $\hbar k/M_{Rb}$, $2\hbar k/M_{Rb}$ and $4\hbar k/M_{Rb}$; for $\hbar k/M_{Rb}$ in Fig. 6.3(a) the asymmetric wave packets are moving in the opposite direction as

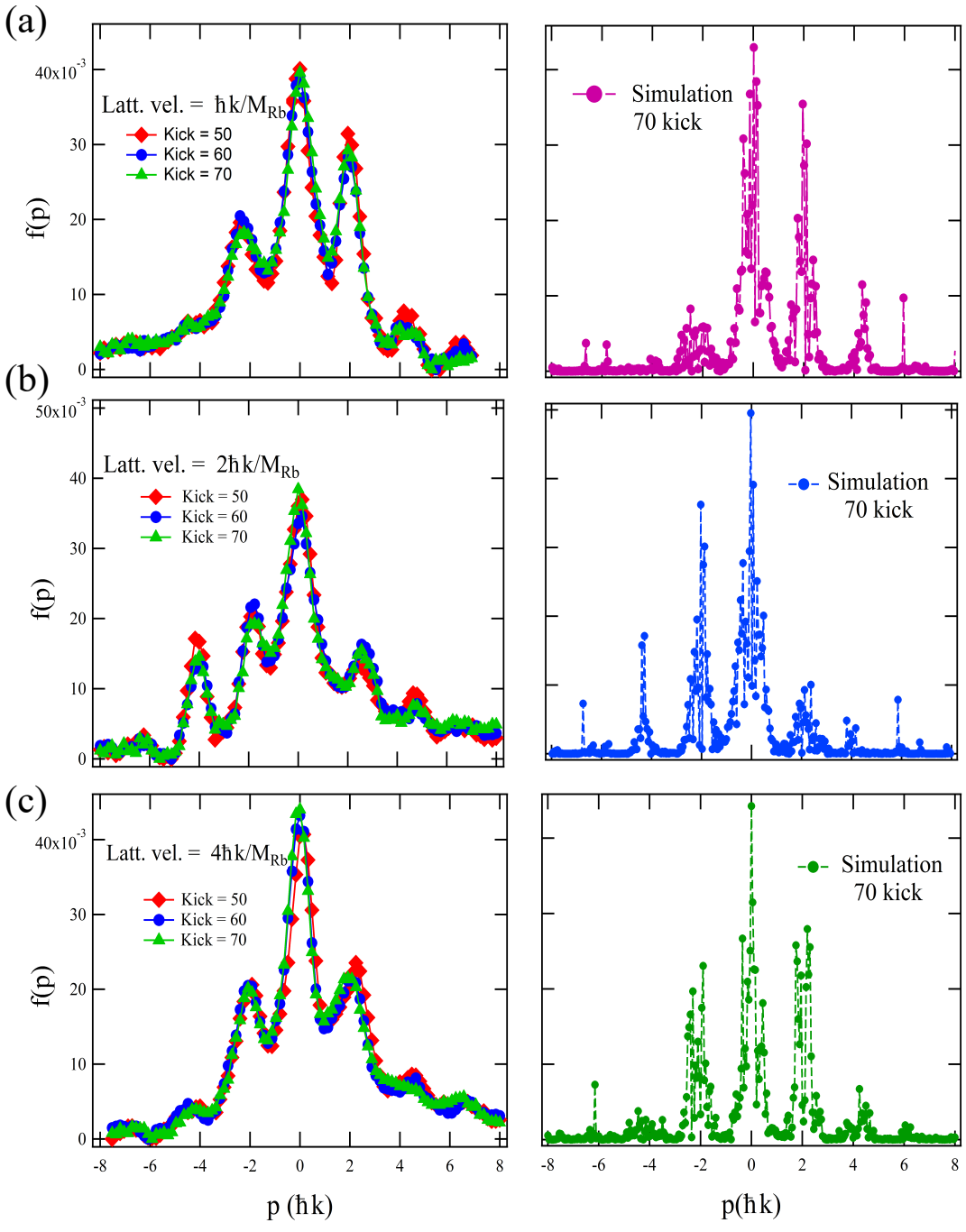

Figure 6.3: Dynamically localization for three different lattice velocity: (a) $\hbar k/M_{Rb}$, (b) $2\hbar k/M_{Rb}$ and (c) $4\hbar k/M_{Rb}$. (left side) experimental data shown as symbols for three different kick numbers, (right side) simulation results shown as symbols at 70th kick.

lattice (left direction), for $2\hbar k/M_{Rb}$ in Fig. 6.3(b), the asymmetric wave packets are moving in the same direction as lattice (left direction), and for $4\hbar k/M_{Rb}$ in Fig. 6.3(c), small asymmetric wave packet is moving again in the opposite direction as lattice.

The right panel in Fig. 6.3 shows the corresponding localization pattern obtained from QKR simulations. The simulation results confirm the emergence of asymmetric dynamical localization when the optical lattice is moved by velocities of $\hbar k/M_{Rb}$, $2\hbar k/M_{Rb}$ and $4\hbar k/M_{Rb}$.

6.5 Measurement of Early Time Dynamics

To understand asymmetry induced by relative motion between the atomic cloud and the optical lattice, early-time dynamics after two kicks is analyzed. The optical lattice is moved by creating a frequency difference between two laser beams, ranging from 0 to $5\hbar k/M_{Rb}$. Subsequently, two kicks are applied separated by time interval $T = 24.3$ μs for different initial velocity v of lattice and $\langle p \rangle$ is measured after a 10 ms time-of-flight. Remarkably, pronounced oscillations in $\langle p \rangle$ are observed, consistent with Eq. 6.4. This is shown in Fig. 6.4, and suggests that $\langle p \rangle$ exhibits a linear relationship in the limit of $v \to 0$. This linearity provides a promising avenue to measure the micromotion discussed in Section 6.6. Fig. 6.4 also shows simulation results (blue line), which agrees with the experimental results in the limit $v \to 0$. For the large v, where the lattice velocity is high, experiment deviates from the simulation due to finite pulse time.

Another intriguing feature observed in Fig. 6.4 is the difference in the sign of $\langle p \rangle$ for $\hbar k/M_{Rb}$ and $2\hbar k/M_{Rb}$. The opposite signs for $\langle p \rangle$ in the early-time dynamics is a consequence of the asymmetric distribution observed after long-time evolution, as demonstrated in Section 6.4. In general, short time asymptotic carry the signature of the long-term behavior at other velocities as well. In particular, for velocities that are integer multiples of $1.37\hbar k/M_{Rb}$ (observed $1.35\hbar k/M_{Rb}$ from Fig. 6.4), asymmetry is absent in the distribution. This corresponds to the condition $vT/\lambda = n/4$, when asymmetry is expected to vanish. Irrespective of the speed of lattice, if the velocity is an integer multiple of $1.37\hbar k/M_{Rb}$, no asymmetry is expected to manifest in the distribution, as a consequence of Eq. 6.4.

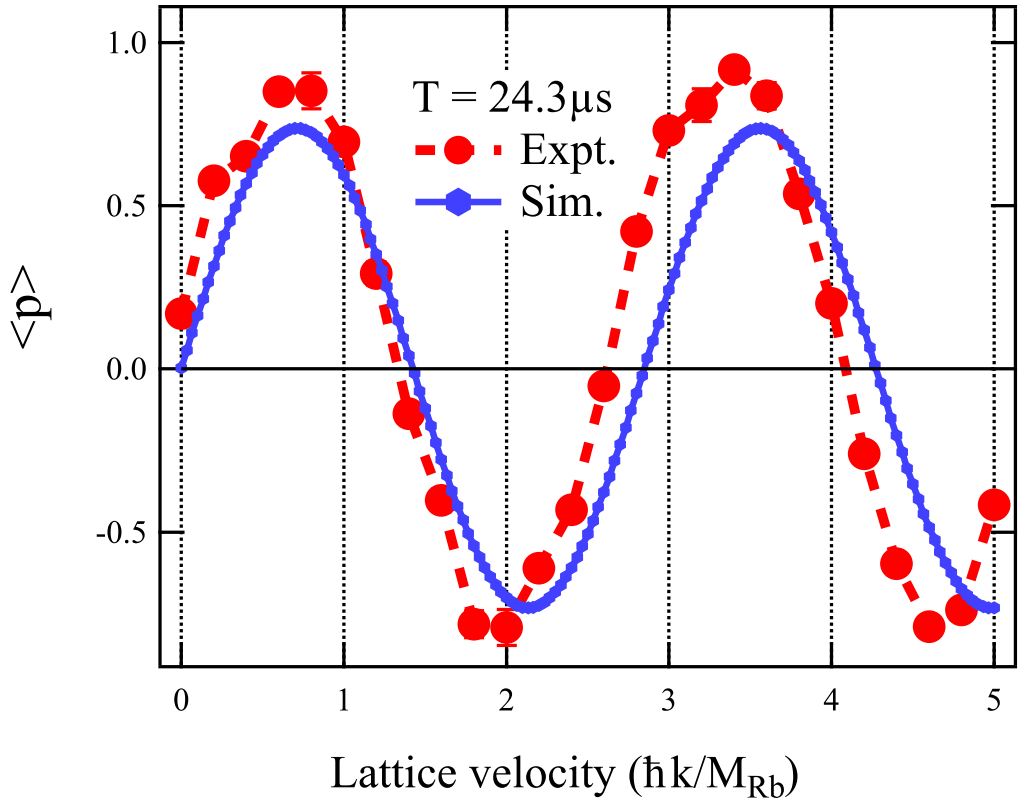

Figure 6.4: Oscillatory behavior of $\langle p \rangle$ as a function of lattice velocity. In this experiment, $\langle p \rangle$ is measured after two kicks

6.6 Measurement of Micromotion of BEC

Measuring the micromotion of the BEC poses a challenge due to its very small magnitude in the direction of the lattice [221]. This small magnitude of the velocity is difficult to measure accurately using conventional time-of-flight methods, which typically require long time-of-flight duration. One such measurement is performed in Ref. [133] through a 225 ms time-of-flight. To address this challenge and accurately measure micromotion, early-time measurements are conducted by systematically tuning α (frequency difference) of the lattice. A single-shot measurement can also measure micromotion if the lattice phase is stable. In these measurements, two different time delays, $T = 24.3\mu$s and $T = 50\mu$s, between two kicks, are employed. The BEC micromotion is measured by tuning the lattice velocity in steps of $0.017\hbar k/M_{Rb}$ corre-

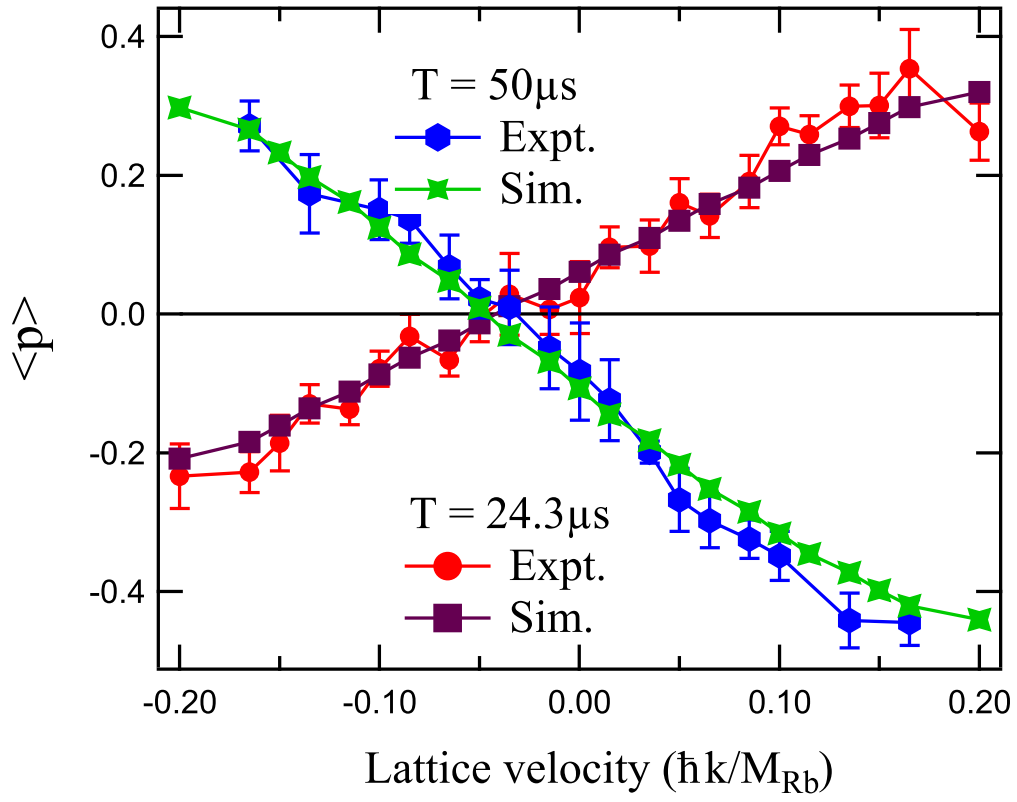

Figure 6.5: Measured $\langle p \rangle$ as a function of lattice velocity by changing the frequency difference α for two different time delays. Micromotion of BEC is measured by scanning over a range of lattice velocity. See text for details.

sponding frequency difference of 250 Hz, as illustrated in Fig. 6.5. The phase evolution induced by micromotion is effectively balanced by the lattice motion. When the net average momentum $\langle p \rangle = 0$, the BEC micromotion velocity can be deduced from the corresponding lattice velocity by linear fit. The calculated lattice velocity at points of $\langle p \rangle = 0$ are $(0.039 \pm 0.003)\hbar k/M_{Rb}$, corresponding to BEC micromotion velocity of (230 ± 17) μm/s for $T = 24.3$ μs, and $(0.043 \pm 0.002)\hbar k/M_{Rb}$, corresponding to a velocity of (254 ± 10) μm/s for $T = 50$ μs. The micromotion can also be obtained by measuring asymmetry, keeping the lattice velocity at $v = 0$, if the proportionality constant c of Eq. 6.4 is known. However, the former method is favoured as it offers a direct and precise measurement of the micromotion.

6.7 Conclusion

This work gives insights about the nature of dynamical localization under two scenarios; (i) when a wave packet is launched with initial momenta $p_0 \neq 0$ in the lab frame, and (ii) when the optical lattice is moved in lab frame. In both scenarios, after a short diffusive timescale, the wavepacket is localized in momentum space with an asymmetric distribution profile. This asymmetry emerges during the early time dynamics – driven by the breaking of parity symmetry due to the motion of the wavepacket or the lattice. This feature is employed for precisely measuring the micromotion of the BEC. For the parameters of the experimental system we employed, velocity measurements yielded (230 ± 17) μm/s for $T = 24.3$ μs and (254 ± 10) μm/s for $T = 50$ μs in our system. This micromotion measurement is crucial for precision instruments such as atom interferometers and atomic gyroscopes, to correct for systematic shifts and uncertainties. The micromotion velocity is an order of magnitude smaller than one recoil photon momentum, as well as comparable to mean velocity associated with BEC temperature. The broken parity symmetry induced by the micromotion is utilized to measure such small velocity. Further, it might not be significantly affected by velocity distribution of the BEC, a common challenge in spectroscopy technique. This work contributes to our understanding of the precision measurement techniques using BEC-based quantum kicked rotor models.

Chapter 7

Conclusion and Future Outlook

7.1 Summary

In summary, this thesis has explored the Floquet engineering for coherent control of chaotic system in periodically kicked optical lattice. It provides a precise control over quantum interference for tuning dynamical localization in the quantum kicked rotor (QKR) system. Additionally, the QKR system serves as a unique tool for probing quantum chaos, strength of quantum coherence over exponentially sensitive classically chaotic systems.

The journey of this thesis began with the task of rebuilding our ^{87}Rb BEC setup, which had stopped working during the COVID-shutdown for almost six months. After reconstructing our robust setup with some modifications and simplifications in the ultra-high vacuum system, implementing homemade control electronics, and creating a flexible LabVIEW program for easy integration with an external Python program, we employed machine learning for optimized evaporation to achieve BEC. Additionally, we also developed a new 'pulse-width modulation technique' to cool the atoms through time-averaged potential. Ultimately, we rebuilt a robust BEC setup that produces a BEC with 8×10^4 atoms and temperature around 70 nK, with an overall production cycle of 8 seconds.

The primary goal of this thesis has been to achieve coherent control over quantum interference without introducing decoherence. Through systematic engineering, two methods have been investigated for controlling dynamical localization in periodically

kicked cold atoms: periodic modulation of a control parameter and a single knob coherent control using Bose-Einstein condensates.

In the first problem, we have investigated a modified kicked rotor model and its experimental implementation using an equivalent atom-optics based test bed. By introducing periodic time delays in the kicking sequence, we effectively flipped the sign of the kick strength after every M kicks, leading to drastic changes in the dynamics with competing effects between localization induced by periodic kick sequences and diffusion induced by sequences with delay times equal to the half-Talbot time. Our findings reveal enhanced quantum mean energies in the modified atom-optics kicked rotor system compared to the standard model, regardless of the presence of transporting islands in classical phase space. Notably, we demonstrate that quantum mean energy enhancement can be achieved without relying on classical features in the atom-optics kicked rotor system, as evidenced by numerical simulations and experimental results. These findings contribute to our understanding of quantum chaos and have broader implications for quantum control.

In the second problem, we utilized BEC for the quantum kicked rotor experiment due to the high phase coherence between momentum states resulting from the narrow quasi-momentum distribution of BEC. Through the proper encoding of relative phase between momentum states via a single time evolution, we effectively steered the QKR dynamics, maintaining robust coherence in the absence of noise and decoherence. This control paradigm allowed for precise adjustments of a single parameter, facilitating targeted alterations in the momentum distribution of the final localized state. We have also demonstrated that such control remains effective even when the system is in a localized state by applying periodic kick, as it maintains quite good coherence. Our quantification of control, measured by the normalized population of zeroth momentum state, showcased an impressive degree of manipulation exceeding 90%, with systematic tunability.

In the final problem, our investigation into the asymmetric localization of momentum distribution in a BEC launched with varying recoil velocities into a periodically kicked optical lattice has yielded valuable insights. We explored this phenomenon in two scenarios: when the BEC is in motion in the laboratory frame and when the op-

tical lattice is in motion. Our findings reveal that this asymmetric behavior emerges during the early-time dynamics and stabilizes as dynamical localization sets in. The early time asymmetry comes from breaking of the parity symmetry due to motion of the wave-function or lattice, so this velocity-dependent features leading to the development of a method for measuring micromotion of BEC. We measure the velocity of the BEC (230 ± 17) μm/s in our system. This micromotion measurement, unaffected by Doppler broadening, offers precise velocity measurements crucial for precision instruments like atom interferometer and atomic gyroscope.

7.2 Future Outlook:

This thesis has focused on studying Floquet engineering in the Quantum Kicked Rotor (QKR) system to achieve coherent control over quantum chaos. Additionally, we have utilized the kicked rotor system for precision measurements of micromotion. The results obtained from these investigations open up possibilities for further experiments in both directions, depending on the goals of the research.

The other aspect involves utilizing Bose-Einstein condensate (BEC) setups with certain modifications to explore momentum-synthesized lattices and BEC loaded into periodically driven optical lattices. These experiments hold promise for advancing our understanding of quantum systems and exploring novel quantum phenomena related to tight-binding model, quantum random walk and Bose-Hubbard Model with arbitrary freedom over parameter space.

Some possibilities for these experiments include:

- Utilizing the QKR system for coherent control of quantum chaos suggests the possibility of extending this approach for optimal coherent targeting. In classical phase space, it's conceivable to connect two points with arbitrary precision, as first discussed in Ulam's conjecture. Can we implement a similar idea in quantum chaotic systems, where tailored perturbations can effectively lead us from one point in phase space to another? Challenge is managing the dynamical spreading of the evolving quantum state and necessitate a delicate balance by tailored perturbation. The QKR system may be an ideal candidate for addressing such a problem, as discussed in a recent theoretical paper [73, 195].

- The measurement of micromotion techniques opens a path for nullifying systematic shifts in precision measurements. The advantage lies in the direct utilization of micromotion pulse schemes in BEC based atom interferometers without the need to change any optical alignment. The concept can be implemented by first applying two delta pulses of moving optical lattices for the measurement of micromotion. Subsequently, $\frac{\pi}{2} - \pi - \frac{\pi}{2}$ pulses are applied for the atom interferometer (AI). Choosing a higher order or opposite order for the AI ensures that it does not get mixed up with the micromotion signal, making it feasible. Additionally, using two delta pulses for micromotion measurement maintains very high fidelity (typically more than 80%, depending on the strength of micromotion) in the zeroth momentum state for the AI. This simultaneous implementation of micromotion measurement and AI has the potential to significantly improve precision measurements.

- The most exciting physics can be explored by utilizing BEC setup for Momentum-Synthesized Lattice (MSL). 1D-MSL has already been utilized as a quantum simulator for single-particle tight-binding Hamiltonians, featuring nearly arbitrary arrangements of tunneling terms, artificial gauge fields, and controllable on-site energy. However, there are many open problems in 2D-MSL and 3D-MSL systems that have not yet been explored by any group.

  A 2D-MSL may open the path for cross-tunneling and cross-hopping in-plane, providing a more logical implementation for exploring artificial gauge fields and kinetic frustration. Similarly, 3D-MSL opens the path for synthesized Weyl materials, dimensionality-dependent localization phenomena, and the possibility to couple the internal states of atoms, as spin, for spin-dependent coupling in MSL.

Bibliography

[1] Z. Ficek and S. Swain, *Quantum interference and coherence: theory and experiments*, vol. 100. Springer Science & Business Media, 2005.

[2] A. Haché, J. Sipe, and H. Van Driel, "Quantum interference control of electrical currents in gaas," *IEEE Journal of Quantum Electronics*, vol. 34, no. 7, pp. 1144–1154, 1998.

[3] H. Mabuchi and N. Khaneja, "Principles and applications of control in quantum systems," *International Journal of Robust and Nonlinear Control: IFAC-Affiliated Journal*, vol. 15, no. 15, pp. 647–667, 2005.

[4] H. Rabitz, R. de Vivie-Riedle, M. Motzkus, and K. Kompa, "Whither the future of controlling quantum phenomena?," *Science*, vol. 288, no. 5467, pp. 824–828, 2000.

[5] M. Shapiro and P. Brumer, *Quantum control of molecular processes*. John Wiley & Sons, 2012.

[6] F. L. Lewis, D. Vrabie, and V. L. Syrmos, *Optimal control*. John Wiley & Sons, 2012.

[7] C. A. Klausmeier, "Floquet theory: a useful tool for understanding nonequilibrium dynamics," *Theoretical Ecology*, vol. 1, pp. 153–161, 2008.

[8] I. M. Georgescu, S. Ashhab, and F. Nori, "Quantum simulation," *Rev. Mod. Phys.*, vol. 86, pp. 153–185, Mar 2014.

[9] L. P. Parazzoli, A. M. Hankin, and G. W. Biedermann, "Observation of free-space single-atom matter wave interference," *Phys. Rev. Lett.*, vol. 109, no. 23, p. 230401, 2012.

[10] H. J. Metcalf and P. Van der Straten, *Laser cooling and trapping*. Springer Science & Business Media, 1999.

[11] C. S. Adams, M. Sigel, and J. Mlynek, "Atom optics," *Physics Reports*, vol. 240, no. 3, pp. 143–210, 1994.

[12] P. Meystre, *Atom optics*, vol. 33. Springer Science & Business Media, 2001.

[13] B. Gadway, "Atom-optics approach to studying transport phenomena," *Phys. Rev. A*, vol. 92, p. 043606, Oct 2015.

[14] S. Bose, "Plancks gesetz und lichtquantenhypothese," *Zeitschrift für Physik*, vol. 26, no. 1, pp. 178–181, 1924.

[15] A. Einstein, "Quantentheorie des einatomigen idealen gases, sitzungsberichte kgl," *Preuss. Akad. Wiss*, vol. 261, 1924.

[16] M. H. Anderson, J. R. Ensher, M. R. Matthews, C. E. Wieman, and E. A. Cornell, "Observation of Bose-Einstein condensation in a dilute atomic vapor," *science*, vol. 269, no. 5221, pp. 198–201, 1995.

[17] K. B. Davis, M.-O. Mewes, M. R. Andrews, N. J. van Druten, D. S. Durfee, D. Kurn, and W. Ketterle, "Bose-Einstein condensation in a gas of sodium atoms," *Phys. Rev. Lett.*, vol. 75, no. 22, p. 3969, 1995.

[18] A. J. Leggett, "Bose-Einstein condensation in the alkali gases: Some fundamental concepts," *Rev. Mod. Phys.*, vol. 73, pp. 307–356, Apr 2001.

[19] C. Deppner, W. Herr, M. Cornelius, P. Stromberger, T. Sternke, C. Grzeschik, A. Grote, J. Rudolph, S. Herrmann, M. Krutzik, A. Wenzlawski, R. Corgier, E. Charron, D. Guéry-Odelin, N. Gaaloul, C. Lämmerzahl, A. Peters, P. Windpassinger, and E. M. Rasel, "Collective-mode enhanced matter-wave optics," *Phys. Rev. Lett.*, vol. 127, p. 100401, Aug 2021.

[20] S. Burger, F. S. Cataliotti, C. Fort, F. Minardi, M. Inguscio, M. L. Chiofalo, and M. P. Tosi, "Superfluid and dissipative dynamics of a Bose-Einstein condensate in a periodic optical potential," *Phys. Rev. Lett.*, vol. 86, pp. 4447–4450, May 2001.

[21] B. P. Anderson and M. A. Kasevich, "Macroscopic quantum interference from atomic tunnel arrays," *Science*, vol. 282, no. 5394, pp. 1686–1689, 1998.

[22] M.-S. Chang, C. D. Hamley, M. D. Barrett, J. A. Sauer, K. M. Fortier, W. Zhang, L. You, and M. S. Chapman, "Observation of spinor dynamics in optically trapped $^{87}\mathrm{Rb}$ Bose-Einstein condensates," *Phys. Rev. Lett.*, vol. 92, p. 140403, Apr 2004.

[23] Y. Kawaguchi and M. Ueda, "Spinor Bose-Einstein condensates," *Physics Reports*, vol. 520, no. 5, pp. 253–381, 2012.

[24] J. R. Abo-Shaeer, C. Raman, J. M. Vogels, and W. Ketterle, "Observation of vortex lattices in Bose-Einstein condensates," *Science*, vol. 292, no. 5516, pp. 476–479, 2001.

[25] M. R. Matthews, B. P. Anderson, P. C. Haljan, D. S. Hall, C. E. Wieman, and E. A. Cornell, "Vortices in a Bose-Einstein condensate," *Phys. Rev. Lett.*, vol. 83, pp. 2498–2501, Sep 1999.

[26] O. Lahav, A. Itah, A. Blumkin, C. Gordon, S. Rinott, A. Zayats, and J. Steinhauer, "Realization of a sonic black hole analog in a Bose-Einstein condensate," *Phys. Rev. Lett.*, vol. 105, p. 240401, Dec 2010.

[27] P. W. Anderson, "Absence of diffusion in certain random lattices," *Phys. Rev.*, vol. 109, pp. 1492–1505, Mar 1958.

[28] E. Abrahams, P. Anderson, D. Licciardello, and T. Ramakrishnan, "Scaling theory of localization: Absence of quantum diffusion in two dimensions," *Phys. Rev. Lett.*, vol. 42, no. 10, p. 673, 1979.

[29] D. J. Thouless, "A relation between the density of states and range of localization for one dimensional random systems," *Journal of Physics C: Solid State Physics*, vol. 5, no. 1, p. 77, 1972.

[30] F. Domınguez-Adame and V. Malyshev, "A simple approach to anderson localization in one-dimensional disordered lattices," *American Journal of Physics*, vol. 72, no. 2, pp. 226–230, 2004.

[31] J. Billy, V. Josse, Z. Zuo, A. Bernard, B. Hambrecht, P. Lugan, D. Clément, L. Sanchez-Palencia, P. Bouyer, and A. Aspect, "Direct observation of anderson localization of matter waves in a controlled disorder," *Nature*, vol. 453, pp. 891–894, Jun 2008.

[32] D. H. White, T. A. Haase, D. J. Brown, M. D. Hoogerland, M. S. Najafabadi, J. L. Helm, C. Gies, D. Schumayer, and D. A. W. Hutchinson, "Observation of two-dimensional anderson localisation of ultracold atoms," *Nat Commun*, vol. 11, p. 4942, Oct 2020.

[33] G. Semeghini, M. Landini, P. Castilho, S. Roy, G. Spagnolli, A. Trenkwalder, M. Fattori, M. Inguscio, and G. Modugno, "Measurement of the mobility edge for 3d anderson localization," *Nat. Phys.*, vol. 11, no. 7, pp. 554–559, 2015.

[34] C. Guan and X. Guan, "A brief introduction to anderson localization," *Department of Physics, Massachusetts Institute of Technology*, 2019.

[35] R. Omnes, "Logical reformulation of quantum mechanics. ii. interferences and the einstein-podolsky-rosen experiment," *Journal of Statistical Physics*, vol. 53, pp. 933–955, 1988.

[36] U. Sinha, C. Couteau, T. Jennewein, R. Laflamme, and G. Weihs, "Ruling out multi-order interference in quantum mechanics," *Science*, vol. 329, no. 5990, pp. 418–421, 2010.

[37] T. Schumm, S. Hofferberth, L. M. Andersson, S. Wildermuth, S. Groth, I. Bar-Joseph, J. Schmiedmayer, and P. Krüger, "Matter-wave interferometry in a double well on an atom chip," *Nature physics*, vol. 1, no. 1, pp. 57–62, 2005.

[38] K. Li, L. Deng, E. W. Hagley, M. G. Payne, and M. S. Zhan, "Matter-wave self-imaging by atomic center-of-mass motion induced interference," *Phys. Rev. Lett.*, vol. 101, p. 250401, Dec 2008.

[39] M. S. Santhanam, S. Paul, and J. Bharathi Kannan, "Quantum kicked rotor and its variants: Chaos, localization and beyond," *Physics Reports*, vol. 956, pp. 1–87, 2022.

[40] F. L. Moore, J. C. Robinson, C. Bharucha, P. E. Williams, and M. G. Raizen, "Observation of dynamical localization in atomic momentum transfer: A new testing ground for quantum chaos," *Phys. Rev. Lett.*, vol. 73, pp. 2974–2977, Nov 1994.

[41] M. Bitter and V. Milner, "Experimental observation of dynamical localization in laser-kicked molecular rotors," *Phys. Rev. Lett.*, vol. 117, no. 14, p. 144104, 2016.

[42] M. Bitter and V. Milner, "Experimental demonstration of coherent control in quantum chaotic systems," *Phys. Rev. Lett.*, vol. 118, no. 3, p. 034101, 2017.

[43] S. S. Maurya, S. B. Kannan, K. Patel, P. Dutta, K. Biswas, J. Mangaonkar, M. Santhanam, and U. D. Rapol, "Control of dynamical localization in atom-optics kicked rotor," *arXiv preprint arXiv:2202.02820*, 2022.

[44] S. Dadras, A. Gresch, C. Groiseau, S. Wimberger, and G. S. Summy, "Quantum walk in momentum space with a Bose-Einstein condensate," *Phys. Rev. Lett.*, vol. 121, p. 070402, Aug 2018.

[45] H.-J. Stöckmann, *Quantum Chaos: An Introduction*. American Association of Physics Teachers, 2000.

[46] R. M. Steck DA, Oskay WH, "Observation of chaos-assisted tunneling between islands of stability," *Science (New York, N.Y.)*, vol. 293, Jul 2001.

[47] C. Eltschka and P. Schlagheck, "Resonance-and chaos-assisted tunneling in mixed regular-chaotic systems," *Phys. Rev. Lett.*, vol. 94, no. 1, p. 014101, 2005.

[48] S. Fishman, D. R. Grempel, and R. E. Prange, "Chaos, quantum recurrences, and anderson localization," *Phys. Rev. Lett.*, vol. 49, pp. 509–512, Aug 1982.

[49] F. L. Moore, J. C. Robinson, C. F. Bharucha, B. Sundaram, and M. G. Raizen, "Atom optics realization of the quantum δ-kicked rotor," *Phys. Rev. Lett.*, vol. 75, pp. 4598–4601, Dec 1995.

[50] I. Manai, J.-F. m. c. Clément, R. Chicireanu, C. Hainaut, J. C. Garreau, P. Szriftgiser, and D. Delande, "Experimental observation of two-dimensional anderson localization with the atomic kicked rotor," *Phys. Rev. Lett.*, vol. 115, p. 240603, Dec 2015.

[51] R. C. Kuhn, C. Miniatura, D. Delande, O. Sigwarth, and C. A. Müller, "Localization of matter waves in two-dimensional disordered optical potentials," *Phys. Rev. Lett.*, vol. 95, p. 250403, Dec 2005.

[52] J. Ringot, P. Szriftgiser, J. C. Garreau, and D. Delande, "Experimental evidence of dynamical localization and delocalization in a quasiperiodic driven system," *Phys. Rev. Lett.*, vol. 85, pp. 2741–2744, Sep 2000.

[53] J. Chabé, G. Lemarié, B. Grémaud, D. Delande, P. Szriftgiser, and J. C. Garreau, "Experimental observation of the anderson metal-insulator transition with atomic matter waves," *Phys. Rev. Lett.*, vol. 101, p. 255702, Dec 2008.

[54] G. Lemarié, H. Lignier, D. Delande, P. Szriftgiser, and J. C. Garreau, "Critical state of the anderson transition: Between a metal and an insulator," *Phys. Rev. Lett.*, vol. 105, p. 090601, Aug 2010.

[55] M. Lopez, J.-F. m. c. Clément, P. Szriftgiser, J. C. Garreau, and D. Delande, "Experimental test of universality of the anderson transition," *Phys. Rev. Lett.*, vol. 108, p. 095701, Feb 2012.

[56] S. Sarkar, S. Paul, C. Vishwakarma, S. Kumar, G. Verma, M. Sainath, U. D. Rapol, and M. S. Santhanam, "Nonexponential decoherence and subdiffusion in atom-optics kicked rotor," *Phys. Rev. Lett.*, vol. 118, p. 174101, Apr 2017.

[57] D. A. Steck, V. Milner, W. H. Oskay, and M. G. Raizen, "Quantitative study of amplitude noise effects on dynamical localization," *Phys. Rev. E*, vol. 62, pp. 3461–3475, Sep 2000.

[58] D. H. White, S. K. Ruddell, and M. D. Hoogerland, "Phase noise in the delta kicked rotor: from quantum to classical," *New Journal of Physics*, vol. 16, p. 113039, nov 2014.

[59] H. Ammann, R. Gray, I. Shvarchuck, and N. Christensen, "Quantum delta-kicked rotor: Experimental observation of decoherence," *Phys. Rev. Lett.*, vol. 80, pp. 4111–4115, May 1998.

[60] H. Schomerus and E. Lutz, "Controlled decoherence in a quantum lévy kicked rotator," *Phys. Rev. A*, vol. 77, p. 062113, Jun 2008.

[61] B. Gadway, J. Reeves, L. Krinner, and D. Schneble, "Evidence for a quantum-to-classical transition in a pair of coupled quantum rotors," *Phys. Rev. Lett.*, vol. 110, p. 190401, May 2013.

[62] J. H. S. Toh, M. Du, X. Tang, Y. Su, T. Rojo, C. O. Patterson, N. R. Williams, C. Zhang, and S. Gupta, "Evidence for a many-body anderson metal-insulator transition using kicked quantum gases," *arXiv preprint arXiv:2305.14817*, 2023.

[63] J. H. See Toh, K. C. McCormick, X. Tang, Y. Su, X.-W. Luo, C. Zhang, and S. Gupta, "Many-body dynamical delocalization in a kicked one-dimensional ultracold gas," *Nature Physics*, vol. 18, pp. 1297–1301, Nov 2022.

[64] A. Cao, R. Sajjad, H. Mas, E. Q. Simmons, J. L. Tanlimco, E. Nolasco-Martinez, T. Shimasaki, H. E. Kondakci, V. Galitski, and D. M. Weld, "Interaction-driven breakdown of dynamical localization in a kicked quantum gas," *Nature Physics*, vol. 18, no. 11, pp. 1302–1306, 2022.

[65] M. Sadgrove, M. Horikoshi, T. Sekimura, and K. Nakagawa, "Rectified momentum transport for a kicked Bose-Einstein condensate," *Phys. Rev. Lett.*, vol. 99, p. 043002, Jul 2007.

[66] I. Dana, V. Ramareddy, I. Talukdar, and G. S. Summy, "Experimental realization of quantum-resonance ratchets at arbitrary quasimomenta," *Phys. Rev. Lett.*, vol. 100, p. 024103, Jan 2008.

[67] R. Sajjad, J. L. Tanlimco, H. Mas, A. Cao, E. Nolasco-Martinez, E. Q. Simmons, F. L. N. Santos, P. Vignolo, T. Macrì, and D. M. Weld, "Observation of the quantum boomerang effect," *Phys. Rev. X*, vol. 12, p. 011035, Feb 2022.

[68] L. Tessieri, Z. Akdeniz, N. Cherroret, D. Delande, and P. Vignolo, "Quantum boomerang effect: Beyond the standard anderson model," *Phys. Rev. A*, vol. 103, p. 063316, Jun 2021.

[69] F. Noronha, J. A. Lourenço, and T. Macrì, "Robust quantum boomerang effect in non-hermitian systems," *Phys. Rev. B*, vol. 106, no. 10, p. 104310, 2022.

[70] J. Ni, W. K. Lam, S. Dadras, M. F. Borunda, S. Wimberger, and G. S. Summy, "Initial-state dependence of a quantum resonance ratchet," *Phys. Rev. A*, vol. 94, p. 043620, Oct 2016.

[71] T. Prat, D. Delande, and N. Cherroret, "Quantum boomeranglike effect of wave packets in random media," *Phys. Rev. A*, vol. 99, no. 2, p. 023629, 2019.

[72] A. J. Daley and A. S. Parkins, "Early time diffusion for the quantum kicked rotor with narrow initial momentum distributions," *Phys. Rev. E*, vol. 66, p. 056210, Nov 2002.

[73] S. Tomsovic, J. D. Urbina, and K. Richter, "Controlling quantum chaos: Optimal coherent targeting," *Phys. Rev. Lett.*, vol. 130, p. 020201, Jan 2023.

[74] C. Gross and I. Bloch, "Quantum simulations with ultracold atoms in optical lattices," *Science*, vol. 357, no. 6355, pp. 995–1001, 2017.

[75] F. Schäfer, T. Fukuhara, S. Sugawa, Y. Takasu, and Y. Takahashi, "Tools for quantum simulation with ultracold atoms in optical lattices," *Nature Reviews Physics*, vol. 2, no. 8, pp. 411–425, 2020.

[76] J. Simon, W. S. Bakr, R. Ma, M. E. Tai, P. M. Preiss, and M. Greiner, "Quantum simulation of antiferromagnetic spin chains in an optical lattice," *Nature*, vol. 472, no. 7343, pp. 307–312, 2011.

[77] W. Zwerger, "Mott–hubbard transition of cold atoms in optical lattices," *Journal of Optics B: quantum and semiclassical optics*, vol. 5, no. 2, p. S9, 2003.

[78] M. Greiner, O. Mandel, T. Esslinger, T. W. Hänsch, and I. Bloch, "Quantum phase transition from a superfluid to a mott insulator in a gas of ultracold atoms," *nature*, vol. 415, no. 6867, pp. 39–44, 2002.

[79] W. S. Bakr, A. Peng, M. E. Tai, R. Ma, J. Simon, J. I. Gillen, S. Foelling, L. Pollet, and M. Greiner, "Probing the superfluid–to–mott insulator transition at the single-atom level," *Science*, vol. 329, no. 5991, pp. 547–550, 2010.

[80] W. S. Bakr, J. I. Gillen, A. Peng, S. Fölling, and M. Greiner, "A quantum gas microscope for detecting single atoms in a hubbard-regime optical lattice," *Nature*, vol. 462, no. 7269, pp. 74–77, 2009.

[81] N. Gemelke, X. Zhang, C.-L. Hung, and C. Chin, "In situ observation of incompressible mott-insulating domains in ultracold atomic gases," *Nature*, vol. 460, no. 7258, pp. 995–998, 2009.

[82] N. Dupont, G. Chatelain, L. Gabardos, M. Arnal, J. Billy, B. Peaudecerf, D. Sugny, and D. Guéry-Odelin, "Quantum state control of a Bose-Einstein condensate in an optical lattice," *PRX Quantum*, vol. 2, p. 040303, Oct 2021.

[83] N. Dupont, L. Gabardos, F. Arrouas, N. Ombredane, J. Billy, B. Peaudecerf, and D. Guéry-Odelin, "Hamiltonian ratchet for matter-wave transport," *Phys. Rev. Lett.*, vol. 131, p. 133401, Sep 2023.

[84] E. J. Meier, F. A. An, and B. Gadway, "Atom-optics simulator of lattice transport phenomena," *Phys. Rev. A*, vol. 93, p. 051602, May 2016.

[85] M. Kozuma, L. Deng, E. W. Hagley, J. Wen, R. Lutwak, K. Helmerson, S. Rolston, and W. D. Phillips, "Coherent splitting of Bose-Einstein condensed atoms

with optically induced bragg diffraction," *Phys. Rev. Lett.*, vol. 82, no. 5, p. 871, 1999.

[86] E. J. Meier, F. A. An, and B. Gadway, "Observation of the topological soliton state in the su–schrieffer–heeger model," *Nat Commun*, vol. 7, no. 1, p. 13986, 2016.

[87] E. J. Meier, F. A. An, A. Dauphin, M. Maffei, P. Massignan, T. L. Hughes, and B. Gadway, "Observation of the topological anderson insulator in disordered atomic wires," *Science*, vol. 362, no. 6417, pp. 929–933, 2018.

[88] F. A. An, K. Padavić, E. J. Meier, S. Hegde, S. Ganeshan, J. H. Pixley, S. Vishveshwara, and B. Gadway, "Interactions and mobility edges: Observing the generalized aubry-andré model," *Phys. Rev. Lett.*, vol. 126, p. 040603, Jan 2021.

[89] J. Bollinger, J. Prestage, W. M. Itano, and D. Wineland, "Laser-cooled-atomic frequency standard," *Phys. Rev. Lett.*, vol. 54, no. 10, p. 1000, 1985.

[90] M. O. Scully and J. P. Dowling, "Quantum-noise limits to matter-wave interferometry," *Phys. Rev. A*, vol. 48, pp. 3186–3190, Oct 1993.

[91] K. S. Hardman, P. J. Everitt, G. D. McDonald, P. Manju, P. B. Wigley, M. A. Sooriyabandara, C. C. N. Kuhn, J. E. Debs, J. D. Close, and N. P. Robins, "Simultaneous precision gravimetry and magnetic gradiometry with a Bose-Einstein condensate: A high precision, quantum sensor," *Phys. Rev. Lett.*, vol. 117, p. 138501, Sep 2016.

[92] Z.-K. Hu, B.-L. Sun, X.-C. Duan, M.-K. Zhou, L.-L. Chen, S. Zhan, Q.-Z. Zhang, and J. Luo, "Demonstration of an ultrahigh-sensitivity atom-interferometry absolute gravimeter," *Phys. Rev. A*, vol. 88, p. 043610, Oct 2013.

[93] J. E. Debs, P. A. Altin, T. H. Barter, D. Döring, G. R. Dennis, G. McDonald, R. P. Anderson, J. D. Close, and N. P. Robins, "Cold-atom gravimetry with a Bose-Einstein condensate," *Phys. Rev. A*, vol. 84, p. 033610, Sep 2011.

[94] A. Peters, K. Y. Chung, and S. Chu, "Measurement of gravitational acceleration by dropping atoms," *Nature*, vol. 400, no. 6747, pp. 849–852, 1999.

[95] P. Dutta, S. S. Maurya, K. Biswas, K. Patel, and U. D. Rapol, "Comparative analysis of phase noise for different configurations of bragg lattice for an atomic gravimeter with Bose-Einstein condensate," *AIP Advances*, vol. 14, no. 1, 2024.

[96] T. D. Ladd, F. Jelezko, R. Laflamme, Y. Nakamura, C. Monroe, and J. L. O Brien, "Quantum computers," *nature*, vol. 464, no. 7285, pp. 45–53, 2010.

[97] J. Preskill, "Reliable quantum computers," *Proceedings of the Royal Society of London. Series A: Mathematical, Physical and Engineering Sciences*, vol. 454, no. 1969, pp. 385–410, 1998.

[98] M. Saffman, T. G. Walker, and K. Mølmer, "Quantum information with rydberg atoms," *Rev. Mod. Phys.*, vol. 82, pp. 2313–2363, Aug 2010.

[99] D. Bluvstein, S. J. Evered, A. A. Geim, S. H. Li, H. Zhou, T. Manovitz, S. Ebadi, M. Cain, M. Kalinowski, D. Hangleiter, *et al.*, "Logical quantum processor based on reconfigurable atom arrays," *Nature*, vol. 626, no. 7997, pp. 58–65, 2024.

[100] M. Saffman, "Quantum computing with atomic qubits and rydberg interactions: progress and challenges," *Journal of Physics B: Atomic, Molecular and Optical Physics*, vol. 49, no. 20, p. 202001, 2016.

[101] S. J. Evered, D. Bluvstein, M. Kalinowski, S. Ebadi, T. Manovitz, H. Zhou, S. H. Li, A. A. Geim, T. T. Wang, N. Maskara, *et al.*, "High-fidelity parallel entangling gates on a neutral atom quantum computer," *arXiv preprint arXiv:2304.05420*, 2023.

[102] T. F. Gallagher, "Rydberg atoms," in *Springer Handbook of Atomic, Molecular, and Optical Physics*, pp. 231–240, Springer, 1994.

[103] E. Urban, T. A. Johnson, T. Henage, L. Isenhower, D. Yavuz, T. Walker, and M. Saffman, "Observation of rydberg blockade between two atoms," *Nat. Phys.*, vol. 5, no. 2, pp. 110–114, 2009.

[104] J. Honer, H. Weimer, T. Pfau, and H. P. Büchler, "Collective many-body interaction in rydberg dressed atoms," *Phys. Rev. Lett.*, vol. 105, no. 16, p. 160404, 2010.

[105] L. E. Reichl, *Transition to Chaos*. Springer, 2021.

[106] G. Casati, B. Chirikov, F. Izraelev, and J. Ford, "Stochastic behavior of a quantum pendulum under a periodic perturbation," in *Stochastic Behavior in Classical and Quantum Hamiltonian Systems: Volta Memorial Conference, Como, 1977*, pp. 334–352, Springer, 2005.

[107] B. Chirikov and D. Shepelyansky, "Chirikov standard map," *Scholarpedia*, vol. 3, no. 3, p. 3550, 2008.

[108] D. Delande, "Kicked rotor and anderson localization," *Boulder School on Condensed Matter Physics*, 2013.

[109] B. V. Chirikov, "A universal instability of many-dimensional oscillator systems," *Physics reports*, vol. 52, no. 5, pp. 263–379, 1979.

[110] J. Gong and P. Brumer, "Directed anomalous diffusion without a biased field: A ratchet accelerator," *Phys. Rev. E*, vol. 70, p. 016202, Jul 2004.

[111] C. Hainaut, A. Rançon, J.-F. m. c. Clément, J. C. Garreau, P. Szriftgiser, R. Chicireanu, and D. Delande, "Ratchet effect in the quantum kicked rotor and its destruction by dynamical localization," *Phys. Rev. A*, vol. 97, p. 061601, Jun 2018.

[112] S. S. Maurya, J. B. Kannan, K. Patel, P. Dutta, K. Biswas, J. Mangaonkar, M. S. Santhanam, and U. D. Rapol, "Interplay between quantum diffusion and localization in the atom-optics kicked rotor," *Phys. Rev. E*, vol. 106, p. 034207, Sep 2022.

[113] G. Casati, B. Chirikov, F. Izrailev, and J. Ford, "Stochastic behavior of a quantum pendulum under a periodic perturbation, vol. 93 of lecture notes in physics springer-verlag," 1979.

[114] M. B. d'Arcy, R. M. Godun, M. K. Oberthaler, D. Cassettari, and G. S. Summy, "Quantum enhancement of momentum diffusion in the delta-kicked rotor," *Phys. Rev. Lett.*, vol. 87, p. 074102, Jul 2001.

[115] G. Floquet, "Sur les équations différentielles linéaires à coefficients périodiques," in *Annales scientifiques de l'École normale supérieure*, vol. 12, pp. 47–88, 1883.

[116] S. Barone, M. Narcowich, and F. Narcowich, "Floquet theory and applications," *Phys. Rev. A*, vol. 15, no. 3, p. 1109, 1977.

[117] M. Saunders, P. L. Halkyard, K. J. Challis, and S. A. Gardiner, "Manifestation of quantum resonances and antiresonances in a finite-temperature dilute atomic gas," *Phys. Rev. A*, vol. 76, p. 043415, Oct 2007.

[118] M. Shapiro and P. Brumer, "Coherent control of atomic, molecular, and electronic processes," in *Advances in atomic, molecular, and optical physics*, vol. 42, pp. 287–345, Elsevier, 2000.

[119] J. Gong, H. J. Wörner, and P. Brumer, "Control of dynamical localization," *Phys. Rev. E*, vol. 68, p. 056202, Nov 2003.

[120] L. Deng, E. W. Hagley, J. Denschlag, J. E. Simsarian, M. Edwards, C. W. Clark, K. Helmerson, S. L. Rolston, and W. D. Phillips, "Temporal, matter-wave-dispersion talbot effect," *Phys. Rev. Lett.*, vol. 83, pp. 5407–5411, Dec 1999.

[121] J. Wen, Y. Zhang, and M. Xiao, "The talbot effect: recent advances in classical optics, nonlinear optics, and quantum optics," *Advances in optics and photonics*, vol. 5, no. 1, pp. 83–130, 2013.

[122] M. Weiß, C. Groiseau, W. K. Lam, R. Burioni, A. Vezzani, G. S. Summy, and S. Wimberger, "Steering random walks with kicked ultracold atoms," *Phys. Rev. A*, vol. 92, p. 033606, Sep 2015.

[123] J. Mangaonkar, C. Vishwakarma, S. S. Maurya, S. Sarkar, J. L. MacLennan, P. Dutta, and U. D. Rapol, "Effects of finite momentum width on the reversal

dynamics in a BEC based atom optics Î´-kicked rotor," *Journal of Physics B: Atomic, Molecular and Optical Physics*, vol. 53, p. 235502, nov 2020.

[124] L. Wang, G. Benenti, G. Casati, and B. Li, "Ratchet effect and the transporting islands in the chaotic sea," *Phys. Rev. Lett.*, vol. 99, no. 24, p. 244101, 2007.

[125] D. L. Shepelyansky, "Some statistical properties of simple classically stochastic quantum systems," *Physica D: Nonlinear Phenomena*, vol. 8, no. 1-2, pp. 208–222, 1983.

[126] F. Haake, *Quantum signatures of chaos*. Springer, 1991.

[127] B. V. Chirikov, F. M. Izrailev, and D. L. Shepelyansky, "Dynamical stochasticity in classical and quantum mechanics," *Sov. Sci. Rev. C*, vol. 2, no. 4, pp. 209–267, 1981.

[128] J. Gong and P. Brumer, "Coherent control of quantum chaotic diffusion," *Phys. Rev. Lett.*, vol. 86, pp. 1741–1744, Feb 2001.

[129] J. Gong and P. Brumer, "Coherent control of quantum chaotic diffusion: Diatomic molecules in a pulsed microwave field," *The Journal of Chemical Physics*, vol. 115, no. 8, pp. 3590–3597, 2001.

[130] J. Gong, H. J. Woerner, and P. Brumer, "Coherent manipulation of quantum δ-kicked dynamics: Faster-than-classical anomalous diffusion," *Phys. Rev. E*, vol. 68, no. 2, p. 026209, 2003.

[131] G. Lemarié, H. Lignier, D. Delande, P. Szriftgiser, and J. C. Garreau, "Critical state of the anderson transition: between a metal and an insulator," *Phys. Rev. Lett.*, vol. 105, no. 9, p. 090601, 2010.

[132] J.-A. Currivan, A. Ullah, and M. Hoogerland, "The initial velocity dependence of the quantum resonance in the delta-kicked rotor," *Europhysics Letters*, vol. 85, no. 3, p. 30005, 2009.

[133] K. S. Hardman, "A BEC-based precision gravimeter and magnetic gradiometer: Design and implementation," *The Australian National University*, 2016.

[134] P. Jones, M. Goonasekera, D. Meacher, T. Jonckheere, and T. Monteiro, "Directed motion for delta-kicked atoms with broken symmetries: Comparison between theory and experiment," *Phys. Rev. Lett.*, vol. 98, no. 7, p. 073002, 2007.

[135] P. Jones, M. Goonasekera, H. Saunders-Singer, and D. Meacher, "Shifting the boundaries: Pulse-shape effects in the atom-optics kicked rotor," *Europhysics Letters*, vol. 67, no. 6, p. 928, 2004.

[136] G. Hur, C. Creffield, P. Jones, and T. Monteiro, "Chaotic quantum ratchets and filters with cold atoms in optical lattices: Analysis using floquet states," *Phys. Rev. A*, vol. 72, no. 1, p. 013403, 2005.

[137] J. W. Cooley and J. W. Tukey, "An algorithm for the machine calculation of complex fourier series," *Mathematics of computation*, vol. 19, no. 90, pp. 297–301, 1965.

[138] J. A. Fleck, J. Morris, and M. Feit, "Time-dependent propagation of high energy laser beams through the atmosphere," *Applied physics*, vol. 10, pp. 129–160, 1976.

[139] A. D. Bandrauk and H. Shen, "Exponential split operator methods for solving coupled time-dependent schrödinger equations," *The Journal of chemical physics*, vol. 99, no. 2, pp. 1185–1193, 1993.

[140] U. Fano, "Description of states in quantum mechanics by density matrix and operator techniques," *Rev. Mod. Phys.*, vol. 29, pp. 74–93, Jan 1957.

[141] D. Sundararajan, *The discrete Fourier transform: theory, algorithms and applications*. World Scientific, 2001.

[142] G. Strang, "On the construction and comparison of difference schemes," *SIAM journal on numerical analysis*, vol. 5, no. 3, pp. 506–517, 1968.

[143] S. Kumar, *Towards Distributed Quantum Information Processing Using Coupling of Neutral Atoms to Plasmonic Nanostructures*. PhD thesis, Department of Physics, IISER Pune, 2017.

[144] S. Sarkar, *Ultracold Atoms in 1-D Optical Lattices: Experiments Towards Quantum Chaos and Atom Interferometry*. PhD thesis, Department of Physics, IISER Pune, 2019.

[145] W. D. Phillips, "Nobel lecture: Laser cooling and trapping of neutral atoms," *Rev. Mod. Phys.*, vol. 70, no. 3, p. 721, 1998.

[146] C. J. Foot, *Atomic physics*, vol. 7. OUP Oxford, 2004.

[147] C. Cohen-Tannoudji, J. Dupont-Roc, and G. Grynberg, *Atom-photon interactions: basic processes and applications*. John Wiley & Sons, 1998.

[148] S. Chu, L. Hollberg, J. E. Bjorkholm, A. Cable, and A. Ashkin, "Three-dimensional viscous confinement and cooling of atoms by resonance radiation pressure," *Phys. Rev. Lett.*, vol. 55, no. 1, p. 48, 1985.

[149] D. A. Steck, "Rubidium 87 d line data," *Self Journal*, 2001.

[150] C. J. Dedman, J. Nes, T. Hanna, R. Dall, K. Baldwin, and A. Truscott, "Optimum design and construction of a zeeman slower for use with a magneto-optic trap," *Review of Scientific Instruments*, vol. 75, no. 12, pp. 5136–5142, 2004.

[151] M. Fox, "Oxford master series in atomic, optical and laser physics," *Quantum optics: an introduction, Oxford Univ. Press, Oxford*, 2006.

[152] C. Townsend, N. Edwards, C. Cooper, K. Zetie, C. Foot, A. Steane, P. Szriftgiser, H. Perrin, and J. Dalibard, "Phase-space density in the magneto-optical trap," *Phys. Rev. A*, vol. 52, no. 2, p. 1423, 1995.

[153] P. Cheiney, O. Carraz, D. Bartoszek-Bober, S. Faure, F. Vermersch, C. Fabre, G. L. Gattobigio, T. Lahaye, D. Guéry-Odelin, and R. Mathevet, "A zeeman slower design with permanent magnets in a halbach configuration," *Review of Scientific Instruments*, vol. 82, no. 6, 2011.

[154] U. D. Rapol, A. Wasan, and V. Natarajan, "Loading of a Rb magneto-optic trap from a getter source," *Phys. Rev. A*, vol. 64, no. 2, p. 023402, 2001.

[155] W. Petrich, M. H. Anderson, J. R. Ensher, and E. A. Cornell, "Behavior of atoms in a compressed magneto-optical trap," *JOSA B*, vol. 11, no. 8, pp. 1332–1335, 1994.

[156] R. Grimm, M. Weidemüller, and Y. B. Ovchinnikov, "Optical dipole traps for neutral atoms," in *Advances in atomic, molecular, and optical physics*, vol. 42, pp. 95–170, Elsevier, 2000.

[157] S. Kuppens, K. Corwin, K. Miller, T. Chupp, and C. Wieman, "Loading an optical dipole trap," *Phys. Rev. A*, vol. 62, no. 1, p. 013406, 2000.

[158] A. J. Olson, R. J. Niffenegger, and Y. P. Chen, "Optimizing the efficiency of evaporative cooling in optical dipole traps," *Phys. Rev. A*, vol. 87, no. 5, p. 053613, 2013.

[159] A. Marchant, S. Händel, S. Hopkins, T. Wiles, and S. Cornish, "Bose-Einstein condensation of 85 rb by direct evaporation in an optical dipole trap," *Phys. Rev. A*, vol. 85, no. 5, p. 053647, 2012.

[160] S. Chaudhuri, S. Roy, and C. Unnikrishnan, "Evaporative cooling of atoms to quantum degeneracy in an optical dipole trap," in *Journal of Physics: Conference Series*, vol. 80, p. 012036, IOP Publishing, 2007.

[161] P. B. Wigley, P. J. Everitt, A. van den Hengel, J. W. Bastian, M. A. Sooriyabandara, G. D. McDonald, K. S. Hardman, C. D. Quinlivan, P. Manju, C. C. Kuhn, *et al.*, "Fast machine-learning online optimization of ultra-cold-atom experiments," *Sci Rep*, vol. 6, no. 1, p. 25890, 2016.

[162] Z. Vendeiro, J. Ramette, A. Rudelis, M. Chong, J. Sinclair, L. Stewart, A. Urvoy, and V. Vuletić, "Machine-learning-accelerated Bose-Einstein condensation," *Phys. Rev. Res.*, vol. 4, no. 4, p. 043216, 2022.

[163] E. Davletov, V. Tsyganok, V. Khlebnikov, D. Pershin, D. Shaykin, and A. Akimov, "Machine learning for achieving Bose-Einstein condensation of thulium atoms," *Phys. Rev. A*, vol. 102, no. 1, p. 011302, 2020.

[164] K. Biswas, K. Patel, S. S. Maurya, P. Dutta, and U. D. Rapol, "Machine-learning-based automated loading of strontium isotopes into magneto-optical trap," *AIP Advances*, vol. 13, no. 7, 2023.

[165] S. Paul, S. Sarkar, C. Vishwakarma, J. Mangaonkar, M. Santhanam, and U. Rapol, "Nonmonotonic diffusion rates in an atom-optics lévy kicked rotor," *Phys. Rev. E*, vol. 100, no. 6, p. 060201, 2019.

[166] P. Dutta, S. S. Maurya, K. Patel, K. Biswas, J. Mangaonkar, S. Sarkar, and U. D. Rapol, "A decade of advancement of quantum sensing and metrology in india using cold atoms and ions," *Journal of the Indian Institute of Science*, vol. 103, no. 2, pp. 609–632, 2023.

[167] S. Sarkar, J. Mangaonkar, C. Vishwakarma, and U. D. Rapol, "Diffraction of an atom laser in the raman-nath regime," *Phys. Rev. A*, vol. 98, no. 4, p. 043625, 2018.

[168] P. Jessen and I. Deutsch, "Optical lattices," *Advances in Atomic, Molecular, and Optical Physics*, vol. 37, pp. 95–138, 1996.

[169] I. Bloch, "Ultracold quantum gases in optical lattices," *Nat. phys.*, vol. 1, no. 1, pp. 23–30, 2005.

[170] B. Gadway, D. Pertot, R. Reimann, M. G. Cohen, and D. Schneble, "Analysis of kapitza-dirac diffraction patterns beyond the raman-nath regime," *Optics express*, vol. 17, no. 21, pp. 19173–19180, 2009.

[171] E. Brion, L. H. Pedersen, and K. Mølmer, "Adiabatic elimination in a lambda system," *Journal of Physics A: Mathematical and Theoretical*, vol. 40, no. 5, p. 1033, 2007.

[172] H. Müller, S.-w. Chiow, and S. Chu, "Atom-wave diffraction between the raman-nath and the bragg regime: Effective rabi frequency, losses, and phase shifts," *Phys. rev. A*, vol. 77, no. 2, p. 023609, 2008.

[173] G. Casati and B. Chirikov, "Quantum chaos: between order and disorder," *Cambridge University Press, New York,*, 1995.

[174] G. Benenti, G. Casati, I. Guarneri, and M. Terraneo, "Quantum fractal fluctuations," *Phys. Rev. Lett.*, vol. 87, p. 014101, Jun 2001.

[175] R. Blümel, S. Fishman, and U. Smilansky, "Excitation of molecular rotation by periodic microwave pulses: A testing ground for anderson localization," *The Journal of Chemical Physics*, vol. 84, no. 5, pp. 2604–2614, 1986.

[176] I. S. Averbukh and R. Arvieu, "Angular focusing, squeezing, and rainbow formation in a strongly driven quantum rotor," *Phys. Rev. Lett.*, vol. 87, p. 163601, Sep 2001.

[177] P. Facchi, S. Pascazio, and A. Scardicchio, "Measurement-induced quantum diffusion," *Phys. Rev. Lett.*, vol. 83, pp. 61–64, Jul 1999.

[178] B. Georgeot and D. L. Shepelyansky, "Exponential gain in quantum computing of quantum chaos and localization," *Phys. Rev. Lett.*, vol. 86, pp. 2890–2893, Mar 2001.

[179] E. Ott, T. M. Antonsen, and J. D. Hanson, "Effect of noise on time-dependent quantum chaos," *Phys. Rev. Lett.*, vol. 53, pp. 2187–2190, Dec 1984.

[180] D. Cohen, "Quantum chaos, dynamical correlations, and the effect of noise on localization," *Phys. Rev. A*, vol. 44, pp. 2292–2313, Aug 1991.

[181] R. Graham and S. Miyazaki, "Dynamical localization of atomic de broglie waves: The influence of spontaneous emission," *Phys. Rev. A*, vol. 53, pp. 2683–2693, Apr 1996.

[182] S. Paul and A. Bäcker, "Linear and logarithmic entanglement production in an interacting chaotic system," *Phys. Rev. E*, vol. 102, p. 050102, Nov 2020.

[183] I. Dana, E. Eisenberg, and N. Shnerb, "Antiresonance and localization in quantum dynamics," *Phys. Rev. E*, vol. 54, pp. 5948–5963, Dec 1996.

[184] F. M. Izrailev, "Simple models of quantum chaos: Spectrum and eigenfunctions," *Physics Reports*, vol. 196, no. 5, pp. 299–392, 1990.

[185] H. Schanz, M.-F. Otto, R. Ketzmerick, and T. Dittrich, "Classical and quantum hamiltonian ratchets," *Phys. Rev. Lett.*, vol. 87, p. 070601, Jul 2001.

[186] W. K. Hensinger, H. Häffner, A. Browaeys, N. R. Heckenberg, K. Helmerson, C. McKenzie, G. J. Milburn, W. D. Phillips, S. L. Rolston, H. Rubinsztein-Dunlop, and B. Upcroft, "Dynamical tunnelling of ultracold atoms," *Nature*, vol. 412, pp. 52–55, Jul 2001.

[187] M. K. Oberthaler, R. M. Godun, M. B. d'Arcy, G. S. Summy, and K. Burnett, "Observation of quantum accelerator modes," *Phys. Rev. Lett.*, vol. 83, pp. 4447–4451, Nov 1999.

[188] R. M. Godun, M. B. d'Arcy, M. K. Oberthaler, G. S. Summy, and K. Burnett, "Quantum accelerator modes: A tool for atom optics," *Phys. Rev. A*, vol. 62, p. 013411, Jun 2000.

[189] S. Fishman, I. Guarneri, and L. Rebuzzini, "Stable quantum resonances in atom optics," *Phys. Rev. Lett.*, vol. 89, p. 084101, Aug 2002.

[190] M. Sheinman, S. Fishman, I. Guarneri, and L. Rebuzzini, "Decay of quantum accelerator modes," *Phys. Rev. A*, vol. 73, p. 052110, May 2006.

[191] J. Edwards and D. Thouless, "Numerical studies of localization in disordered systems," *Journal of Physics C: Solid State Physics*, vol. 5, no. 8, p. 807, 1972.

[192] N. C. Murphy, R. Wortis, and W. A. Atkinson, "Generalized inverse participation ratio as a possible measure of localization for interacting systems," *Phys. Rev. B*, vol. 83, p. 184206, May 2011.

[193] R. Sankaranarayanan, A. Lakshminarayan, and V. B. Sheorey, "Quantum chaos of a particle in a square well: Competing length scales and dynamical localization," *Phys. Rev. E*, vol. 64, p. 046210, Sep 2001.

[194] R. Sankaranarayanan and V. B. Sheorey, "Accelerator modes of square well system," *Physics Letters A*, vol. 338, no. 3, pp. 288–296, 2005.

[195] S. Tomsovic, J. D. Urbina, and K. Richter, "Controlling quantum chaos: Time-dependent kicked rotor," *Phys. Rev. E*, vol. 108, p. 044202, Oct 2023.

[196] K. Bongs, M. Holynski, J. Vovrosh, P. Bouyer, G. Condon, E. Rasel, C. Schubert, W. P. Schleich, and A. Roura, "Taking atom interferometric quantum sensors from the laboratory to real-world applications," *Nat. Rev. Phys.*, vol. 1, no. 12, pp. 731–739, 2019.

[197] C. F. Ockeloen, R. Schmied, M. F. Riedel, and P. Treutlein, "Quantum metrology with a scanning probe atom interferometer," *Phys. Rev. Lett.*, vol. 111, p. 143001, Oct 2013.

[198] P. Berg, S. Abend, G. Tackmann, C. Schubert, E. Giese, W. P. Schleich, F. A. Narducci, W. Ertmer, and E. M. Rasel, "Composite-light-pulse technique for high-precision atom interferometry," *Phys. Rev. Lett.*, vol. 114, p. 063002, Feb 2015.

[199] I. Dutta, D. Savoie, B. Fang, B. Venon, C. L. Garrido Alzar, R. Geiger, and A. Landragin, "Continuous cold-atom inertial sensor with $1\ \mathrm{nrad/sec}$ rotation stability," *Phys. Rev. Lett.*, vol. 116, p. 183003, May 2016.

[200] M.-K. Zhou, Z.-K. Hu, X.-C. Duan, B.-L. Sun, J.-B. Zhao, and J. Luo, "Precisely mapping the magnetic field gradient in vacuum with an atom interferometer," *Phys. Rev. A*, vol. 82, p. 061602, Dec 2010.

[201] R. Bouchendira, P. Cladé, S. Guellati-Khélifa, F. m. c. Nez, and F. m. c. Biraben, "New determination of the fine structure constant and test of the quantum electrodynamics," *Phys. Rev. Lett.*, vol. 106, p. 080801, Feb 2011.

[202] S.-Y. Lan, P.-C. Kuan, B. Estey, P. Haslinger, and H. Müller, "Influence of the coriolis force in atom interferometry," *Phys. Rev. Lett.*, vol. 108, p. 090402, Feb 2012.

[203] A. Peters, K. Y. Chung, and S. Chu, "High-precision gravity measurements using atom interferometry," *Metrologia*, vol. 38, no. 1, p. 25, 2001.

[204] J. Stenger, S. Inouye, A. P. Chikkatur, D. M. Stamper-Kurn, D. E. Pritchard, and W. Ketterle, "Bragg spectroscopy of a Bose-Einstein condensate," *Phys. Rev. Lett.*, vol. 82, pp. 4569–4573, Jun 1999.

[205] J. Ringot, P. Szriftgiser, and J. C. Garreau, "Subrecoil raman spectroscopy of cold cesium atoms," *Phys. Rev. A*, vol. 65, p. 013403, Dec 2001.

[206] H. Lignier, C. Sias, D. Ciampini, Y. Singh, A. Zenesini, O. Morsch, and E. Arimondo, "Dynamical control of matter-wave tunneling in periodic potentials," *Phys. Rev. Lett.*, vol. 99, p. 220403, Nov 2007.

[207] C. E. Creffield, F. Sols, D. Ciampini, O. Morsch, and E. Arimondo, "Expansion of matter waves in static and driven periodic potentials," *Phys. Rev. A*, vol. 82, p. 035601, Sep 2010.

[208] N. Goldman and J. Dalibard, "Periodically driven quantum systems: Effective hamiltonians and engineered gauge fields," *Phys. Rev. X*, vol. 4, p. 031027, Aug 2014.

[209] M. Bukov, L. D'Alessio, and A. Polkovnikov, "Universal high-frequency behavior of periodically driven systems: from dynamical stabilization to floquet engineering," *Advances in Physics*, vol. 64, no. 2, pp. 139–226, 2015.

[210] M. Arnal, G. Chatelain, C. Cabrera-Gutiérrez, A. Fortun, E. Michon, J. Billy, P. Schlagheck, and D. Guéry-Odelin, "Beyond effective hamiltonians: Micromotion of Bose-Einstein condensates in periodically driven optical lattices," *Phys. Rev. A*, vol. 101, p. 013619, Jan 2020.

[211] J. Sun, R. Liao, P. Zhao, Z. Hu, Z. Wang, X.-J. Liu, X. Zhou, and X. Chen, "A quantitative study of the micromotion of a p-band superfluid in a shaking lattice," *Journal of Physics B: Atomic, Molecular and Optical Physics*, vol. 56, no. 9, p. 095302, 2023.

[212] J. H. Müller, O. Morsch, D. Ciampini, M. Anderlini, R. Mannella, and E. Arimondo, "Atomic micromotion and geometric forces in a triaxial magnetic trap," *Phys. Rev. Lett.*, vol. 85, pp. 4454–4457, Nov 2000.

[213] L. Fallani, C. Fort, N. Piovella, M. Cola, F. S. Cataliotti, M. Inguscio, and R. Bonifacio, "Collective atomic recoil in a moving Bose-Einstein condensate: From superradiance to bragg scattering," *Phys. Rev. A*, vol. 71, p. 033612, Mar 2005.

[214] J. Janarek, B. Grémaud, J. Zakrzewski, and D. Delande, "Quantum boomerang effect in systems without time-reversal symmetry," *Phys. Rev. B*, vol. 105, p. L180202, May 2022.

[215] S. Chai, J. Fekete, and M. F. Andersen, "Measuring the local gravitational field using survival resonances in a dissipatively driven atom-optics system," *Phys. Rev. A*, vol. 98, p. 063614, Dec 2018.

[216] R. Dubertrand, I. Guarneri, and S. Wimberger, "Fidelity for kicked atoms with gravity near a quantum resonance," *Phys. Rev. E*, vol. 85, p. 036205, Mar 2012.

[217] P. H. Jones, M. Goonasekera, D. R. Meacher, T. Jonckheere, and T. S. Monteiro, "Directed motion for delta-kicked atoms with broken symmetries: Comparison between theory and experiment," *Phys. Rev. Lett.*, vol. 98, p. 073002, Feb 2007.

[218] A. Kenfack, J. Gong, and A. K. Pattanayak, "Controlling the ratchet effect for cold atoms," *Phys. Rev. Lett.*, vol. 100, p. 044104, Jan 2008.

[219] M. Lepers, V. Zehnlé, and J. C. Garreau, "Kicked-rotor quantum resonances in position space: application to situations of experimental interest," *The European Physical Journal D*, vol. 63, pp. 449–456, Aug 2011.

[220] S.-w. Chiow, T. Kovachy, H.-C. Chien, and M. A. Kasevich, "$102\hbar k$ large area atom interferometers," *Phys. Rev. Lett.*, vol. 107, p. 130403, Sep 2011.

[221] Yosri Ben-Aïcha, Zain Mehdi, Christian Freier, Stuart S. Szigeti, Paul B. Wigley, LorcÃ¡n O. Conlon, Ryan Husband, Samuel Legge, Rhys H. Eagle, Joseph J.

Hope, Nicholas P. Robins, John D. Close, Kyle S. Hardman, Simon A. Haine, and Ryan J. Thomas, “A dual open atom interferometer for compact, mobile quantum sensing,” 2024.